S.F. van der Sandt

Forming of sandwich panels on a reconfigurable mould

Exploratory research on quality improvement

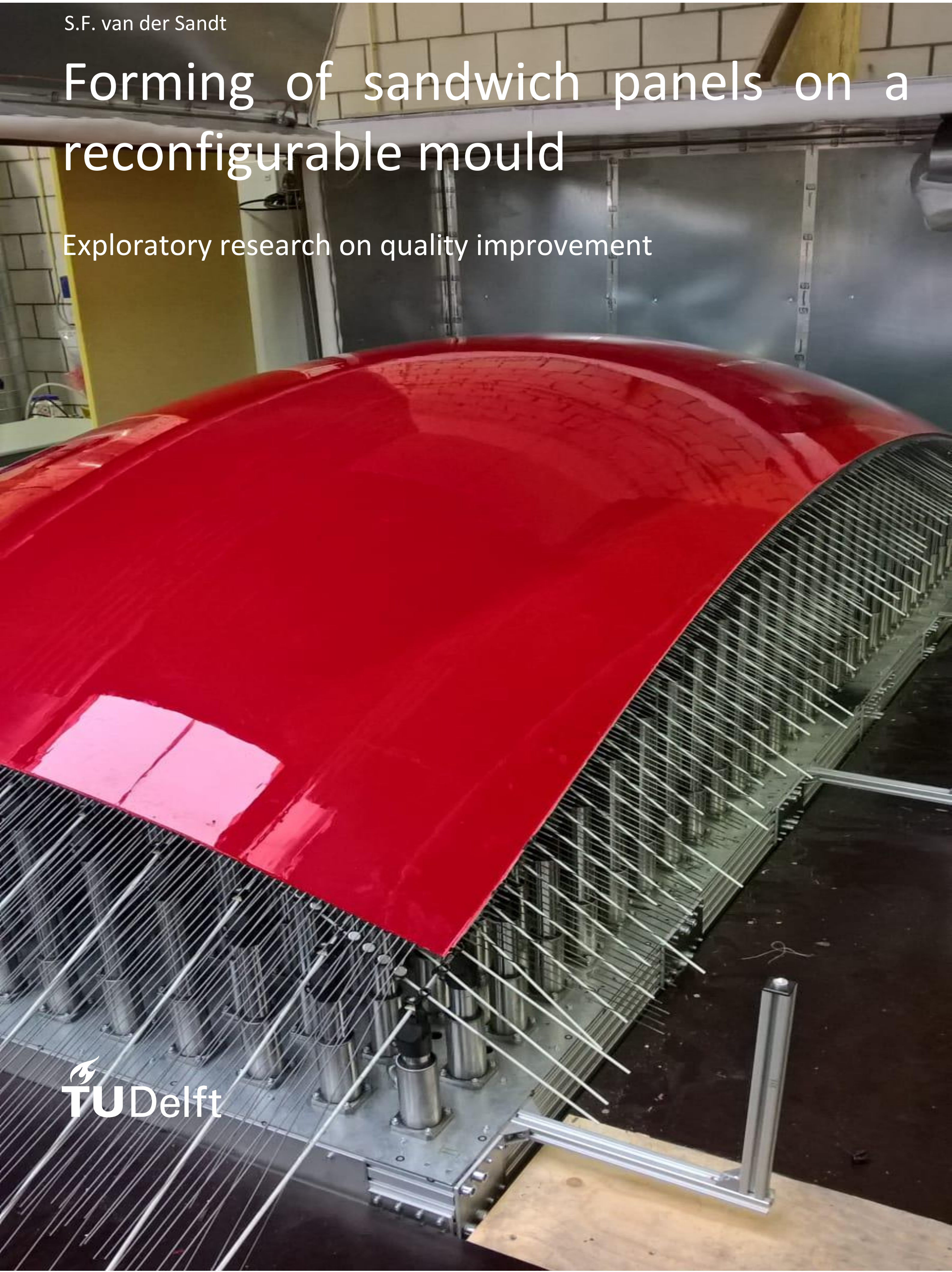

TU Delft

Forming of sandwich panels on a reconfigurable mould

Exploratory research on quality improvement

By

S.F. van der Sandt

in partial fulfilment of the requirements for the degree of

Master of Science
in Aerospace Engineering

at the Delft University of Technology,
to be defended publicly on Tuesday July 10, 2018 at 02:00 PM.

Supervisor:	Dr.ir. O.K. Bergsma,	TU Delft
Thesis committee:	ir. J. Sinke,	TU Delft
	Dr.ir. J.M.F. van Campen,	TU Delft
	Dr.ir. F.J.J.M.M. Geuskens,	Curve Works BV

This thesis is confidential and cannot be made public until July 10, 2023.

An electronic version of this thesis is available at http://repository.tudelft.nl/.

TU Delft

Abstract

The subject of this thesis is the forming of sandwich panels on a reconfigurable mould. The field of research is composite sheet forming. This novel manufacturing process at Curve Works has problems with panel quality, especially out-of-plane wrinkles. Exploratory research on quality improvement is performed by analysing the underlying mechanisms of single curved resin infused sandwich panels where the tooling surface is reconfigured to a concave shape. This will be done under the influence of diaphragm reinforcement, infusion pressure, and forming speed. It has become clear that a reinforced diaphragm reduces out-of-plane wrinkle displacement at the cost of residual stress. The effect of forming speed and infusion pressure on out-of-plane wrinkles is considered to be insignificantly small under the testing conditions as described in this work. For future research it is suggested to look in to reducing frictional forces and the application of tensile stresses to improve formability and panel quality.

Acknowledgements

I would like to thank a number of people who have helped me during the course of this thesis project, as it would not have been possible without them:

First of all, I would like to thank François Geuskens and his wife Tahira Ahmed from Curve Works for having provided me with this thesis opportunity. Their feedback has helped me learn some valuable lessons on how to perform research.

I would like to thank Otto Bergsma as my thesis supervisor, for his constructive support during the insightful and fun meetings we had.

Those involved from Delft Aerospace Structures and Materials Laboratory who enabled me to make use of their facility.

Finally, I am very grateful for the love and support from my girlfriend, family, and friends, during the course of my studies at TU Delft and especially during the work presented in this thesis.

Table of Contents

1 Introduction

Nowadays, the demand for products made from composites is at an all-time high and is expected to keep increasing in the years to come. To meet this demand and to drop prices, innovative manufacturing methods are essential. One of those innovations is taking place at a company called Curve Works situated in Zoetermeer, The Netherlands. They have devised a unique production-line, with an automated reconfigurable mould as a centrepiece, to create single and double curved composite panels starting from a flat impregnated preform. Therefore, reducing; tooling costs, lead times, storage/disposal issues of moulds, which are common for low-volume production or prototyping.

For Curve Works it is of specific interest to form composite sandwich panels, as sandwich panels have a high bending stiffness to weight ratio which is of interest to the marine and architecture markets they try to serve. The goal is to form double curved sandwich panels of a high quality in a short time at low cost. Quality refers to sandwich panels without unwanted deformation modes like out-of-plane wrinkles. Out-of-plane wrinkles have been detected in formed panels, undermining the desired quality. Forming of concave shapes has shown to create significantly worse forms of wrinkling compared to convex. Also, the forming of double curved panels has proven difficult due to high forming forces. In some cases, the tool surface disconnected from the supporting pin bed.

The choice was made to conduct an exploratory research, due to the fact that composite sheet forming in combination with this new type of tooling has not been studied before. This is done by performing a literature study, followed by a first series of tests. For future research on this topic it is suggested to use this exploratory research as a starting point.

The aim of the test series is to investigate the underlying forming mechanisms of resin infused sandwich panels under the influence of diaphragm reinforcement, infusion pressure, and forming speed. Single curved panels mainly experience inter-ply slip, whereas double curved panels also experience intra-ply shear. To limit the complexity of this first series of tests to a reasonable level it makes sense to only consider single curved panels. These tests will be performed with the tooling surface reconfiguring itself to a concave shape.

This thesis starts off with chapter 2, a literature review briefly exploring the topics which have been identified to be of importance for this research. The literature review will provide perspective and also enable the creation of some hypotheses. These hypotheses are formulated in section 3.1 and form a starting point for chapter 3. Chapter 3 elaborates on the methods and materials used for the current research. It covers a geometrical slip model of the forming experiments, the forming experiments themselves, post processing procedures and data collection. Chapter 4 presents the results and analysis of the data collected. Section 4.3 will review the hypotheses. Chapter 5 will close off the thesis with the conclusions and recommendations.

2 Review of the Literature

The topic of this thesis is the forming of sandwich panels with a reconfigurable mould. Composite sheet forming is therefore the research area of interest. This literature review will briefly explore the topics which have been identified to be of importance. Those topics are: reconfigurable mould forming, diaphragm forming, resin infusion, reinforcements, the deformation mechanisms in both fabrics and laminates, and modelling of deformation.

2.1 Reconfigurable mould forming

2.1.1 Introduction

Common problems for low-volume production or prototyping of curved laminate sheets are the high tooling costs, long lead times, and storage/disposal issues of moulds. At Curve Works a unique production-line, with an automated reconfigurable mould as a centrepiece, to create single and double curved panels from 3D drawings, was developed to overcome these issues. This section on reconfigurable mould forming will provide some detailed information on the reconfigurable mould and how it is used in the reconfigurable mould forming production process.

2.1.2 Reconfigurable mould

The main components of the reconfigurable mould are clearly visible in Figure 1. Those components are the reconfigurable pin bed or pin bed for short and the mould surface on top of the pin bed. The function of the pin bed is to control the mould surface such that it matches the 3D surface digitally supplied to it by the computer aided design (CAD) input. The bed can be seen as a bundle of 528 steel modules with actuators which are driven by step-motors. The mould surface is a rubber membrane which is reinforced with freely sliding carbon fibre rods. The free sliding rods give the rubber membrane the needed bending stiffness without an increase in membrane stiffness. This allows for the rubber membrane to be forced in the desired shape without requiring an unnecessary increase of force needed by the supporting pin bed.

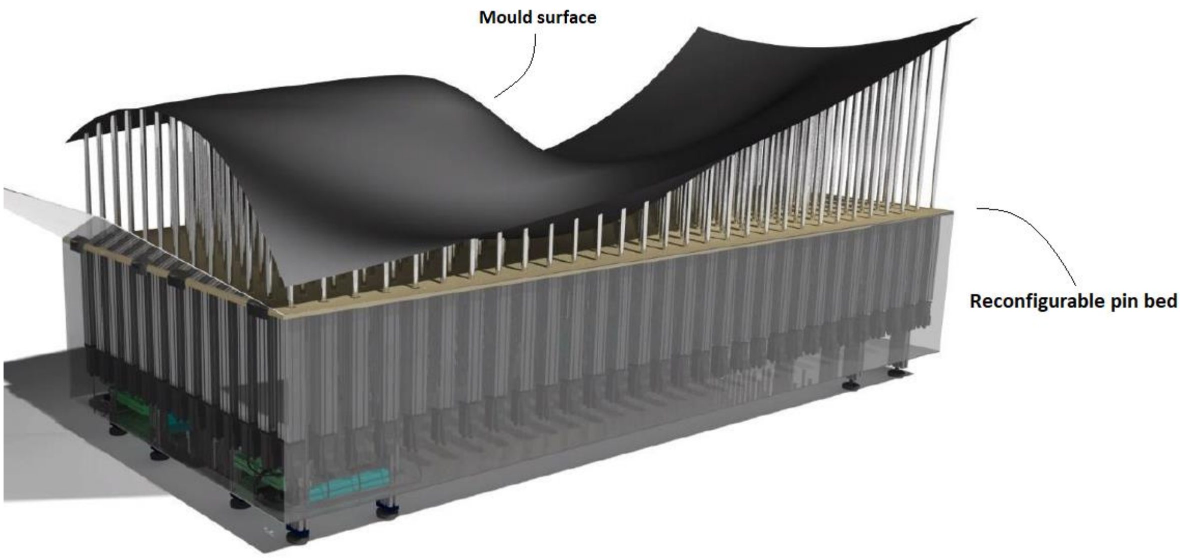

Figure 1: Reconfigurable mould's main components are the reconfigurable pin bed and the mould surface

The structure which connects the pin bed and mould surface is of vital importance to the reconfigurable mould as it is directly driven by the actuators to create the splines which dictate the shape of the mould surface. These splines are physically represented by glass fibre rods. A detailed drawing of this support structure which shows the glass fibre rods is shown in Figure 2. This figure also shows the t-sections which directly connect the pins of the pin bed to the glass fibre rods, and the magnets in their cupholders which form a direct connection between the glass fibre rods and the mould surface. Note that the mould surface contains iron particles on the side of the pin bed to allow for this magnetic attraction.

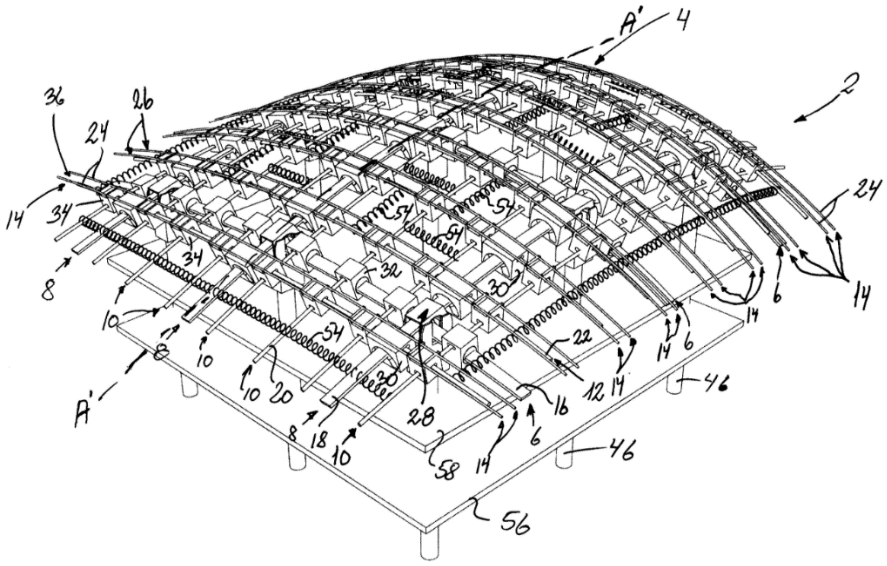

Figure 2: Support structure [1]

The reconfigurable mould at Curve Works comes with some constrains which are briefly described in Table 1.

Table 1: Constraints related to the reconfigurable mould

Size	The maximum part size on a flat mould surface can be up to 3.60 x 1.56 m. Beyond this range it is difficult to guarantee sufficient accuracy as the edges of the mould surface are not directly attached to the supporting structure. The curvature of the edges therefore deviates from the 3D surface supplied digitally to the reconfigurable mould. Another size constraint is a direct consequence of the maximum z-deflection an actuator can reach, i.e., 1 m.
Speed	Maximum forming speed of the mould surface is dictated by the maximum speed of an individual actuator, i.e., 5mm/s.
Geometry	For single curved shapes the minimum radius of curvature is 400 mm. For double curved shapes the minimum radius of curvature is higher and is a function of the product complexity.
Accuracy	For single curved and slightly double curved shapes an accuracy of ±1 mm applies. Whereas more complex double curved shapes have an accuracy of ±2 mm.

Currently, the software of the reconfigurable mould is still limited, i.e., the flat homing plane Z-position of the reconfigurable mould cannot be chosen freely and has just one default position. Also, the required end-shape can only be created starting from the default position. The minimum time it takes to go from start-position to end-position is determined by the actuator that must travel the largest distance divided by the maximum actuator speed (5 mm/s). The other actuators will move with speeds which are scaled to this “reference” actuator. Meaning that all actuators will arrive at their respective end positions at the same moment in time. This is due to the requirement of maintaining a low energy spline during the forming operation, therefore not creating excessive membrane stresses for efficient machine operation. It is possible to decrease the speed of the “reference” actuator and therefore of the entire forming operation. This will probably all change in nearby future updates. The next update should allow for other homing positions to be chosen. Therefore, right now the influence of the user on the forming operation is:

- Choosing the forming speed of the mould, no faster than the maximum which is limited by the maximum speed of the actuators
- Choosing the end position and shape, which is limited by the dimension of the membrane, actuator movement and the low energy spline (minimum radius of curvature).

2.1.3 Production process

The process of producing both single and double curved laminate panels with a reconfigurable mould is a new type of composite sheet forming process. The reconfigurable mould at Curve Works can be used to form various types of products, such as fibre reinforced plastics or thermoplastics. As the thesis focusses itself on the forming of resin infused sandwich panels, this section will only describe specifics related to that process.
Figure 3 shows a process diagram of the currently used method of forming resin infused sandwich panels at Curve Works.

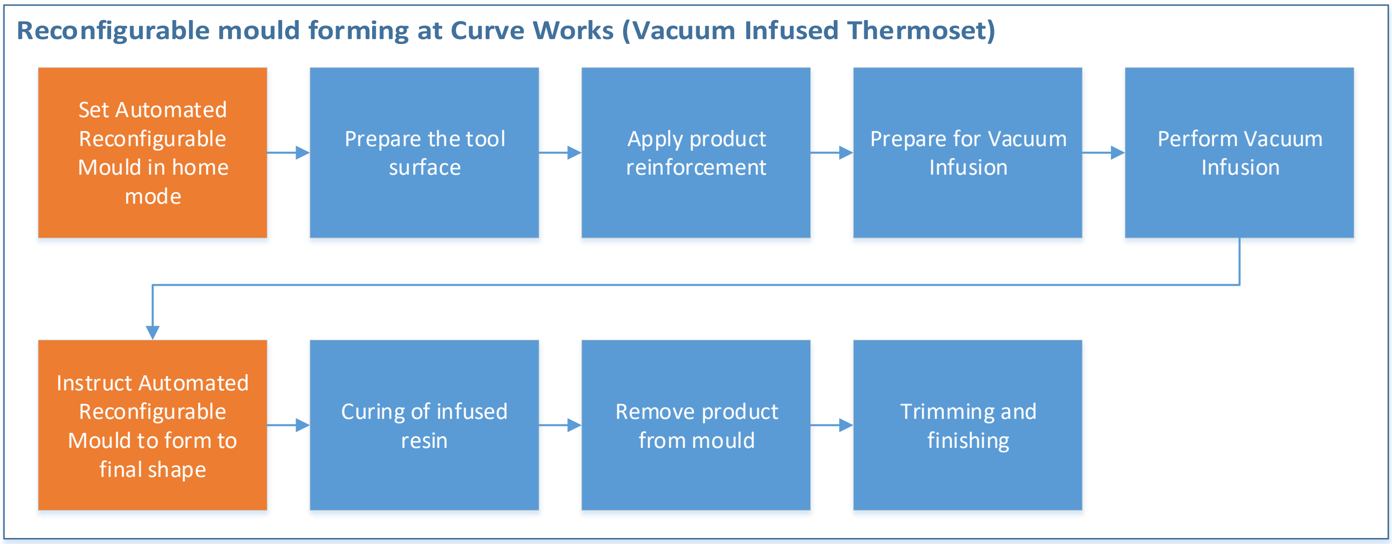

Figure 3: Process diagram of the currently applied production process

The process starts with switching on the machine and putting it in home mode, followed by a calibration step. Now that the reconfigurable mould is in the calibrated flat configuration, the tool surface can be prepared. Preparation of the mould surface is done first by cleaning the silicone rubber mould surface with denatured alcohol. Followed by the application of a thin nylon diaphragm. This diaphragm is applied to the mould surface with the use of tacky tape and a vacuum connection to ensure it is fully applied. Product reinforcement can now be applied in the desired way. Last steps before the forming can commence is putting down consumables for the vacuum infusion (including a top diaphragm) and the vacuum infusion process itself. Instruct the reconfigurable mould to form to the digitally uploaded 3D shape and wait for the resin to be cured. Finally remove the product from the mould such that it can be trimmed and finished.

The *advantages* of this process at Curve Works are:

- Relatively easy to place the laminate on a flat plane, making the “layup” part of the process less time consuming and therefore more cost effective.
- The reconfigurable mould can reconfigure itself within minutes, saving on production time and costs of moulds.
- Moulds can be stored as digital 3D models. This significantly decreases the storage space needed.

The *disadvantages* of this process at Curve Works are:

- The attainable curvature is limited by the actuators (min. radius of curvature 40cm)
- The speed of the reconfigurable mould is limited (scaled speeds with an actuator speed of 5mm/s)
- The reconfigurable mould consists of many parts, such as actuators, magnets, reinforcement rods for the membrane, etc. Resulting in frequently needed maintenance, which causes unwanted downtime of the machine.
- The tool surface/membrane material is high performance rubber (, currently silicone rubber). This is an expensive membrane that needs to be handled carefully during layup and forming procedures.

2.1.4 Findings

- The Reconfigurable Mould Forming process has a lot of potential to compete in the forming of double curved panels. Especially for prototyping or low volume productions, since it can save on the production and storage of moulds, and man hours needed for layup.
- Development of new heating and cooling systems will improve the forming of curved thermoplastic laminate sheets significantly. The thesis however, will limit itself to the forming of curved thermoset laminate sheets.
- Only “slightly” curved parts can be formed due to the limitation on the minimum attainable radius of curvature.
- There is only a limited amount of options on how to influence the kinematics of the membrane during forming operations.

2.2 Diaphragm forming

2.2.1 Introduction

Diaphragm forming was developed together by Superform Ltd. and ICI PLC. in Great Britain [2]. A composite preform is positioned between two diaphragms, the diaphragms are clamped in a frame and the composite preform remains free floating between the two diaphragms. Finally, a vacuum is applied between the diaphragms after which a pressure difference enforces the diaphragms together with the composite preform to conform to the mould underneath. See, Figure 4.

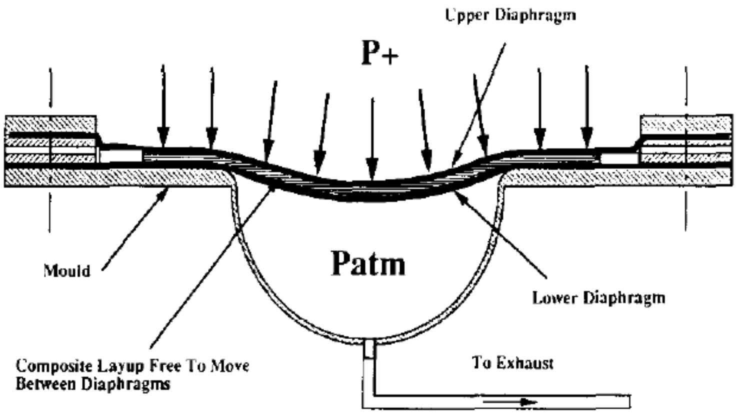

Figure 4: Diaphragm forming [3]

Originally the diaphragm forming process was developed for the forming of thermoplastic laminates. However, at a later stage the process has also been successfully applied for the forming of thermoset prepregs. The main differences are the processing temperatures, pressures, forming speeds, and the type of diaphragms used. An advantage of this process is that the impregnated preform can be applied on a flat surface, which saves man hours and therefore costs. A common downside of composite sheet forming which also plagues diaphragm forming, is the forming of wrinkles. However, by choosing a diaphragm which matches the process this can be suppressed to a large extent.

2.2.2 Diaphragms

The purpose of diaphragms is keep the laminate under control during forming. The requirement for diaphragms is that they can sufficiently deform without rupturing at the processing temperature of the laminate. By stretching, the diaphragms are in tension which can reduce or even eliminate possible wrinkling, i.e., tensile stresses from the diaphragms can prevent laminate wrinkling by reducing compressive stresses in the laminate.

Materials used for diaphragms are: metal; polymeric; and composite [4]. The requirement is that the diaphragm should sufficiently deform without rupturing at the processing temperature. Superplastic aluminium was therefore used for the forming of thermoplastic laminates at a temperature of around 400°C. However, superplastic aluminium diaphragms are expensive. Polymer diaphragms, for example those made from polyimide were much cheaper, resulting in a more economical process.

In Figure 5, the Diaphragm Forming and the Reconfigurable Mould Forming process are shown for the production of an identically curved laminate shell. A noticeable difference which can be observed is that the diaphragms used in Diaphragm Forming are clamped at the edges, therefore allowing tension to build up during forming. However, for Reconfigurable Mould Forming the edges are not clamped by a fixture but held down with tacky tape and vacuum. The question arises whether sufficient tensile forces are built up in the top diaphragm in the current Reconfigurable Mould Forming process. Meaning that a relatively large portion of the compressive stresses that occur would need to be taken up by the laminate. This might be one of the causes for the wrinkling to occur in Reconfigurable Mould Forming of slightly double curved panels.

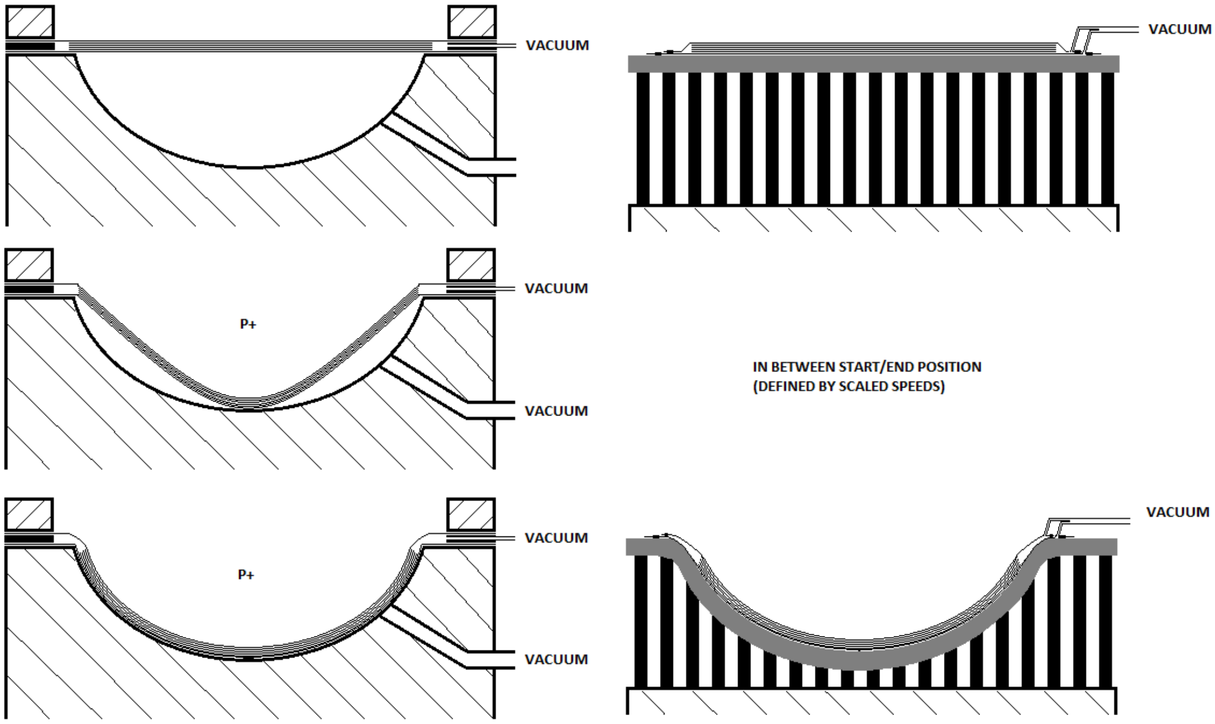

Figure 5: Diaphragm forming versus Reconfigurable Mould Forming

An interesting patent [5] which describes the concept of a reinforced diaphragm (, see Figure 6) has been said to greatly increase the number of plies that could be diaphragm formed in the production of a 61-cm C-channel. It is said to have successfully produced a C-channel with a quasi-isotropic layup that was 32 plies thick [6].

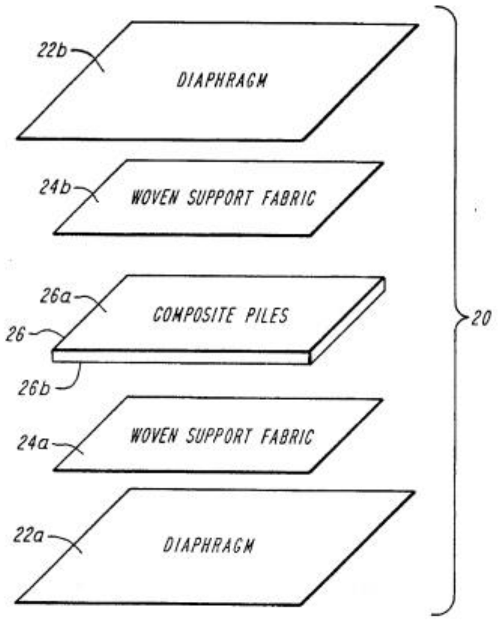

Figure 6: A woven support fabric is added to the "conventional" diaphragm forming package

2.2.3 Findings

- Choice of diaphragm material depends on the processing temperature of the laminate to be formed. Within this temperature range the diaphragms will need to provide sufficient stretching without rupture.
- Diaphragm materials previously used are: metal, polymeric, and composite.
- Diaphragms are under tension when stretched. This tension helps to counteract out-of-plane buckling
- It is questionable if sufficient tension can be built up in Reconfigurable Mould Forming to prevent laminate wrinkling
- Diaphragm tension is backtracked by measuring the strains with GSA, and by applying constitutive relations you can get back to the stress

2.3 Resin infusion

2.3.1 Introduction

Many types of resin infusion exist, the main ones are considered to be Resin Transfer Moulding (RTM), Vacuum Assisted Transfer Moulding (VARTM), and Vacuum Infusion (VI). Apart from the differences in tooling, the main differences between these methods are the pressure differences, see Figure 7 and Table 2. For the resin to flow, the pressure at the inlet (P1) needs to be larger than the pressure at the outlet (P2).

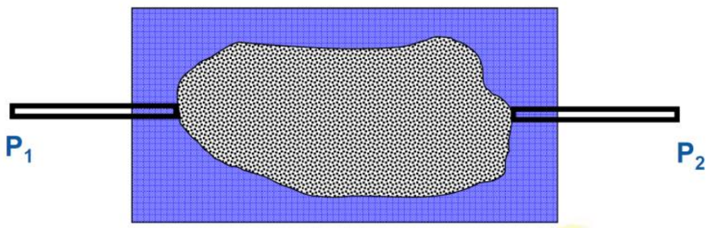

Figure 7: Resin infusion schematic

Table 2: Resin infusion types and their respective in (P1) and outlet (P2) pressures

Resin infusion type	*P1*	*P2*
RTM	> 1 atm	1 atm
VRTM	> 1 atm	< 1 atm
VI	1 atm	< 1 atm

However, this research will limit itself to the VI process.

2.3.2 Vacuum infusion process parameters

The vacuum infusion process for basic line infusion is governed by Darcy's law.

$$Filltime \approx \frac{Viscosity \cdot Porosity \cdot Flowlength^2}{Permeability \cdot Pressure\,difference} \qquad \text{Eq. 1}$$

That means that the time to fill depends on the viscosity of the thermoset, the porosity and permeability of the laminate, the pressure difference between in and outlet, and the length the resin needs to travel. Note that the flow length has a relatively large influence. Therefore, it is important to properly choose the infusion strategy, see Figure 8. Clearly, the infusion strategy has a huge influence on fill time.

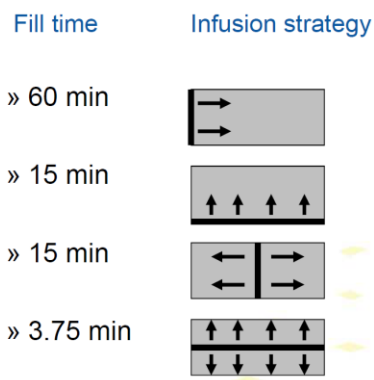

Figure 8: Infusion strategy

More information about the porosity and permeability of the laminate can be found in [7]. The viscosity of the thermoset should be low to improve the flow. Viscosity of a thermoset depends on the temperature and the extent of cure, and it is covered by the field known as rheokinetics. A theoretical description of this viscosity up to the point of gelation has been shown to be [7].

$$\mu = \mu_0(T)\left(\frac{\alpha_g}{\alpha_g - \alpha}\right)^f \qquad \text{Eq. 2}$$

Where, μ_0 is the initial viscosity as a function of temperature, f is a constant which is resin system dependent, α_g is the conversion of gelation, and α is the conversion given by:

$$\alpha = 1 - e^{-\int k dt} \qquad \text{Eq. 3}$$

Where, k is the reaction constant.

The initial dynamic viscosity for polyester, vinyl ester, or epoxy resins is in the order of a 100 to 300 mPa*s [8]. The viscosity build-up of a polyurethane network is depicted in Figure 9. The initial viscosity goes down for a higher temperature; however, a higher temperature also causes a more rapid increase of the viscosity as time progresses. During this research however, room temperature conditions apply and no further heating is applied.

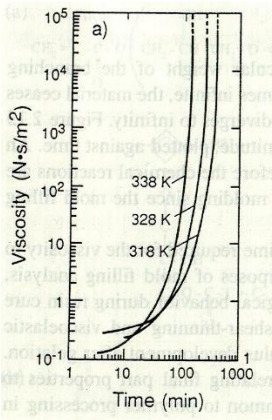

Figure 9: Viscosity build-up of a polyurethane network

2.3.3 Pressure distribution during vacuum infusion

During vacuum infusion, an uneven pressure distribution is created in the product, see Figure 10. After the resin has infused into the product there are several ways to end the vacuum infusion procedure, each having a different effect on the way the pressure is distributed in the infused part. The options are:

- leave inlet and outlet open (Figure 10)
- close the inlet (Figure 11)
- close the outlet (Figure 12)
- close inlet and outlet (Figure 13)

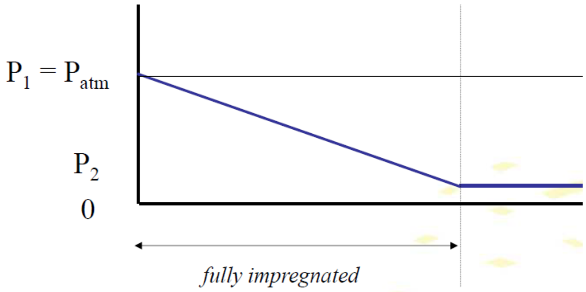

Figure 10: Pressure difference after resin infusion

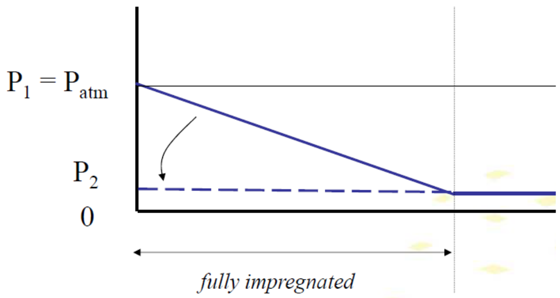

Figure 11: Close inlet

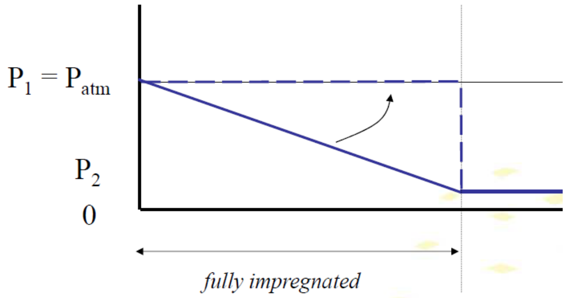

Figure 12: Close outlet

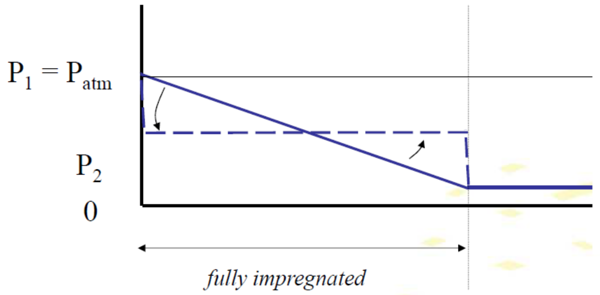

Figure 13: Close inlet and outlet

Leaving both the inlet and outlet open maintains the pressure difference throughout the product. When closing the inlet or the outlet, the pressure will even out to the inlet or outlet that is still open. And when both the inlet and outlet are closed, the resulting pressure will be the average of in the inlet and outlet pressures.

An interesting feature of this is that for vacuum infusion the outlet pressure can be chosen. And by closing the inlet only, the pressure in the infused laminate will become that of the outlet where the vacuum is applied. Therefore, the pressure inside the infused laminate can be anything between the minimum and maximum values of the pressure applied at the outlet.

$$0 < P_{vacuumbag} < 1 atm \qquad \text{Eq. 4}$$

The pressure that is acting on the vacuum infused package is the difference between that of the atmosphere and the pressure inside the vacuum bag.

$$\begin{aligned} &P_{package} = \Delta P = P_{atm} - P_{vacuumbag} \\ &\Rightarrow 0\,atm \leq P_{package} < 1\,atm \end{aligned} \qquad \text{Eq. 5}$$

2.3.4 Findings

- The process used in the thesis is Vacuum Infusion
- The pressure acting on the entire package can be regulated with the outlet pressure and can have values roughly ranging between 0 and 1 atm.
- It is important to have a low viscosity resin that will have an acceptable level of viscosity by the time the forming procedure would start in reconfigurable mould forming.
- Choosing a suitable infusion strategy can save a lot of time.
- Keep in mind that the consumables used might influence the forming process.

2.4 Reinforcements

2.4.1 Introduction
The function of reinforcements is to literally reinforce a matrix, such that the resulting composite has improved mechanical properties when compared to the constituent materials individually. The goal of this chapter is to describe the types of reinforcement and the effect of fabric type on the deformability of an impregnated and uncured laminate during forming.

2.4.2 Reinforcement types
There is a great variety of reinforcement types made from continuous fibres; UD, woven fabrics, knitted fabrics, and multi-axial fabrics.

<u>UD</u>
A true Uni-Directional fabric is one that has all fibres oriented in the same direction (see Figure 14). Note that in practice UD fabrics are kept together by fibres running in different directions. If one wants no fibres in any other direction except the primary, then use impregnated UD tape. The advantage of UD is that it has no crimp and is straight, giving rise to good mechanical properties.

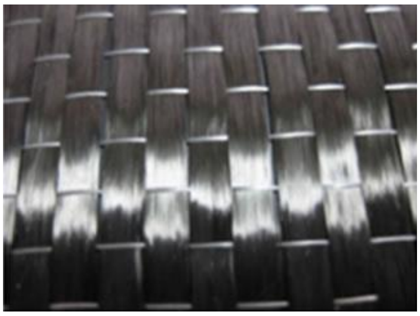

Figure 14: UD fabric with supporting fibres visible

<u>Multi-axial fabrics</u>
A Multi-Axial fabric is one that consists of multiple layers of UD fabric, held together by stitching (see Figure 15). The advantage of Multi-axial fabrics is that the fibres in each layer are straight and have no crimp, giving rise to good mechanical properties. Some common forms of multi-axial fabrics are: biaxials, triaxials, quadriaxials, etc.

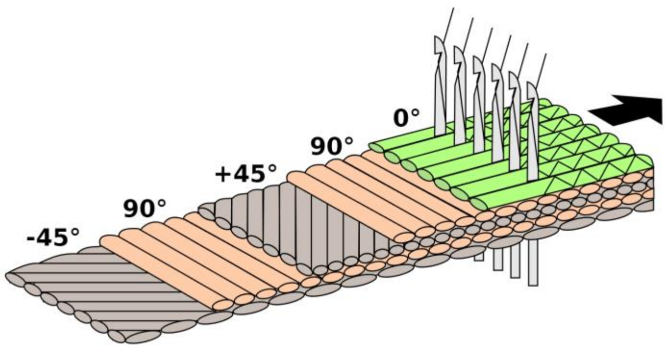

Figure 15: example of a multi-axial fabric as it is stitched during production (Creative Commons, free to share)

<u>Woven fabrics</u>
A woven (or textile) fabric is one that has a woven structure, meaning; warp and weft fibres which cross each other. This cross-over causes mechanical interlocking of the fibres which keeps the fabric together. By using different cross-over patterns of warp and weft fibres a multitude of woven fabrics can be manufactured. Some of the common types

of woven fabrics are; plain weave, twill weave, satin weave (see Figure 16). The advantage is that different types of woven fabrics have different properties with respect to drape-ability, stability, permeability, etc.

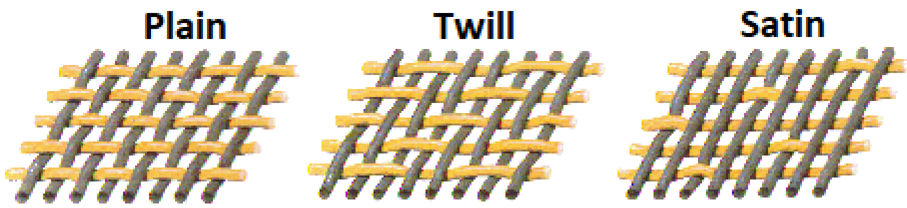

Figure 16: Three common types of woven fabrics

Knitted fabrics
Knitted fabrics differ from woven fabrics in that they are “more flexible and can be more readily constructed into smaller pieces. This has to do with the completely different patterns used to weave knitted fabrics resulting in a different structure altogether, which allows for large strains. See, Figure 17.

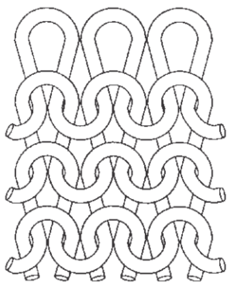

Figure 17: Knitted fabric [9]

2.4.3 Effect of fabric properties on deformation modes
Fabrics have many properties. The ones that are considered the most important in relation to deformation are the fabric weave style, yarn count, and yarn shape.

Weave style
Some common weave styles are the plain weave, twill weave, and satin weave, see the left of Figure 18. The multiaxial fabric has also been included in the figure. On the right of Figure 18 a graph is shown where the different weave styles (including the multiaxial fabric) have been plotted based on their relative drapeability and crimp. It becomes clear that there is a trade-off between the drapeability and crimp of the fabrics. This trend can be explained by the number of crossings in a weave, i.e., less crossings in a weave pattern result in better shear deformation capability [10]. For this reason, the satin weave style has the best drapeability. However, a high drapeability also results in a lower crimp due to a lower number of crossings. Meaning that the distance between the crossings (which act as supports) increases, therefore decreasing the buckling resistance [11]. That is why the plain weave has the highest buckling resistance. Important to note is that a low crimp results in improved mechanical performance.

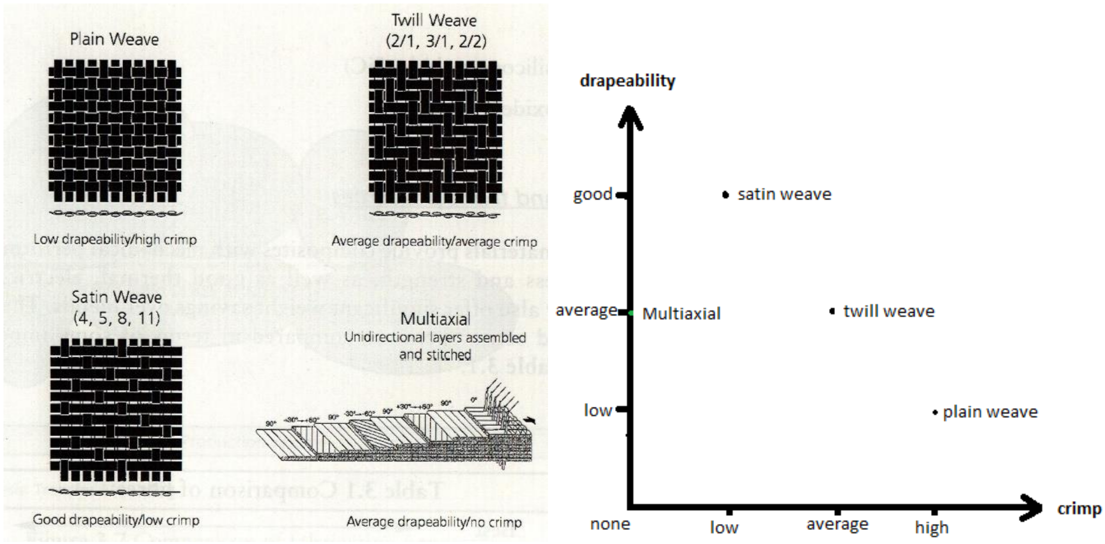

Figure 18: (Left) Common weave styles, (Right) and their relative drapeability and crimp

Choosing the right fabric in this case therefore depends on the forming and mechanical requirements. More properties related to different weave styles are shown in Table 3.

Table 3: Several weave styles and their properties

Property	Plain	Twill	Satin	Basket	Leno	Mock Leno	Knit
Good stability	***	***	**	**	*****	***	***
Good drape	**	****	*****	***	*	**	***
Low porosity	***	****	*****	**	*	***	*
Smoothness	**	***	*****	**	*	**	**
Balance	****	****	**	****	**	****	***
Symmetrical	*****	***	*	***	*	****	***
Low crimp	**	***	*****	**	*****	**	***

***** = excellent, **** = good, *** = acceptable, ** = poor, * = very poor

<u>Yarn count and yarn shape</u>

Looking at Figure 19 it seems evident to say that the higher the yarn count, the more shear deformation is restricted. Decreasing yarn count means that the relative distance between two yarns increases and vice versa. Note that a relatively large gap improves the shear deformation capability. At the same time, a large gap also means that shear slip becomes worse. By careful handling of the fabric this can be avoided [11].

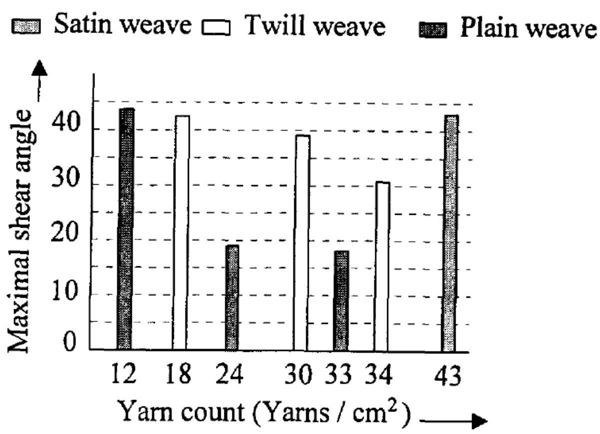

Figure 19: Maximal shear angle as a function of yarn count [11]

The shape of the yarns produced by the industry are usually flat rather than round, see Figure 24. This shape will change when the fabric is sheared. Note that a thin yarn will deform later when sheared compared to a thick yarn, resulting in improved shear deformation capability. Another effect of flat yarns is that the effect of fibre straightening capability decreases [11].

Influence of resin [11]
The influence of resin on fabric deformation cannot be neglected. By looking at Figure 20 it becomes clear that a resin allows for an increase of the maximum shear angle, acting as a lubricant.

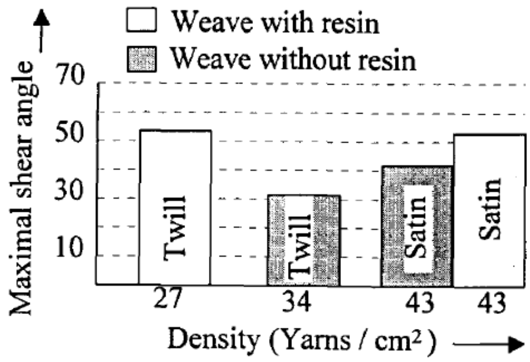

Figure 20: comparison of maximal shear angle for fabrics with and without resin [11]

The viscosity of the resin is an important parameter which depends on both pressure and temperature. The maximal shear angle as a function of both pressure and temperature for thermoplastic PEI is shown in Figure 21. By increasing the pressure, it becomes clear that the shear deformation is obstructed. Two possible reasons for this are the higher resistance to yarns rotating at the crossover points, and the obstruction of yarn shape deformation which occurs during shearing of a fabric. By having small yarn bundles and an increased yarn spacing deformation, characteristics of a fabric can be further improved.

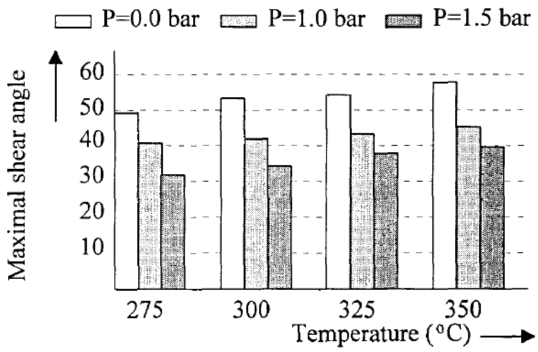

Figure 21: Influence of temperature and pressure on the maximal shearing angle [11]

2.4.4 Findings

- It has become clear that many types of woven reinforcement are available. However, the research for which this literature study is intended is limited to 0/90 biaxials, +45/-45 biaxials, 0/90 woven fabrics, and +45/-45 woven fabrics. Note that the woven fabrics can come in several weave patterns, such as Plain, Twill, Satin, etc.
- The most important fabric properties in relation to deformation are considered to be weave style, yarn count, and yarn shape. The satin weave style has the highest drapeability due to the lower number of crossings, but it has a low buckling resistance. The plain weave style has the lowest drapeability but the highest buckling resistance. Multi-axial fabrics have average drapeability, but very little crimp and therefore the best mechanical properties.

- By having small yarn bundles and an increased yarn spacing, deformation characteristics of a fabric can be further improved.
- Resin seems to have a lubricating effect which positively impacts shear deformation.

2.5 Fabric and laminate deformation mechanisms

2.5.1 Introduction

Forming a flat impregnated preform into a curved shape which is either single or double curved requires for the laminate to deform. Various deformations can play a role, the two main deformation mechanisms for forming of laminate sheets are inter-ply slipping and intra-ply shear. This chapter will however first discuss ways in which fabrics can deform, followed by the section on inter-ply and intra-ply slipping.

2.5.2 Deformation modes of fabric

A flat fabric layer is identified to have five deformation modes, namely: fibre stretching, fibre straightening, shear (or trellis effect), shear slip, and buckling [11].

I Fibre stretching

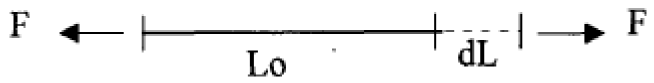

Figure 22: fibre stretching deformation mode [11]

When a tensile stress is applied to a fibre it will stretch. Most high performance fibres can deform up to around 2% strain before failure occurs, for glass fibres this is around 5% [12]. Since fibres are very strong, they are not likely to fail during forming. Also, fibre stretching will result in relatively small deformations when compared to other deformations [11]. Therefore, in most models it is assumed that the fibres are inextensible when forming.

II Fibre straightening

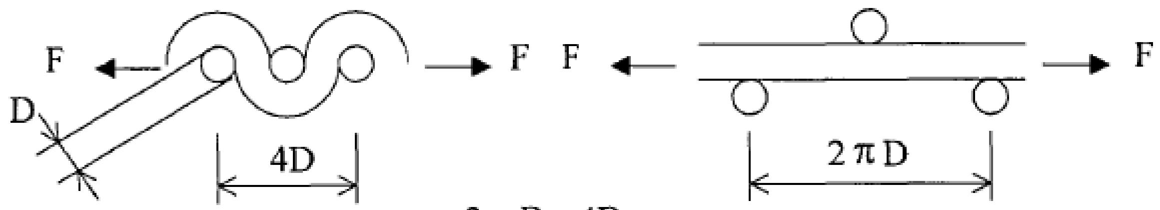

$$\varepsilon_{max} = \frac{2\pi D - 4D}{4D} = 57\,\%$$

Figure 23: Fibre straightening deformation mode [11]

For fabrics with a crimp there is a deformation mode called fibre straightening. When tension is applied the fibres in that direction will straighten, see Figure 23. Note that in this case the maximum amount of strain can be as high as 57%. However, this maximum amount of strain is greatly reduced by the fact that the industry produces fabrics which have relatively flat fibre bundles [11], see Figure 24.

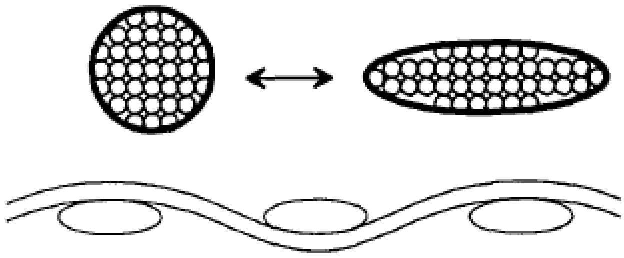

Figure 24: Round versus flat fibre bundles, where flat fibre bundles decrease the maximum amount of strain [11]

Another factor which is of influence on the amount of fibre straightening is the weave style [13], see Figure 25. Note that the fibre straightening factor (FSF) is the highest for the plain weave style, which has the highest crimp.

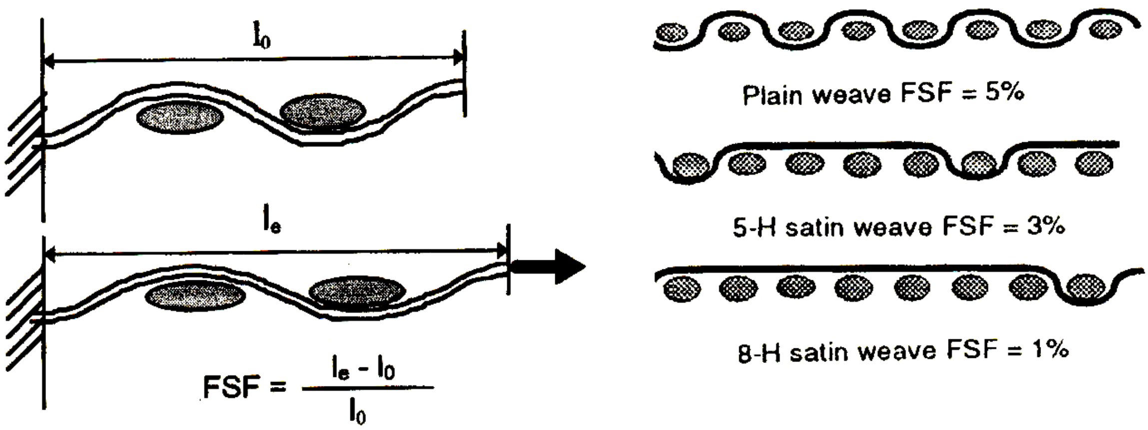

Figure 25: Straightening of different fabric styles [6]

<u>III trellis effect</u>

When a single layer of fabric is sheared in plane, one can observe the trellis effect. The trellis effect occurs when a tensile force is applied in a direction that does not align with the orthogonal fibres, see Figure 26.

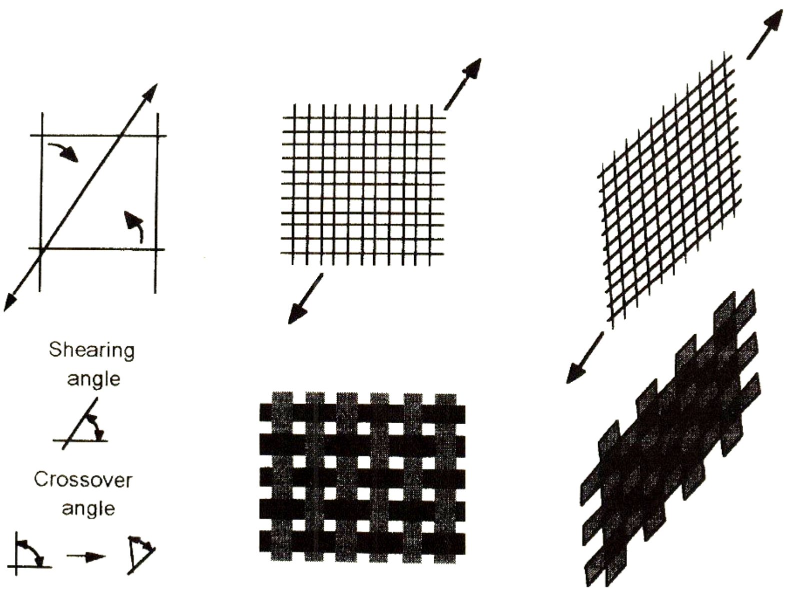

Figure 26: Trellis effect [6]

The effect is that the angle between the fibre bundles decreases. This angle is called the trellis angle, a.k.a. crossover angle. As the trellis angle decreases, it will reach a limiting value called the locking angle. When the trellis angle is coming near the value of the locking angle, the force required to shear the fabric rapidly increases. If an attempt is made to go beyond the locking angle, the fabric will show out-of-plane buckling [6]. Note that the trellis angle will never obtain a value of zero.

IV Shear slip

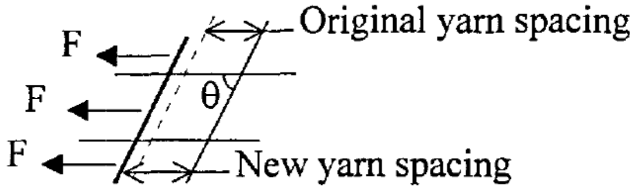

Figure 27: Shear slip [11]

Shear slip is the slipping of yarn bundles w.r.t each other, due to shear [11]. This effect occurs locally in a fabric. The larger the size of the fabric the less shear slip will occur according to [14]. According to [15] the relation between shear slip and the trellis angle theta as shown in Figure 27, is as follows.

$$\frac{new\,yarn\,spacing}{original\,spacing} = 1 + s(1 - \theta / 90) \qquad \text{Eq. 6}$$

V Buckling

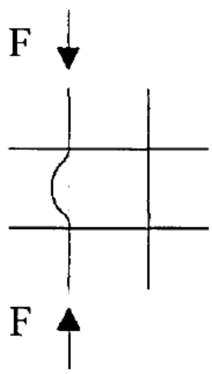

Figure 28: Buckling [11]

Buckling deformation is unwanted because it greatly diminishes the mechanical properties of the product. It occurs at the locking angle as has been explained before. The buckling can either be in-plane or out-of-plane, depending on the constraints imposed during production. Keep in mind that fibres buckle relatively quick under compressive loads. For these reasons, it is important to stay below the locking angle and to prevent compressive loads from building up in the direction of the fibres [11].

2.5.3 Deformation modes of a laminate

In the previous section the various deformation modes of a fabric were shown. However, a composite product also includes the matrix component, and by stacking multiple layers one obtains a laminate. When deforming a laminate, two major deformation modes can occur. Namely, inter-ply slip and intra-ply shear.

2.5.3.1 Inter-ply slip

Inter-ply slip is the relative sliding of neighbouring plies within a laminate. Because of this relative sliding, an amount of slip can become visible at the edge of the laminate. If the edges are constrained the slip is restrained and buckling can occur, see Figure 29.

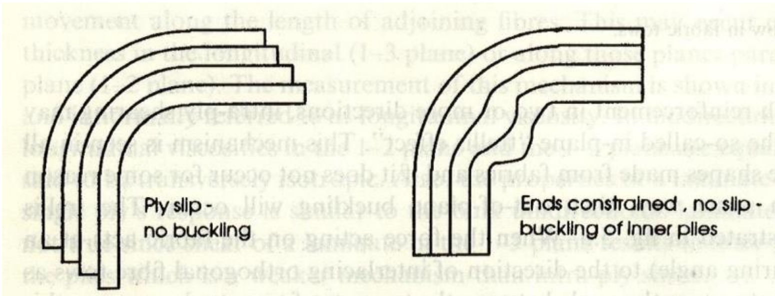

Figure 29: Inter-ply slip [6]

Geometrical considerations

A good starting point to understand inter-ply slip is by looking at it from a geometrical point of view where it is assumed that the matrix layers are infinitely thin and frictionless, and where the fibre layers are inextensible yet flexible as has been done by Robroek et al. [10]. Important findings are repeated here as they can be of great value for the thesis.

A picture of this geometrical model is shown where a flat laminate has been bent with one side fixed and the other side free, see Figure 30.

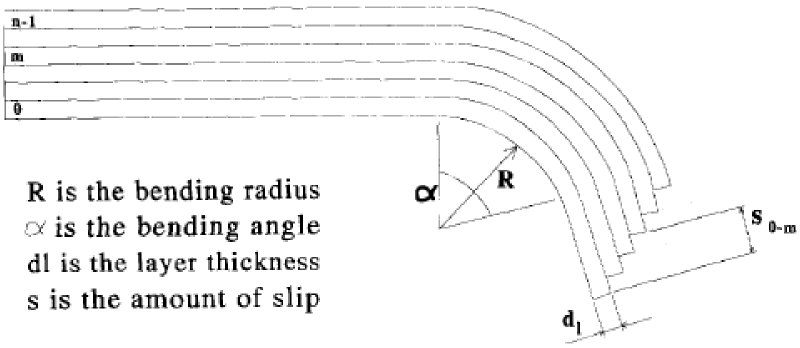

Figure 30: inter-ply slip in a single bend laminate [10]

It now is straightforward to define the slip as a function of the other geometric parameters.

$$S_{0-m} = \alpha \cdot \left(R + m \cdot d_l\right) - \alpha \cdot R = m \cdot \alpha \cdot d_l \qquad \text{Eq. 7}$$

This formula can be easily extended to one that involves more bends. See Figure 31.

$$S_{total} = \sum S_{i,0-m} = m \cdot d_l \cdot \sum \alpha_i \qquad \text{Eq. 8}$$

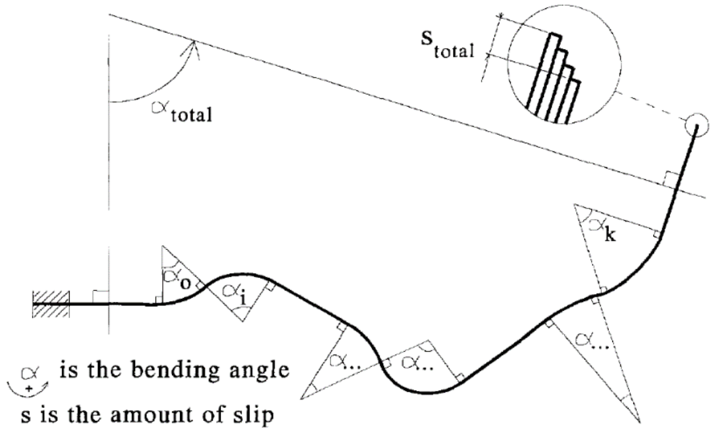

Figure 31: Inter-ply slip in a laminate with multiple bends [10]

From this result Robroek et al. concluded two things.

- If the sum of the angles is the same for two differently formed laminates, they have identical amounts of inter-ply slip deformation.
- The slip rate is directly proportional to the rate of change of the sum of the angles.

Based on these geometrical observations and that it can be shown that the forces needed to form a laminate are mostly dependent on the relative velocity between two layers, Robroek et al. [10] observed that for this case it holds that:

- The forces necessary for inter-ply slip do not depend on the final shape of the product, rather on the geometrical route of the laminate during forming.

Note that this result is of specific interest for starting plane considerations for the reconfigurable mould.

2.5.3.2 Intra-ply shear

Intra-ply shear is the in-plane shearing of a ply. It can give rise to the so-called trellis effect, see Figure 26.

<u>Geometrical considerations</u>

From a geometrical point of view (Robroek et al. [10]) a fabric reinforcement will experience a change in the crossover angle. This shearing is also known as the trellis effect, see Figure 26. The change in crossover angle will influence the overall dimensions of a piece of fabric. See, Figure 32.

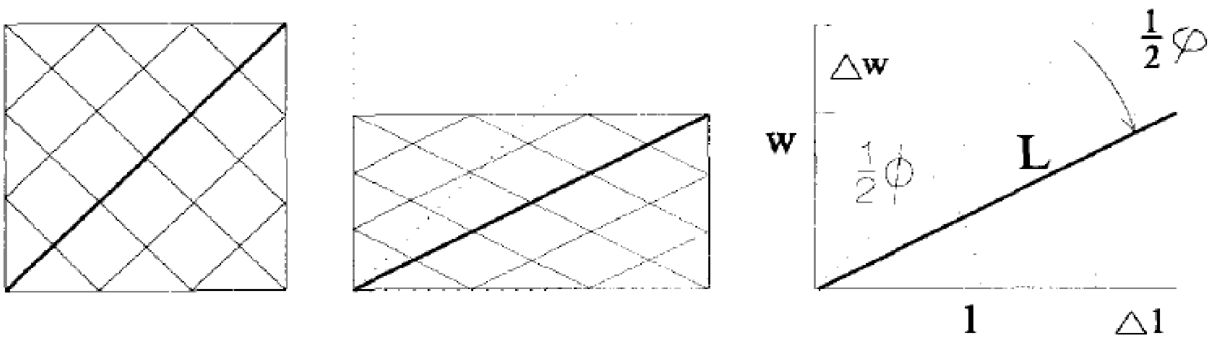

Figure 32: Shearing of a fabric [10]

The width and length of the fabric will change. The lengthening of the fabric length is given by.

$$\Delta l = L\left(\cos\left(\phi/2 - \varphi/2\right) - \cos\left(\phi/2\right)\right) \qquad \text{Eq. 9}$$

The shortening of the fabric width is given by.

$$\Delta w = L\left(\sin\left(\phi/2\right) - \sin\left(\phi/2 - \varphi/2\right)\right) \qquad \text{Eq. 10}$$

For a fabric where the original crossover angle is 90 [deg] it can be shown that.

$$\cos\left(\varphi/2\right) < 1 \quad \Rightarrow \quad \left(1-\cos\left(\varphi/2\right)\right) > \left(-1+\cos\left(\varphi/2\right)\right) \quad \Rightarrow \quad \Delta w > \Delta l \qquad \text{Eq. 11}$$

Where it becomes evident that the absolute decrease of the width dimension (perpendicular to the tensile force) is larger than the absolute increase of the length dimension (in the direction of the tensile force).
Intra-ply shear also influences the thickness of a laminate. The laminate is assumed to be incompressible due to the presence of the matrix, and therefore the volume is considered a constant. With the help of this information Robroek et al. [10] showed that the local change of thickness of a laminate which is sheared can be determined with.

$$\Delta t = t \cdot \frac{\left(1-\cos\varphi\right)}{\cos\varphi} \qquad \text{Eq. 12}$$

By combining the formula for the change of thickness with a software tool such as DRAPE [11], one can now determine the thickness of a laminate locally.

2.5.4 Findings

- Many deformation mechanisms exist. The two main deformation modes are considered to be inter-ply slip and intra-ply shear.
- Restricting deformation modes is a cause for unwanted deformations during forming
- The fabric is ultimately the limiting factor in composite sheet forming as it imposes kinematic constraints
- With the geometrical model of inter-ply slip for a 2-D laminate it was shown that the forces necessary for inter-ply slip do not depend on the final shape of the product, rather on the geometrical route of the laminate during forming.

2.6 Modelling of deformation

2.6.1 Introduction

Modelling of deformation behaviour can help to increase the understanding of the underlying mechanisms involved in composite sheet forming. This chapter will go into more detail concerning the modelling of inter-ply slip, intra-ply shear, and laminate wrinkling.

2.6.2 Modelling inter-ply slip [10]

As shown in earlier, a geometrical point of view helps to visualize the kinematics of a laminate as inter-ply slip occurs. However, that approach gives insufficient information for the understanding of the forces that occur internally during this deformation mode. For that reason, the matrix rich layers can no longer be assumed to be infinitely thin and frictionless. Several models which include both the fibre rich layer and the matrix layer have been devised, namely:

- The linear viscoelastic ply-slip deformation model of Tam [16, 17].
- The yield shear stress and friction model of Scherer et al [18].
- The linear elastic ply-slip deformation model of Talbott and Miller [19].

Some considerations to take into account in relation to the linear viscoelastic ply-slip deformation model of Tam:

Tam's model assumes that the fibre rich layers behave in a linearly elastic way, therefore also assuming Hooke's law to be applicable. The matrix rich layer is assumed to act as a Newtonian fluid. It is important to note that the assumed Newtonian behaviour might not be justified at too high forming speeds, since most fluids are non-Newtonian, i.e., viscosity depends on the shear rate. Therefore, the results of experiments could show a completely different result from the one predicted by this model, see Figure 33.

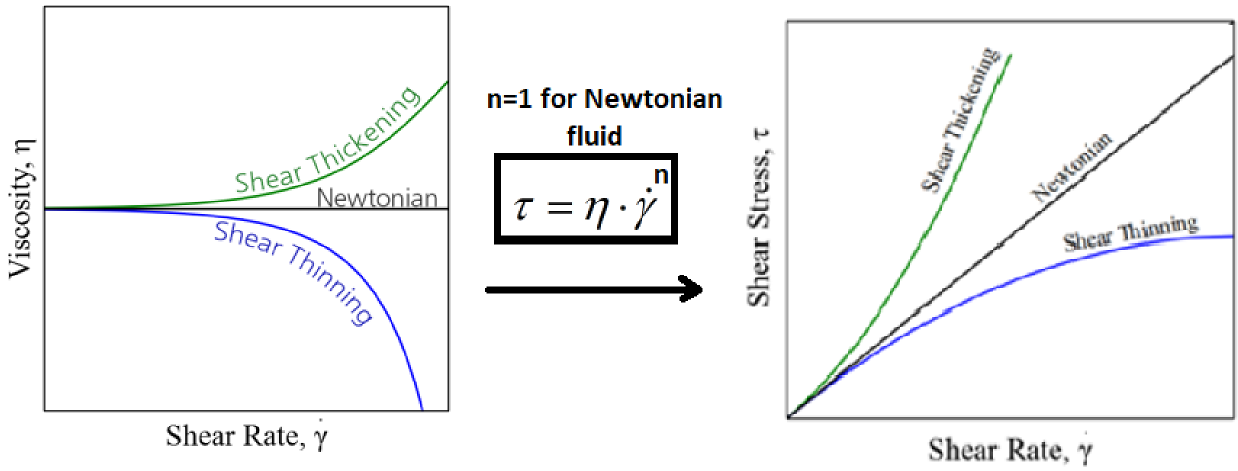

Figure 33: Influence of Newtonian and non-Newtonian behaviour on the viscosity and shear stress

Robroek et al. [10] for example, showed that the viscosity behaviour PEI follows a power-law. Epoxy resins also behave in a non-Newtonian way. Despite this shortcoming of the model, it is still very useful in the understanding of inter-ply slip behaviour.

Some considerations to take into account in relation to the yield shear stress and friction model of Scherer et al.:

This model lacked a proper description of the viscous drag, since an attempt was made to represent it with a friction coefficient which does not take into account the slip velocity. At a later stage, this model was improved upon by using a power-law to describe this behaviour. Also, insufficient experimental results were provided to support this model.

Some considerations to take into account in relation to the linear elastic ply-slip deformation model of Talbott and Miller:

As opposed to Tam's model, Talbott and Miller make use of a Hookian relation for the prediction of shear deformations and internal stresses. According to Robroek et al. [10] this model is considered not accurate enough for the prediction of internal stresses. The linear elastic model however, is considered to be useful to get an indication of changes of the internal stresses relative to each other, as a result of externally applied forming forces.

Modified interply slip model [10]

Robroek et al. made improvements on the previous models and performed several constant velocity inter-ply slip experiments on thermoplastic laminates that have shown that rheological considerations alone are not enough to cover inter-ply slip modelling as a yield stress has also been observed Figure 34. An overview of the models discussed in this section are shown in Table 4.

Table 4: Overview of the discussed interply slip deformation models [10]

Overview of the described interply slip deformation models.				
model	interply slip description			
	fabric behaviour	matrix behaviour	fabric surface	interply slip result
Tam	lineair elastic	newtonian flow	smooth	shear flow
Talbott	lineair elastic	fully elastic	smooth	elastic shear deformation
Scherer	lineair elastic	fully elastic/ powerlaw	smooth	yield stress governed by matrix, followed by shear flow
Robroek	in-extensible	powerlaw flow	rough	yield stress governed by matrix and fabric, followed by shear

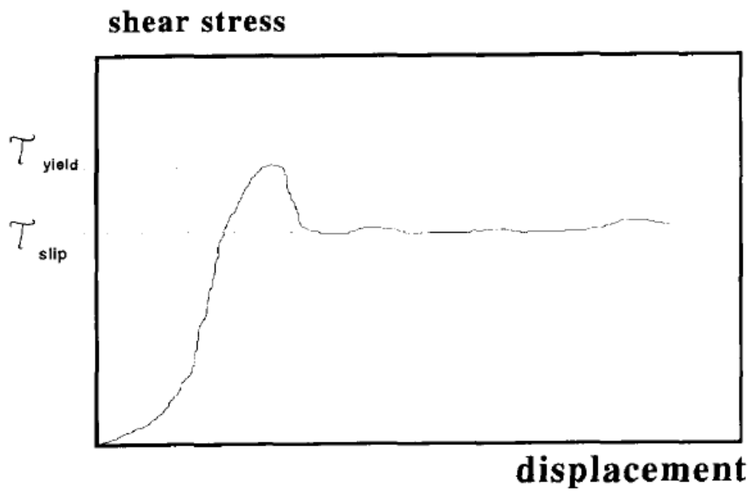

Figure 34: interpretation of Robroek et al inter-ply slip experiments [10]

2.6.3 Modelling intra-ply shear

Robroek et al. [10] gave a review on theory of intra-ply shearing forces, and performed experiments to verify these theories. This has given relevant insights into the prediction of shearing capability of a fabric:

- During shearing of a fabric, the crossover angle decreases and the effectiveness of the applied force which causes this deformation becomes less. This is thought to be caused by not only the change in crossover angle, but also due to the tension that builds up in the fibre which causes compressive forces at the crossover points to increase.
- A lower degree of interlacing causes a lower compression force at the crossover points. At the same time, the lower amount of crossover points will further decrease the force required to shear the fabric.
- A high-density fabric requires relatively high forces for shearing due to a large crossover surface. When shearing such a fabric, the forces needed quickly rise because this further increases the fabric density.
- In general, the intra-ply shearing of a fabric is positively influenced by the thermoplastic matrix

2.6.4 Modelling of laminate wrinkling [6]

When forming single or double curved parts, failure modes such as, in-plane buckling, out-of-plane buckling, tow splitting, and laminate wrinkling may occur. Laminate wrinkling which involves all the layers of the laminate is considered to be the dominating failure mode in the production of double curved parts. Therefore, this section will devote itself to the modelling of this phenomena.

A model for laminate wrinkling needs to have good:

- Constitutive relations of the materials which are deformed (laminate, diaphragm, etc.)
- Failure criterion

This starts with making some assumptions for the behaviour of the laminate. For pure shear, the laminate can be modelled to be anisotropic and viscous [20]. Together with a viscous stability failure criterion this has shown reasonable results [21, 22]. More complex deformations show more of a viscoelastic behaviour, and the laminate will need to be modelled with different assumptions. An example where the shear of a laminate is modelled to be viscous and the failure criterion is based on an elastic behaviour is shown in [source]. Every specific case will need to be considered individually and with care, as the outcome of the model is only as good as its assumptions. An example of how the diaphragm stiffness can be taken into account is shown in [6]. A general overview of the steps taken in a laminate wrinkling model are shown in Figure 35.

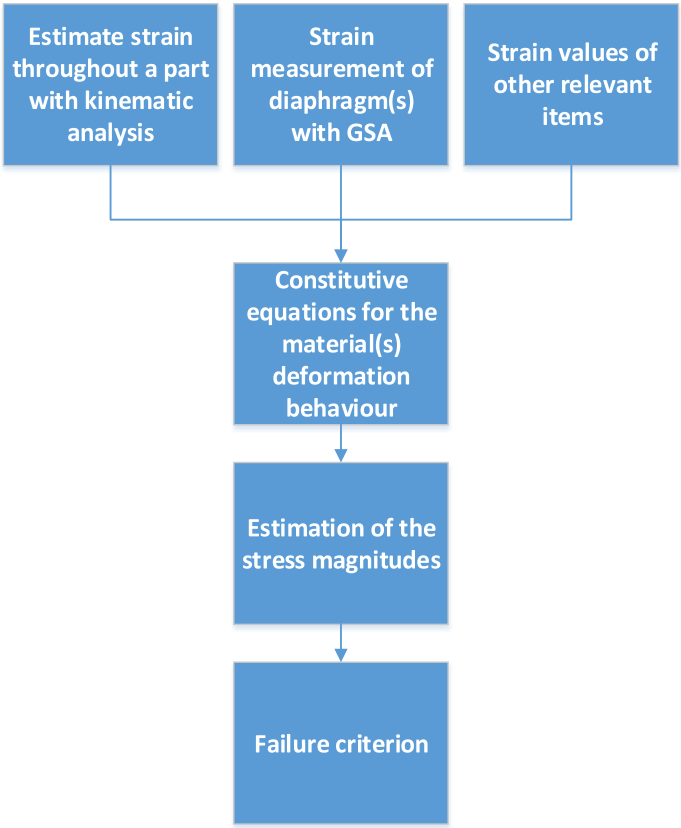

Figure 35: General overview of a laminate wrinkling model

2.6.5 Findings

Modelling and verification of laminate deformation modes can give good insight into the forming behaviour of laminates. One needs to be aware that the outcome of the model is only as good as its assumptions. The findings in this section are mostly based on thermoplastic laminate modelling and testing. Note that the current research considers thermoset laminates only. Thermoset laminates are formed at different temperatures and pressures and have much lower viscosities. Therefore, the results in this section are considered to give a general indication of the deformation mechanism that have been modelled/investigated.

3 Methods and Materials

3.1 Hypotheses

The previous chapter has reviewed key topics w.r.t. the aim of the current research, as stated in the introduction of this thesis. This enables the formulation of some hypotheses which help to better understand the possible influence of diaphragm reinforcement, infusion pressure, and forming speed on the underlying forming mechanisms of single curved resin infused panels on a concave reconfigured tool surface. The hypotheses to be tested are formulated:

1. A reinforcement reduces out-of-plane wrinkles by constraining out-of-plain displacement and therefore promoting the slipping of layers
2. A reduction in pressure reduces out-of-plane wrinkles by lowering the friction between layers and therefore promoting the slipping of layers
3. A reduction in forming speed reduces out-of-plane wrinkles by lowering the friction between layers and therefore promoting the slipping of layers

The theoretical basis for hypothesis 1 is: A reinforcement on top of a forming package introduces an extra layer with a flexural stiffness that will oppose out-of-plane displacement. As the layers are unable to form out-of-plane wrinkles, the deformation will manifest itself in a different form. For example: slipping of layers, in-plane fibre buckling, a thicker fibre bundle, spring back, or a combination. The theoretical basis for hypothesis 2 is: A reduction in pressure will lower the mechanical friction as neighbouring layers of the package are not so much pressed against each other. The theoretical basis for hypothesis 3 is: A reduction in forming speed is equivalent to a reduction in shear rate. The rheological behaviour of either shear thickening, Newtonian, or shear thinning fluids is such that shear stress decrease as shear rate is decreased.

3.2 Approach

The methods described in this section are necessary to evaluate the hypotheses stated in section 3.1. A series of forming experiments is conducted as described in section 3.4. Those tests will form single curved resin infused sandwich panels where the tooling surface is reconfigured to a concave shape. This will be done under different diaphragm reinforcements, infusion pressures, and forming speeds. Post processing of the formed samples is needed to collect displacement data and geometrical data.

<u>Displacement data</u> is collected as relative movement (or slipping) of sample layers w.r.t. each other. The composite sandwich to be formed consists of a core sheet and two facings. The facings consist out of woven glass fabric sheets. The fabric layers are adjusted by inserting black threads in the fabric. The idea is to capture the positions of those threads before and after forming. A measure for displacement will be the difference between the before and after positions of those threads. The positions before forming are captured by taking pictures of individual layers as they are stacked. After the forming experiment the facings of the panel become transparent, except for the black threads. Direct measurements are performed to determine the positions of threads after forming. Displacement data can be measured by inserting threads at multiple locations along the length of the panel. Section 3.5.2 shows in detail how displacement data is collected.

<u>Geometrical data</u> will also be collected. Each sample will be analysed for its wrinkles, if any. The location and geometry of each wrinkle will be recorded. The location of the wrinkles will be determined by mapping the wrinkles in relation to the panel as a whole. The geometry of the wrinkles will be determined by cutting up the panels such that the wrinkles can be inspected under magnification with the use of a microscope. Overall panel geometry will be characterised by the radius of curvature and thickness distribution. More details about geometrical data collection is provided in section 3.5.3.

The results of these tests and a geometrical model of slip (as described in section 3.3) will be analysed in chapter 4. This approach should provide the insight needed to test the hypotheses. Section 4.3 will review the hypotheses.

3.3 Geometrical model for slip

This section will derive a model for the forming experiments as performed during this research. The goal is to obtain a model that represents the theoretically desired deformation. Theoretically desired means forming of a high-quality panel without any unwanted deformation, i.e. only desired deformation. Desired deformation for single curved panels is considered to be inter-ply slipping only. The result would be a panel without unwanted deformation or residual stresses. The displacement data from the forming experiments can be compared to this model.

The starting point in this derivation is the 2d geometrical model of slip [10] for a laminate which is bent while it is fixed on one end and free on the other end, Figure 30. The geometrical model assumes that:

1. The laminate stack is composed out of reinforcement layers with matrix layers in between
2. The laminate stack is in a flat configuration before forming
3. The length and thickness of the reinforcement layers is constant and identical
4. The matrix layers are infinitely thin
5. The friction between the reinforcement layers is zero
6. During forming the reinforcement layers do not separate

The forming experiments in the current research form initially flat laminates into single curved panels. It is assumed that the geometrical model can be applied by recognizing that the laminate layers are fixed at the line of symmetry and free at the ends of the panel, Figure 36. Only having to solve for half the panel to find the absolute values for the entire panel.

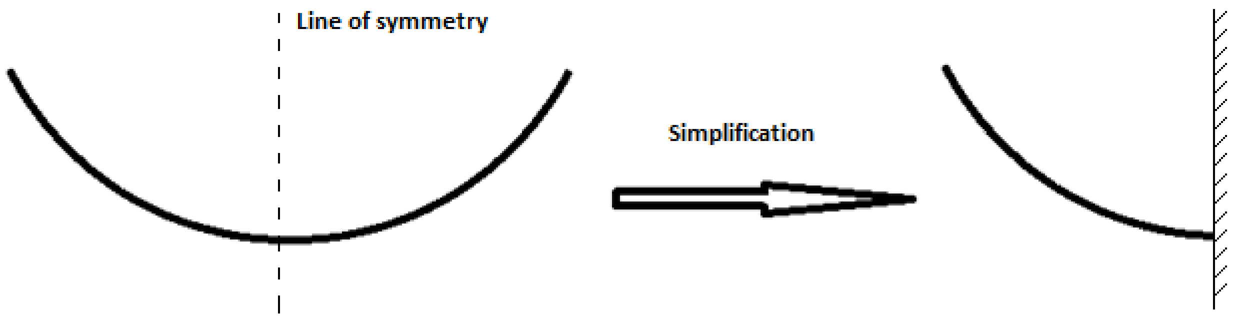

Figure 36: Simplification of the forming geometry as layers do not move at the line of symmetry

The current research uses a sandwich panel. The stacking sequence for the model of the sandwich panels is simplified to 3 layers, i.e. two facings and a core. The results for displacement data in section 4.1 show that the layers of the facings exhibit very little slip w.r.t. each other and they act as one layer, i.e. facing. The thickness of the core usually is much thicker compared to the individual layers of the facing, as this gives a sandwich its high bending stiffness to weight ratio. For that reason, assumption 3 does not hold and requires that Eq. 7 would need to be modified to accommodate for this simplification. Resulting in Figure 37 and Eq. 13.

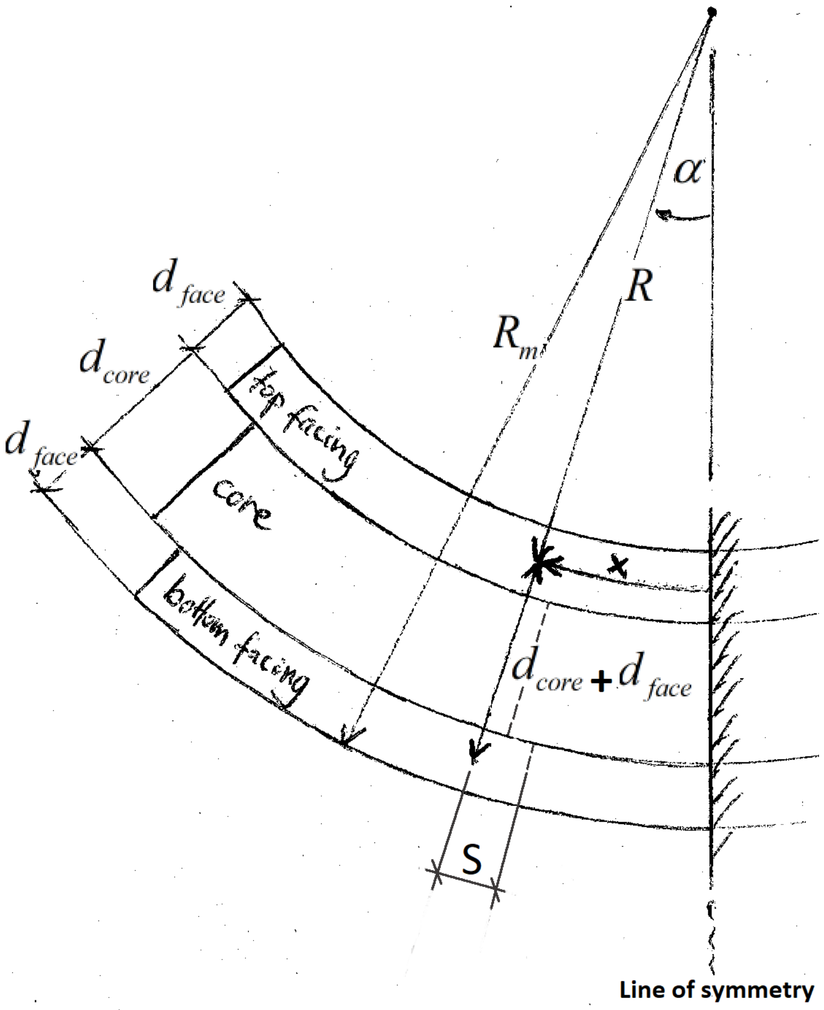

Figure 37: Definition of geometrical parameters of the modified geometrical slip model

$$S = \alpha \cdot \left(d_{core} + d_{face}\right) \qquad \text{Eq. 13}$$

Where S is the amount of slip in [mm] for a given angle α in [radians], core thickness d_{core} in [mm], and facing thickness d_{face} in [mm]. The angle α can be expressed in terms of top facing centreline radius R in [mm] and travelled distance along the top facing centreline from the centre x in [mm]. This results in:

$$S = \left(\frac{x}{R}\right) \cdot \left(d_{core} + d_{face}\right) \qquad \text{Eq. 14}$$

R as defined in Figure 37 can be expressed in terms of the radius of the tool surface R_m in [mm] and d_{core} and d_{face}.

$$R = R_m - d_{core} - \frac{3}{2} d_{face} \qquad \text{Eq. 15}$$

Substituting Eq. 15 in to Eq. 14 results in:

$$S = \left(\frac{x}{R_m - d_{core} - \frac{3}{2} d_{face}} \right) \cdot \left(d_{core} + d_{face} \right)$$ Eq. 16

Reordering leads to:

$$S = x \cdot \left(\frac{d_{core} + d_{face}}{R_m - d_{core} - \frac{3}{2} d_{face}} \right)$$ Eq. 17

The slip between the facings S has now been modelled in terms of the distance along the top facing centreline from the centre of the panel x, tool surface radius R_m, core thickness d_{core}, and facing thickness d_{face}. The sign convention for x for the entire sandwich panel is shown in, Figure 38.

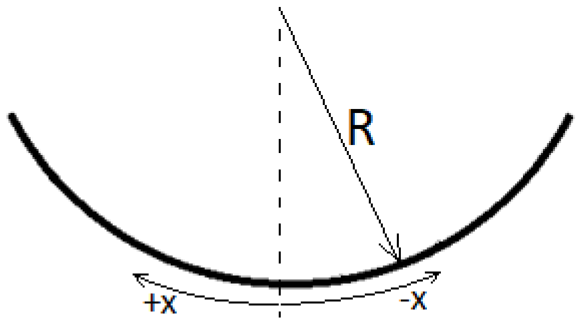

Figure 38: Sign convention for x

This model illustrates the following behaviour:

- For a given sandwich panel and radius of the tool surface, the slip between two facings is directly proportional to the distance from the centre of the panel. The theoretical slip is 0 at the centre and increases linearly to a maximum value at the edge of the panel
- For a given sandwich panel and panel location, the slip between two facings is inversely proportional to the radius of curvature of the panel. The theoretical slip will therefore be 0 throughout the panel when it is in its undeformed configuration since R is infinite. The amount slip will increase as the radius decreases.
- For a given radius of the tool surface and panel location, the slip between two facings increases as the core and facing thickness are increased.

To determine the total amount of theoretically desired slip one simply needs to add the maximum values for slip at the edges of the panel, i.e.:

$$S_{TOT} = 2 \cdot S_{\max}$$ Eq. 18

Where $S_{\max}$ is the slip maximum slip as defined by Eq. 17. This maximum slip occurs at the edge of the panel for $x = x_{\max}$.

3.4 Forming experiments

3.4.1 Tests performed

In total, 7 tests are performed. Each test forms a resin infused sandwich panel from a flat position into a single curved shape. This forming is enforced by reconfiguring the tool surface in a concave configuration. Tool surface radius is set to 40 cm, which is the smallest radius possible on the reconfigurable mould at Curve Works. The tests will be performed under different *speeds*, *pressures*, and *reinforcements*. It should be noted that tests 1 and 2 have a different type of woven glass fabric used in the faces of the test sample compared to tests 3, 4, 5, 6, and 7, see section 3.4.3. Full forming speed means that the actuators move at 5mm/s, translating to a forming time of approximately 3 minutes. Slow forming speed resulted in approximately 10 minutes forming speed. The tests performed and their testing conditions are shown in Table 5.

Table 5: Performed forming experiments and their testing conditions

Tests #	Pressure [mbar]	Speed	Reinforcement	Facing Material Type
Test 1	500	Full	No	1
Test 2	500	Full	Yes	1
Test 3	200	Full	No	2
Test 4	500	Full	No	2
Test 5	200	Low	No	2
Test 6	500	Low	No	2
Test 7	200	Low	Yes	2

3.4.2 Test setup

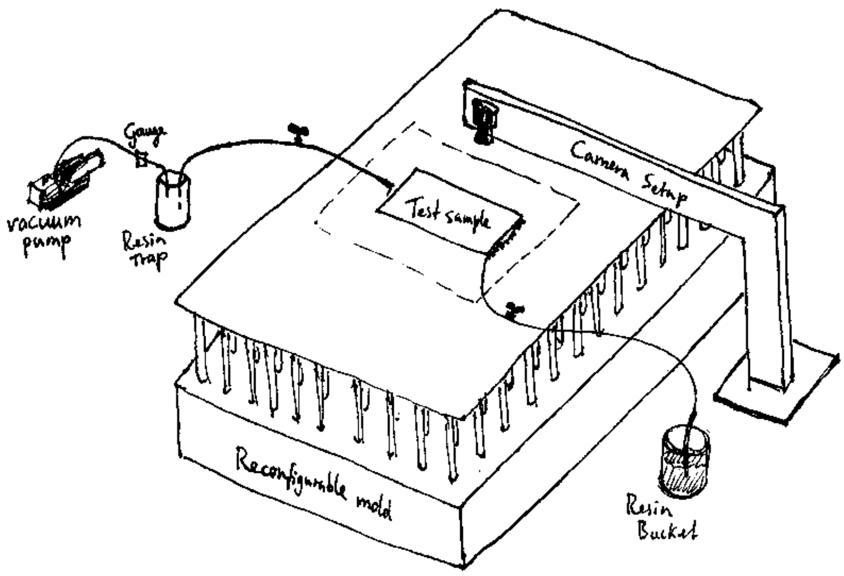

Figure 39: Test setup used for all tests in the current research. It consists of the reconfigurable mould, camera setup, vacuum infusion system, and the test sample.

A schematic representation of the test setup is shown in Figure 39. The main elements are:

- ***Reconfigurable mould setup:*** consisting of the reconfigurable mould as reviewed in section 2.1 and a control panel.
- ***Camera setup:*** consisting of a camera and a stand.
- ***Vacuum infusion setup:*** consisting of a resin bucket, resin trap, and a vacuum pump.
- ***Test Sample:*** Elaborated upon in the following section 3.4.3

3.4.3 Test samples

Each sample is a dry stack, consisting of 30 x 70 cm sheets made from:

- Woven fabric 0/90 and +45/-45 (glass)
    - **Type 1** for tests 1 and 2: Plain weave, approximately 700 g/m^2, initial thickness approximately 0.8mm
    - **Type 2** for tests 3, 4, 5, 6, and 7: Plain weave, 580 g/m^2, initial thickness approximately 0.8mm
- Foam core (6 mm thickness, Lantor Soric® XF)

The stacking sequence is depicted in Figure 40.

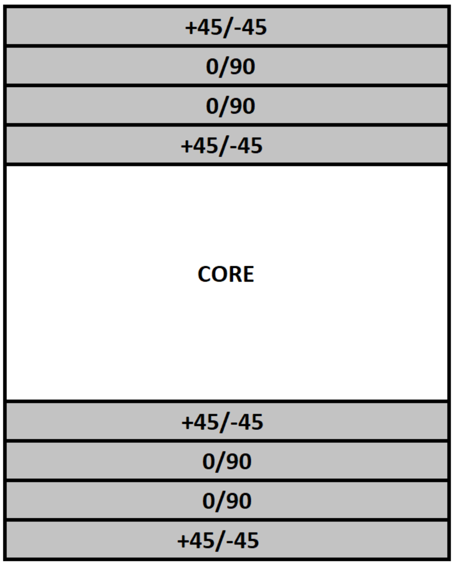

Figure 40: Sample stacking sequence

Both the woven fabric and core layers are cut to size with the help of a template. Note that woven glass fabric layers have been initially cut to a larger size than 30 x 70 cm, allowing for masking tape to be put around the edges. Masking tape serves to protect the edges of the fabric layers such that the material does not fall apart when handled. In this case the fabric of material 1 and 2 was relatively coarse, and yarns at the edges would slide and fall off.

Figure 41: Intermediate result of a test sample

To enable the measurement of slip, threads are inserted. The process of inserting threads in fabric layers is shown in Figure 42. Note that the thread is not inserted directly into the yarns of the fabric, but in between the open spaces. This should help to minimize the interference of inter-ply slip and make for easy insertion.

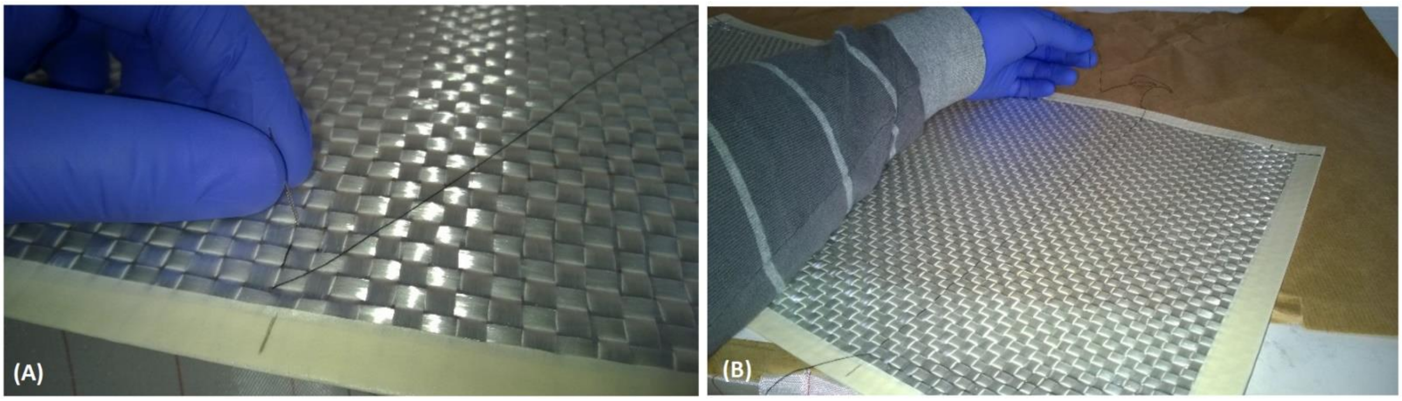

Figure 42: (A) Close up of thread in fabric, (B) thread fully pulled through fabric

The finished patterns are shown in Figure 43. For 0/90 layers the pattern consists of 6 equally spaced and parallel threads, with a spacing of 10 cm +- yarn width. For +-45 the threads form a checkerboard pattern.

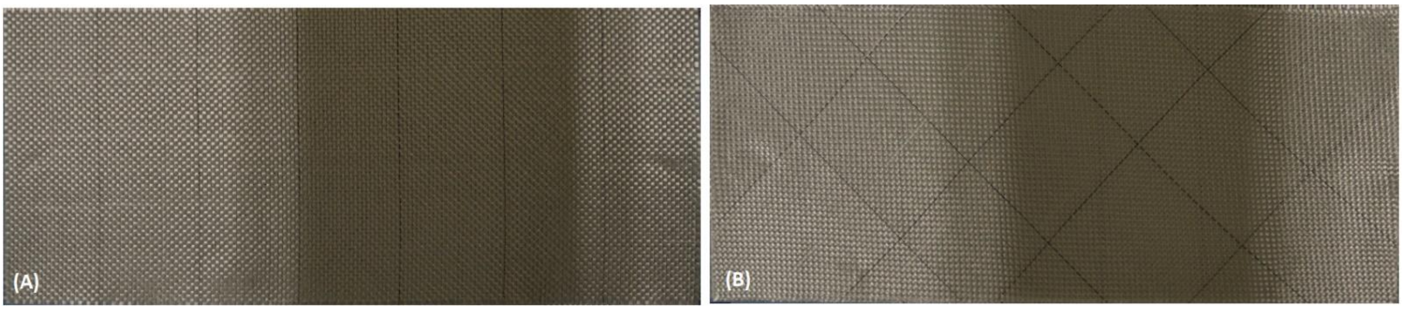

Figure 43: (A) Thread pattern in a 0/90 layer, (B) Thread pattern in a +45/-45 layer

3.4.4 Forming experiment

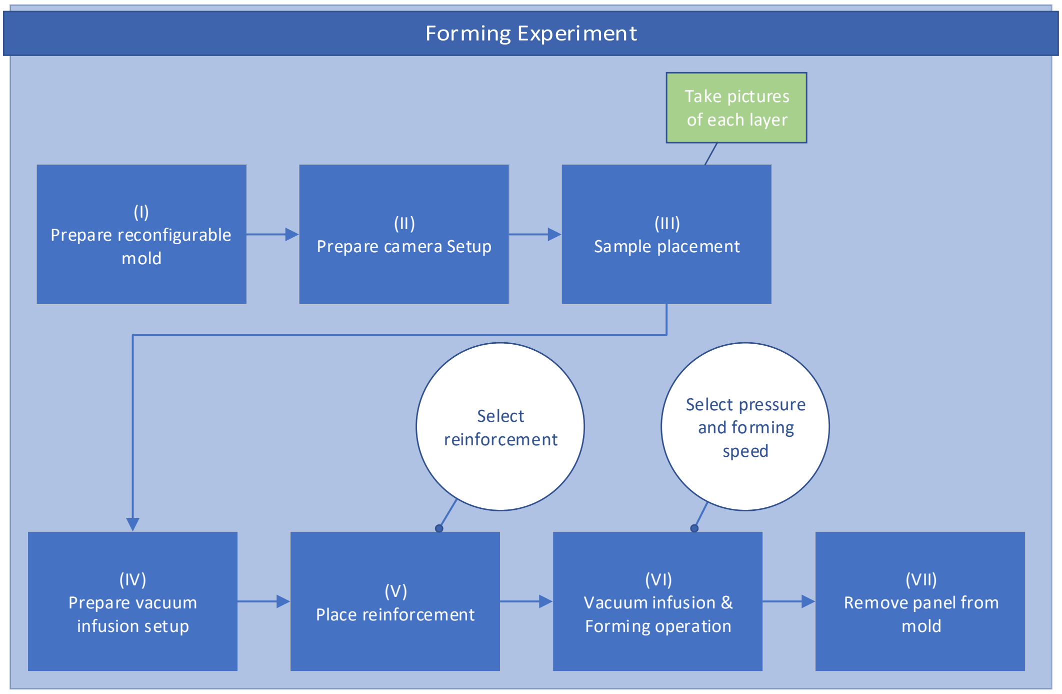

Figure 44: Flow diagram, depicting the steps needed to prepare and execute a forming experiment.

An overview of the steps taken for a forming experiment are shown in the flow diagram, Figure 44.

(I) ***Prepare reconfigurable mould:*** Prepare the reconfigurable mould by calibrating it and setting it in home position, i.e., flat configuration of mould surface. The silicone rubber surface of the mould is cleaned with denatured alcohol. A foil is placed on top and fixed in place with tacky tape and a vacuum connection, see Figure 45.

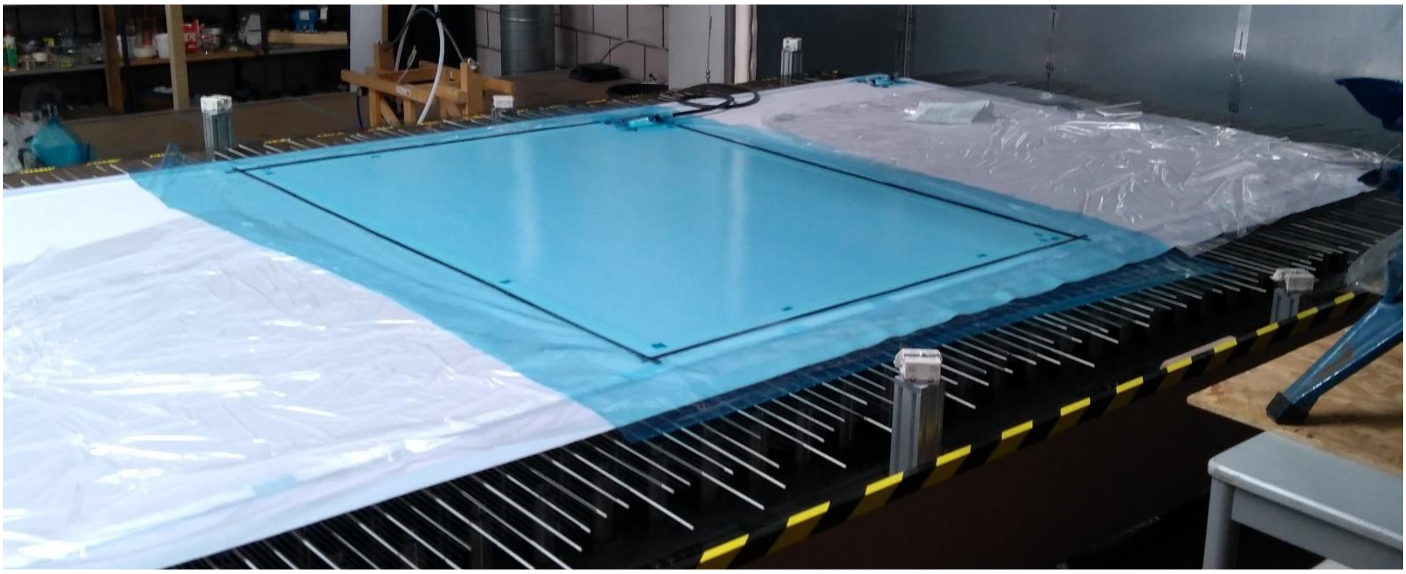

Figure 45: Prepared reconfigurable mould

(II) ***Prepare camera setup:*** The position of the camera setup is determined by the location of the sample. The location of the sample is determined by projecting a reference axis at the center of the panel with a laser projector, see Figure 46.

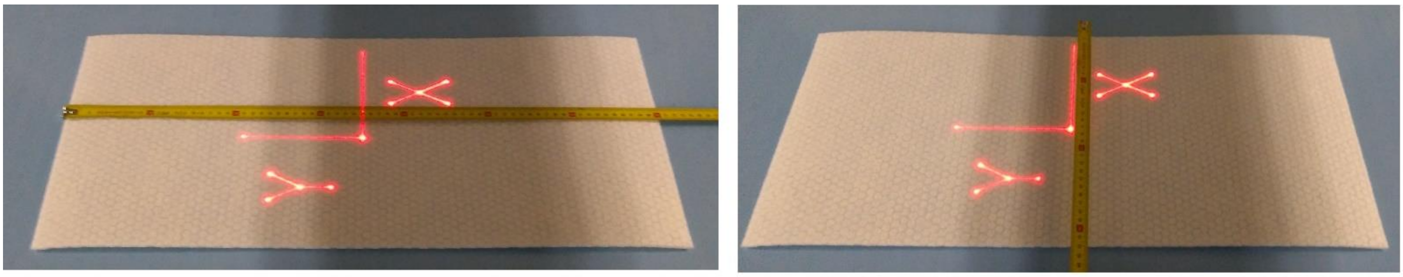

Figure 46: Centering of template (in this case a core sheet of 30x70cm) on top of the prepared tool surface

The centred template is used to mark the foil, see Figure 47.

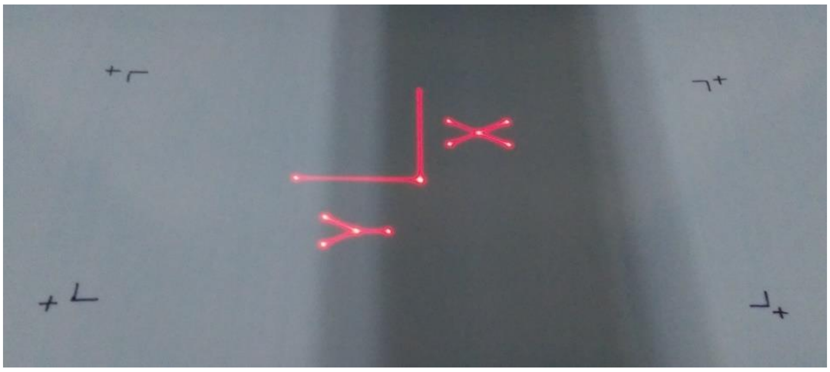

Figure 47: Centred foil markings. The corner pieces provide guidance for the placement of sample layers, and + markings are used for picture alignment.

Position the camera setup such that it is centred above the mould and adjust the zoom and focus so that the sample's layers are fully visible when placed. The view of the camera should extend a little outside the markings to also capture rulers. The intermediate result is seen in Figure 48.

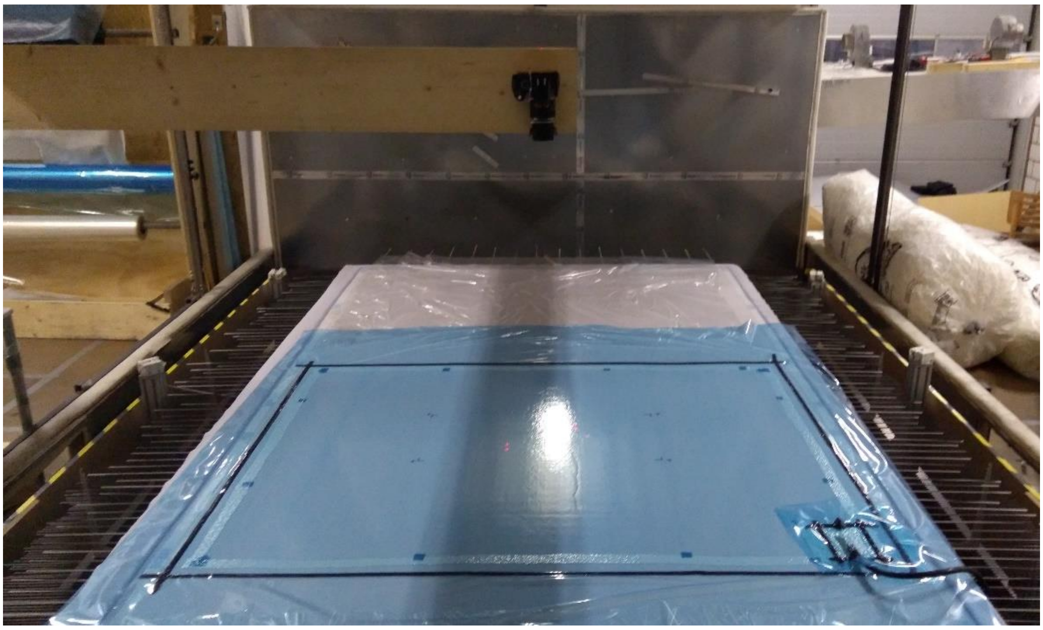

Figure 48: Prepared tool surface and camera setup

(III) *Sample placement:* The sample is put down layer by layer in the stacking sequence shown earlier (Figure 40). Fabric layers are cut one last time before they are stacked to remove the protective tape. The fabric and core layers are placed within the markings of the bottom foil. A picture is taken each time a fabric layer is put in place, see Figure 49. Special care must be taken not to move the layers underneath, as this would ruin thread location measurements.

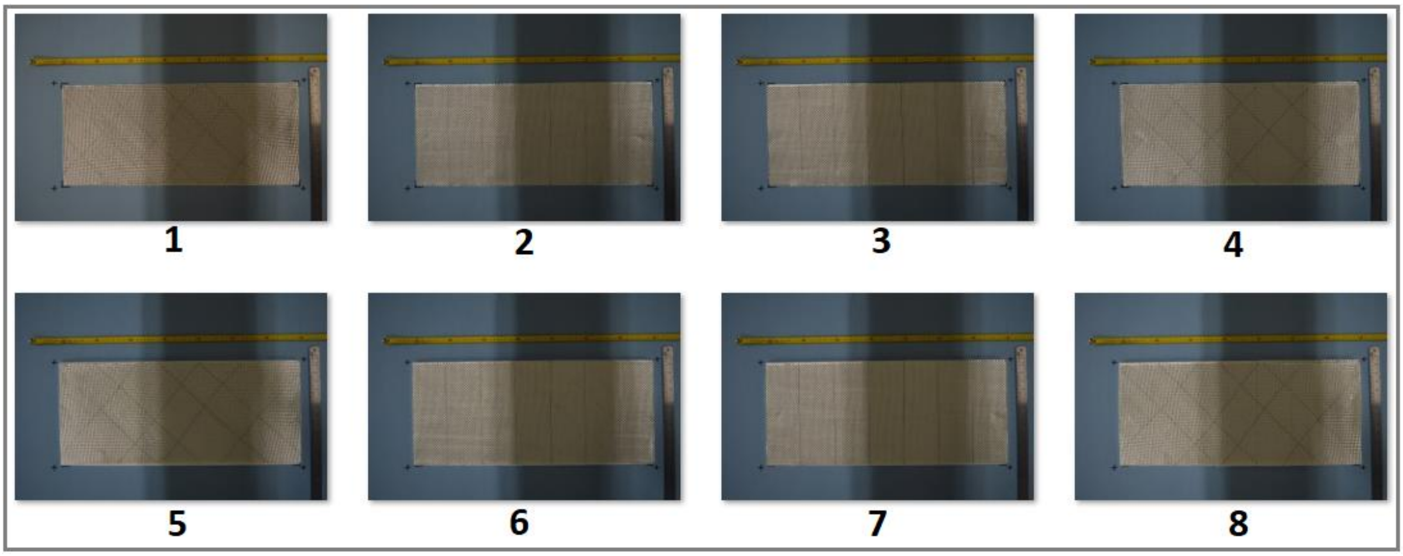

Figure 49: Pictures taken during sample placement. The numbers indicate layer position. Number 1 is the first layer to be placed on top of the tool surface, number 2 is stacked on top, etc.

(IV) Prepare v*acuum infusion setup:* The vacuum infusion setup will require consumables to be placed around the sample stack. The bottom foil is already in place. What remains are the inlet, outlet, and top foil. The top foil is put down first, together with a weight to keep the stack in place. Once all is in place, the top and bottom foil are connected with tacky tape around the edges. See Figure 50 for the intermediate result. The final step is to connect the outlet to the resin trap and vacuum pump.

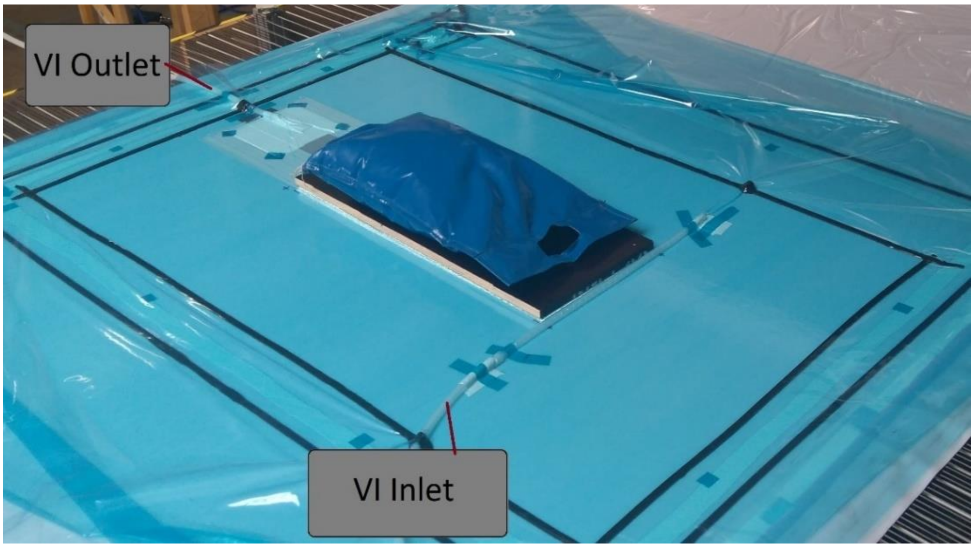

Figure 50: Intermediate result showing the vacuum infusion setup is ready

(V) Place reinforcement: As tests are either reinforced or unreinforced, two types of forming packages exist, see Figure 51. In case of an unreinforced test package step (V) can be skipped. In case of a reinforced tests package, a reinforcement is put on top of the result from step (IV) and it is kept in place with an extra diaphragm/foil under vacuum.

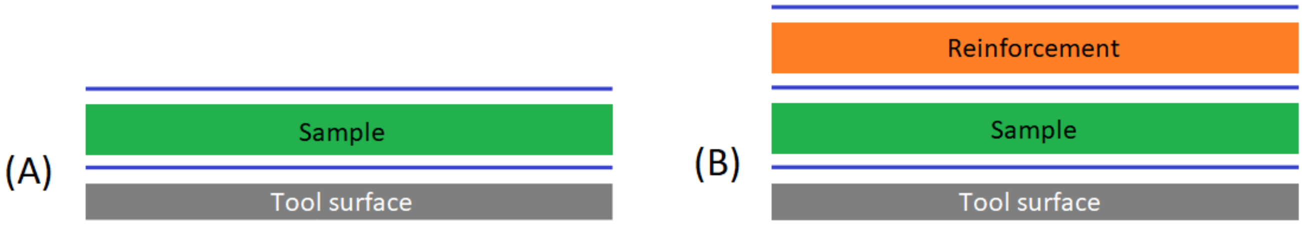

Figure 51: (A) *Unreinforced test package* on top of tool surface. The test package consists of a sample (section 3.4.3) between two diaphragms. Diaphragms are indicated in blue, (B) *Reinforced test package* on top of tool surface. The test package consists of a sample (section 3.4.3) between two diaphragms with an additional reinforcement on top, kept in place with an extra diaphragm. Diaphragms are indicated in blue.

Tests 2 and 7 have a reinforcement added. The reinforcement is cut to the same dimensions as the test sample layers (30 x 70 cm). It is put on the top of the foil. The reinforcement is kept in place putting another foil over it and creating a vacuum. Test 2 has an extra layer of 6mm thick Lantor Soric® XF core material as a reinforcement. Test 7 has an extra layer of approximately 6 mm thick silicone rubber + 6mm thick Lantor Soric® XF core material as a reinforcement, see Figure 52.

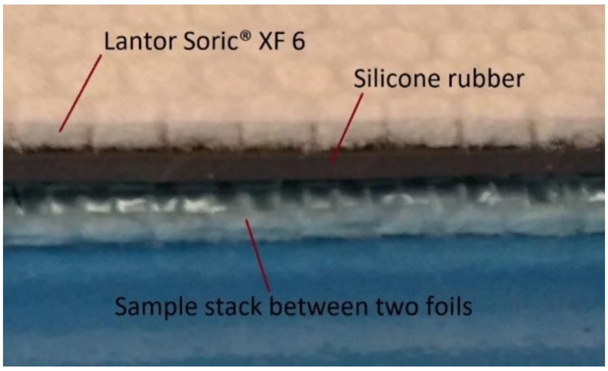

Figure 52: Reinforcements

(VI) Vacuum infusion & Forming operation: The test setup is fully prepared and ready to have the sample infused with resin, followed by the forming operation. This is considered as one step since the resin will cure and is time dependent, i.e., the forming needs to happen before the resin starts to harden. In this step, both pressure and forming speed are set. The resin initiator data sheet in appendix C shows that the gel time is approximately 25 min. After forming, the reconfigurable mould will stay in the final configuration until the polyester is cured. Figure 53 shows a panel after the forming operation.

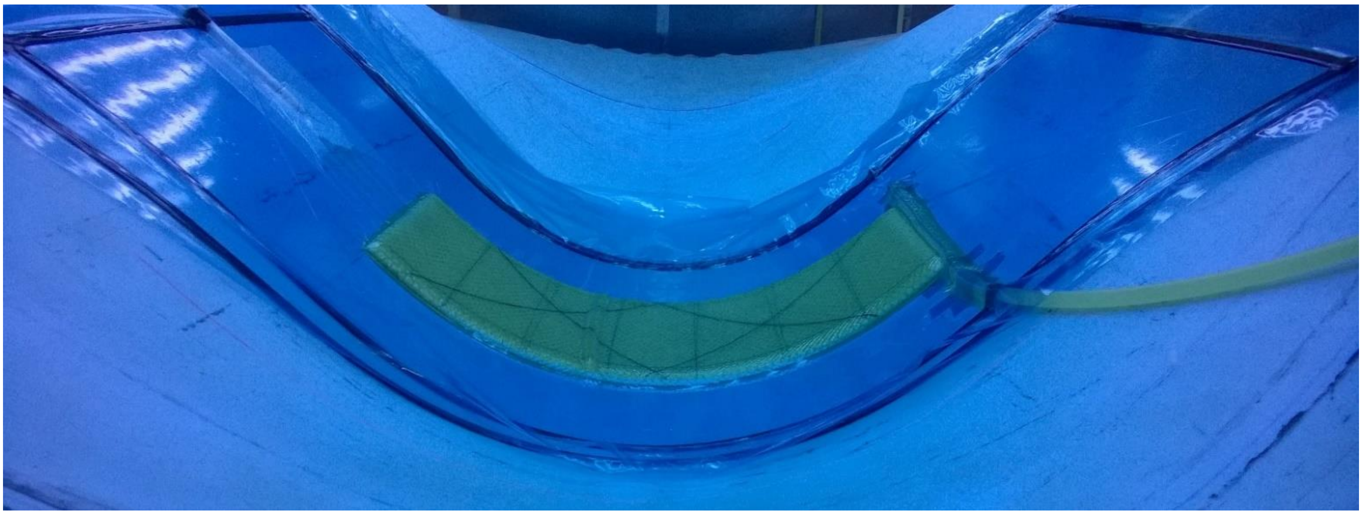

Figure 53: A formed sample in its final shape, left to cure on top of the reconfigurable mould.

(VII) *Remove panel from the mould:* It takes around 2 hours for the polyester to cure. After curing, the panel is removed from the mould by turning off the vacuum pumps and releasing the bottom foil from the tool surface. The sample is stored to post cure at room temperature. Finally, reconfigure the mould to its flat position and turn it off.

3.5 Post Processing and Data Collection

3.5.1 Cutting

Formed panels are cut such that displacement data and geometrical data can be collected. For each panel two cuts are made along the length, see Figure 54.

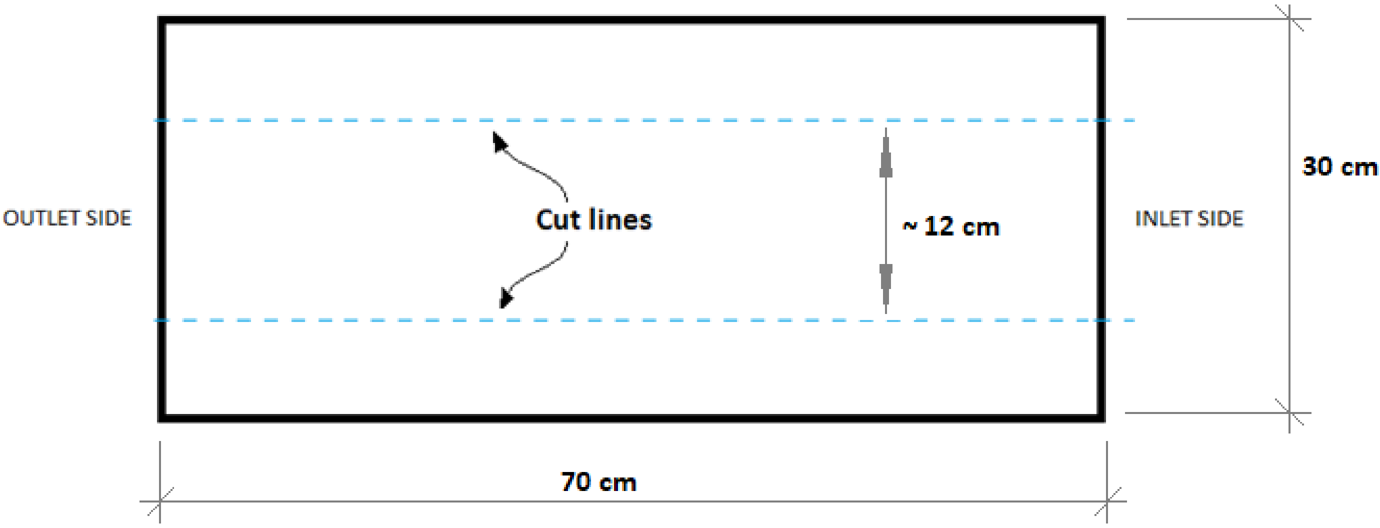

Figure 54: Cut line locations indicated from a top view perspective.

Cutting was performed with the help of a large cutting apparatus suitable for the cutting of glass fiber reinforced composites at the faculty of Aerospace engineering in Delft. This proved difficult because of the size and curvature of the sample. The process of cutting the panels is show in Figure 55.

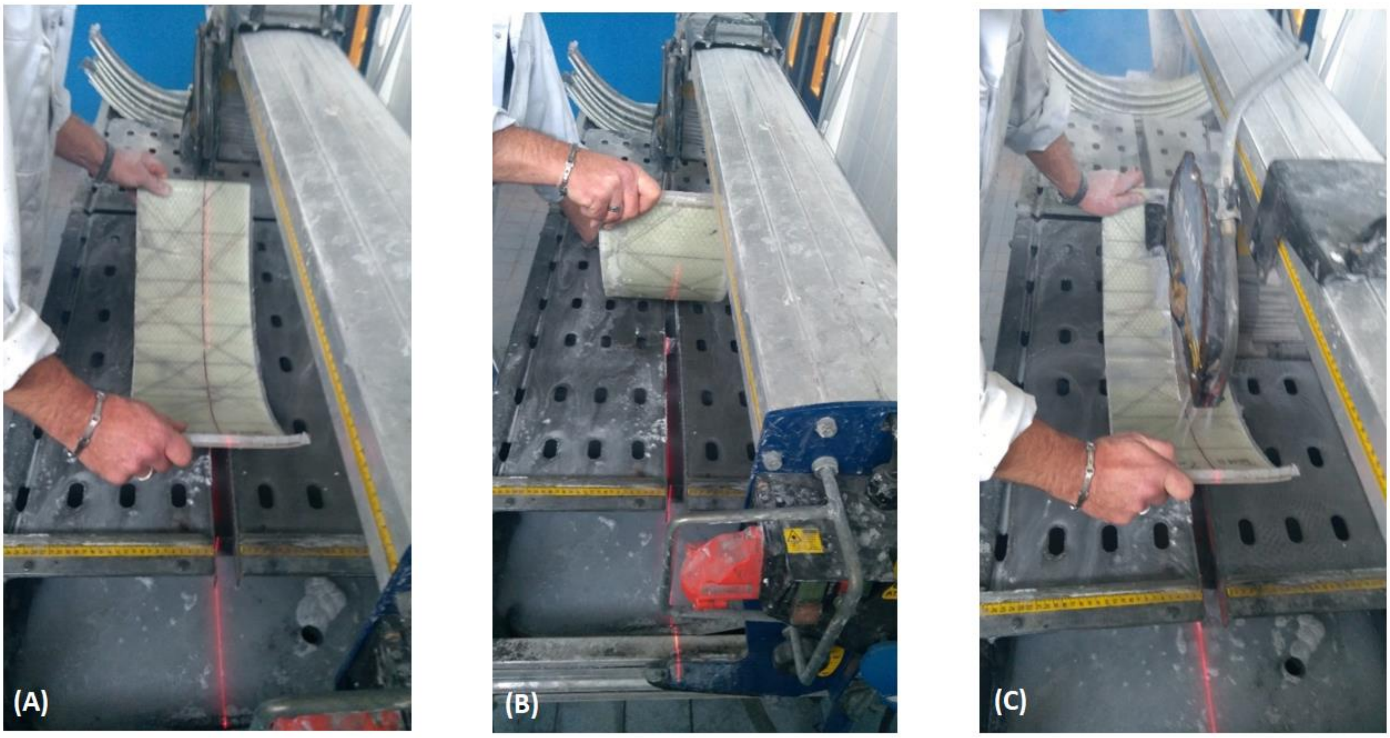

Figure 55: (A) align marked cut line with laser projector, (B) Set panel in starting position for cutting, (C) Rotate panel as sawing blade cuts through to allow for a full cut

3.5.2 Collecting Displacement data

As mentioned before, threads have been inserted into the fabric layers to enable measurement of displacement. *Pictures* taken during the forming experiments have captured the thread positions before forming, see section 3.4.4. Thread positions after forming are captured by *directly measuring* the formed samples.

Measurement locations and sign convention

Displacement data is extracted from the movement of threads of 0/90 layers. Threads in 0/90 layers are spaced 10 cm apart, see section 3.4.3. The measurement locations are shown in Figure 56.

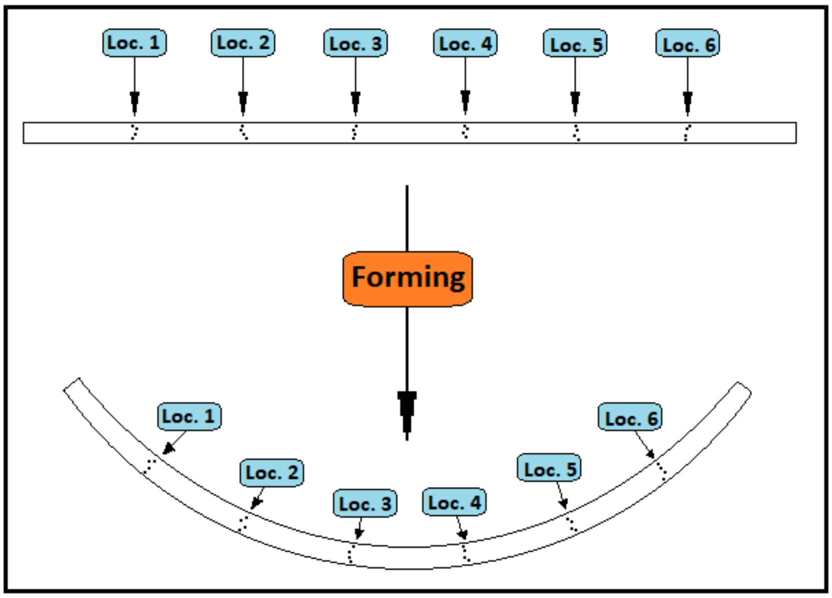

Figure 56: Measurement locations before and after forming.

A local coordinate system is used at each measurement location, see Figure 57.

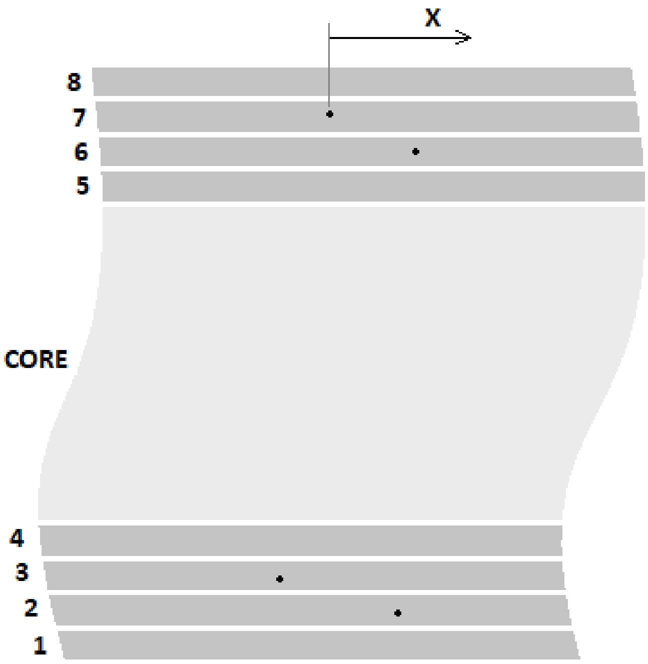

Figure 57: Local coordinate system at a measurement location. The thread at layer 7 is located at X=0 per default.

(Before forming) Thread locations:

The thread locations are extracted from the pictures taken during the forming experiment (Figure 49). In total there are 8 pictures, each picture represents one of the glass fabric layers.

The pictures are geometrically distorted by optical distortion. Optical distortion is a lens error and can be corrected with the use of a geometric distortion profile for that specific lens. For this research a Nikon D3200 camera in combination with a Nikon DX VR AF-S NIKKOR 18-55 1:2.5-5.6 G II lens was used. According to the lens profile, the lens caused a maximum 0.5%-barrel distortion for a focal length of 25mm, as was used for all pictures. In this case the camera was used to correct for this distortion with a built-in tool.

Further processing of the pictures is needed to determine the relative locations of the threads. Image processing software allows to digitally stack pictures. The pictures are centred with the help of the markings on the foil, see Figure 58.

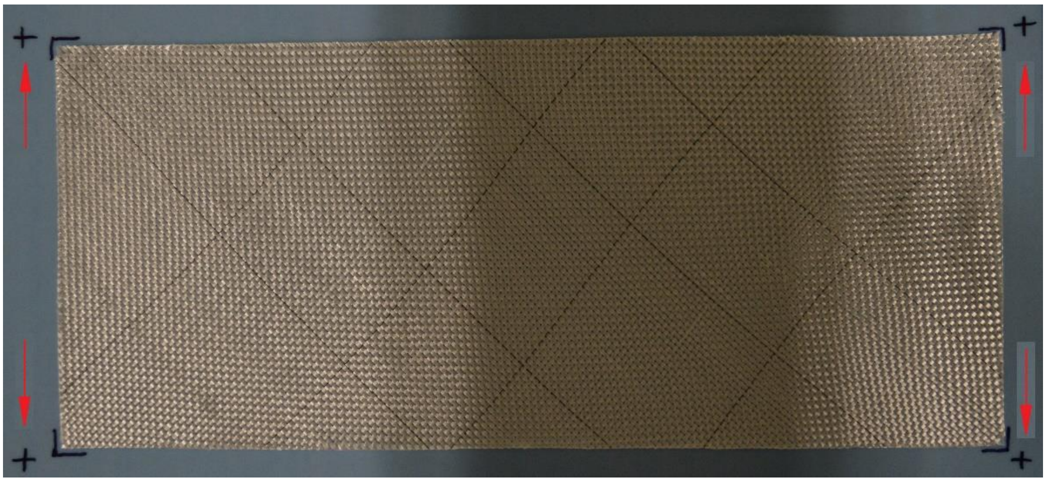

Figure 58: + marks on the foil for alignment of pictures.

For each of the pictures a transparent layer is created on which the threads are traced, see Figure 59.

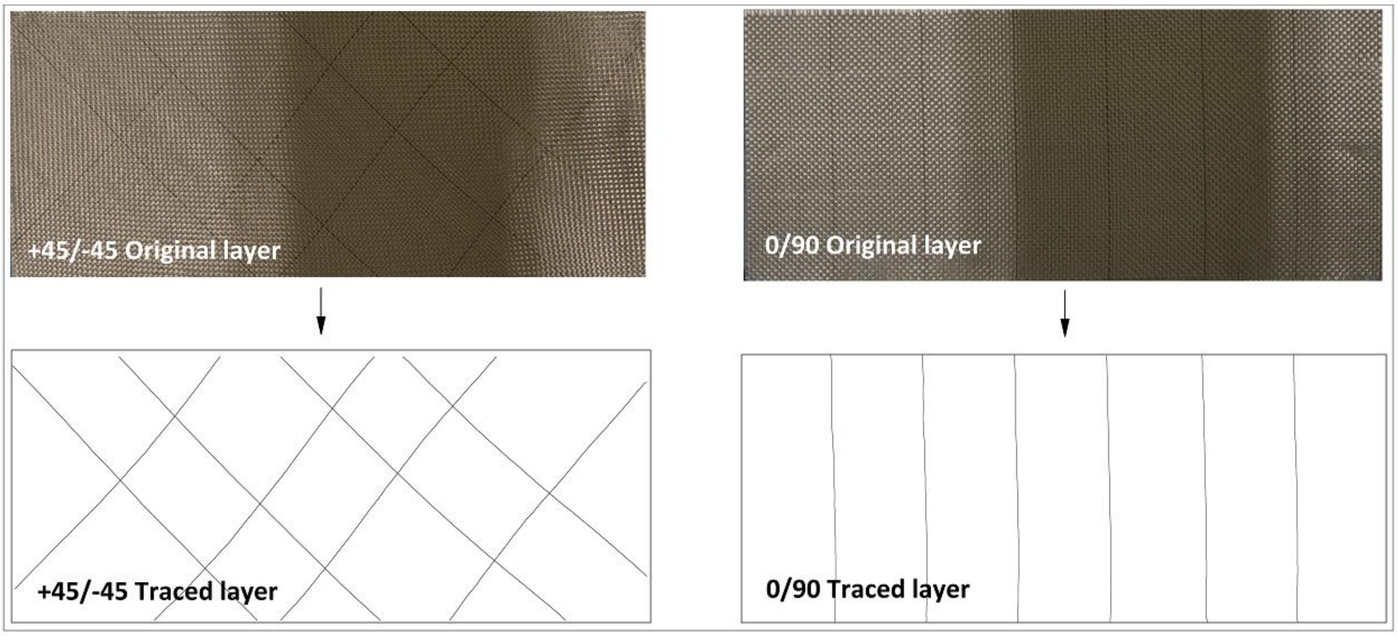

Figure 59: The results obtained from tracing a +45/-45, and 0/90 layer

These new layers form a new stack, containing aligned layers with thread locations only. Now it is possible to select multiple layers and see them all at the same time, allowing for easy measurement of relative thread positions. The relative positions of threads in the digital stack are measured along the same line as where the formed panel is cut. A line representing the location of that cut is created and added to the digital stack. The position of the cutline is found by taking the real panel and measuring the distance between the cutline and the thread intersection on one of the +45/-45 layers, see Figure 60.

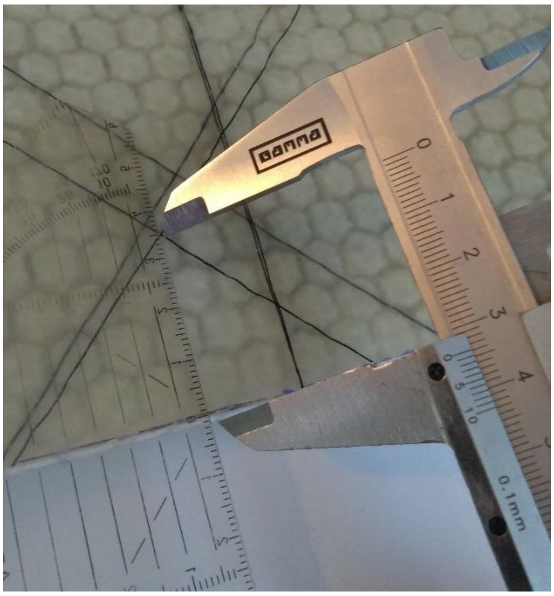

Figure 60: Measuring the distance between a top +45/-45 layer intersection and the cutline

Those measurements are used to find the cutline in the digital stack. An example of such a cutline in a digital stack is shown in Figure 61.

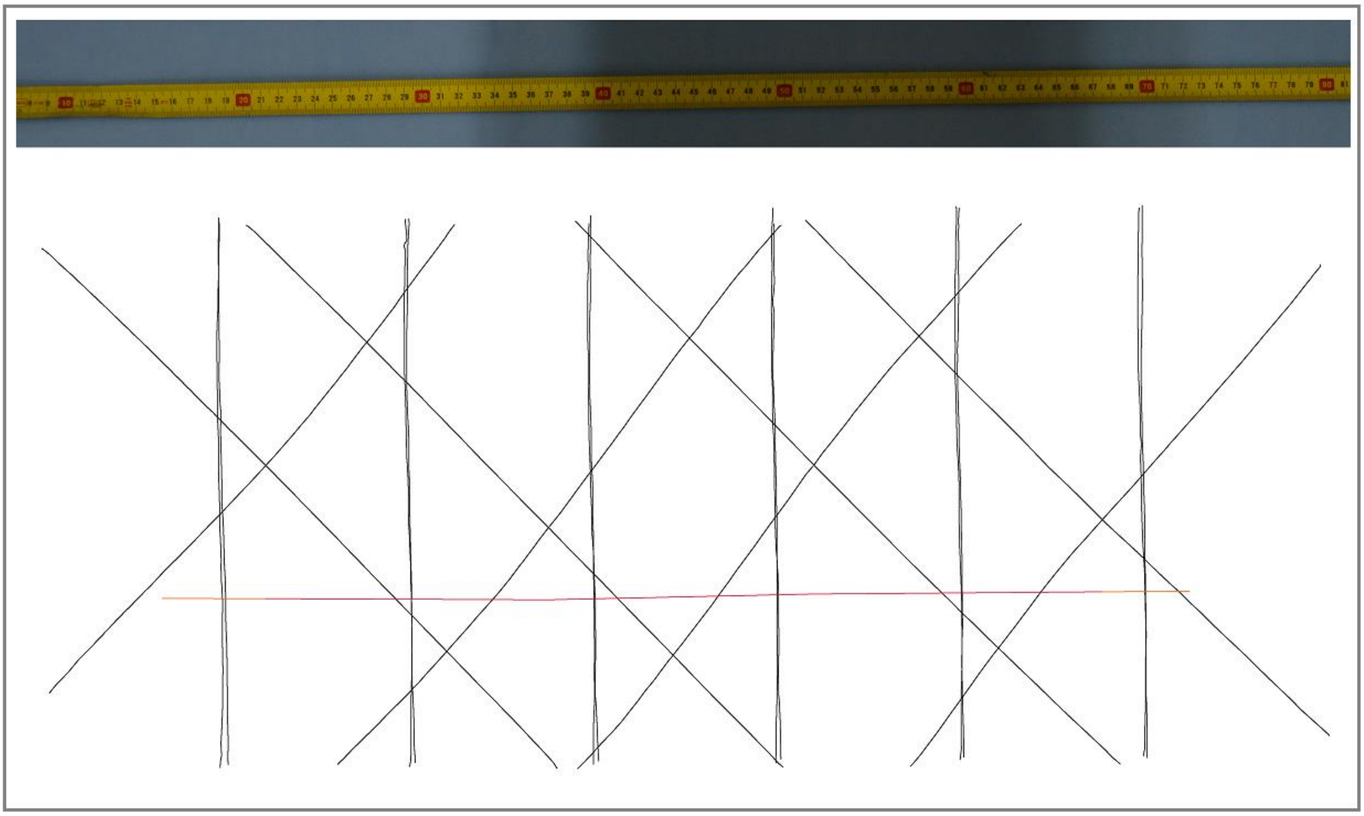

Figure 61: Digital stack of 3 traced layers, including the cutline. The cutline is the red horizontal line. On top is a ruler which will be used as a reference for measurements.

The final step is to measure the relative positions of the threads. Zoom in on the ruler (see top of Figure 61) as shown in Figure 62 (A) and use a real ruler to get scaled measurements from the screen, allowing for a higher accuracy. Figure 62 (B)

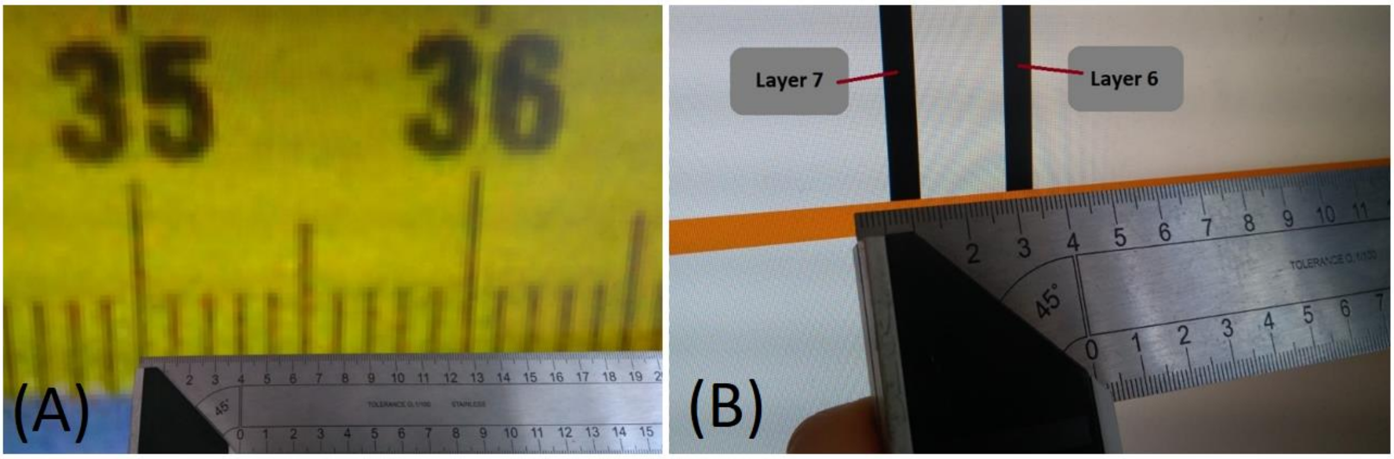

Figure 62: (A) Determine the scale for improved accuracy, (B) Measure the relative position of a thread from layer 6 w.r.t. a thread of layer 7. This measurement is performed at one of the measurement locations along the cutline.

(After forming) Thread locations:

The relative distances after forming can be measured directly at the cut line, without correcting for the curvature of the panel. This assumption is valid as the measurements are taken along no more than 1 cm arc length of the panel, with a radius of around 40 cm. Small angle approximation holds. Rendering the difference in length between the arc length and the accompanying chord length insignificant as this difference is less than the accuracy of the caliper (0.1mm).

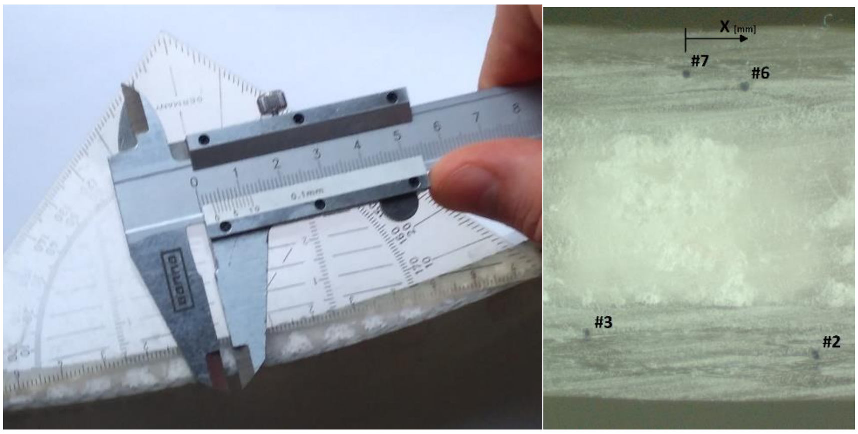

Figure 63: Direct measurement of thread positions w.r.t. thread in layer 7 at that location. A protractor is used to create the X axis, and the calliper measures the positions of the threads in layers 2, 3, and 6.

(Before, After, and Difference) Table format:

The displacement data for each panel is captured in a table. The table of test 1 is provided as an example, see Table 6.

Table 6: Displacement data test 1. Layer numbering is displayed on the left. Measurement locations are indicated in the top, as well as the before, after, and difference at those locations in [mm]. Layer 7 is used as a reference, hence 0 by default in all cases.

Test 1	@ Loc. 1			@ Loc. 2			@ Loc. 3			@ Loc. 4			@ Loc. 5			@ Loc. 6		
Layer #	B[mm]	A[mm]	Δ[mm]	B[mm]	A[mm]	Δ[mm]	B[mm]	A[mm]	Δ[mm]	B[mm]	A[mm]	Δ[mm]	B[mm]	A[mm]	Δ[mm]	B[mm]	A[mm]	Δ[mm]
7	0	0	0	0	0	0	0	0	0	0	0	0	0	0	0	0	0	0
6	2.7	1.9	-0.8	-8.5	-8.9	-0.4	1.2	0.8	-0.4	-0.8	-1.1	-0.3	-6.1	-6.2	-0.1	-2.9	-2.9	0
CORE																		
3	-2.9	-3.1	-0.2	-4.3	-5.6	-1.3	-5	-2.2	2.8	-5.2	-3.2	2	-7.1	-6.2	0.9	-8.1	-8	0.1
2	4.8	4	-0.8	-3.1	-5.2	-2.1	2.7	5	2.3	1.8	3	1.2	-6.9	-6.8	0.1	-1.6	-1.9	-0.3

This method of measuring displacement data is considered to be prone to errors as there are multiple steps involved that need full attention. In case all steps have been performed well, there still are some possible sources of error. A small mismatch in the tracing of threads digitally. This is expected not to exceed 0.3mm, as the width of a thread is less than 0.3mm. The other step where an error could originate is the direct measurement of the sample with a calliper. This is considered to be no larger than 0.2 mm (the calliper has an accuracy of 0.1mm). As the displacement data represents the difference between the before and after conditions, these two errors can add up. The maximum error is therefore approximated to be ±0.5mm.

The results are presented in section 4.1.

3.5.3 Collecting Geometrical data

Geometrical data for each of the formed samples is collected in the form of:

- Top impression and side contour
- Close-up pictures
- Radius of curvature
- Average thickness at non-wrinkled regions
- Total difference in length caused by wrinkling

Top impression and side contour

A large piece of paper is put on top of the panel. By swiftly rubbing back and forth across the surface with a marker, an impression of the top surface appears. Stick the piece of paper to a window with some adhesive tape. Use another piece of paper to trace the impression. Digitize the impression by scanning it. Finally, use image processing software to adjust the contrast.

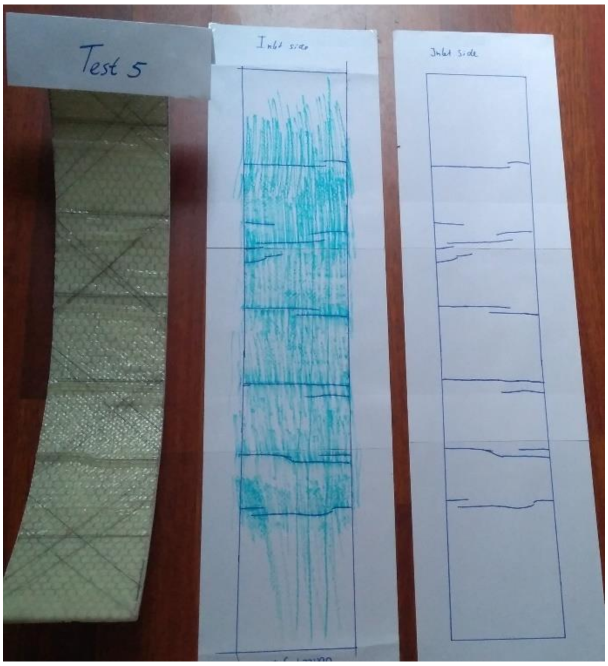

Figure 64: From left to right: Formed panel, impression, traced impression

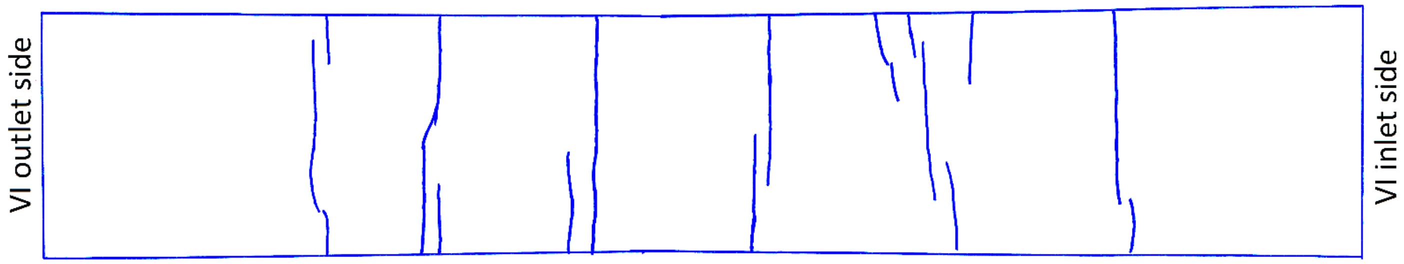

Figure 65: Final top view impression

A contour of the side view is created by laying the panel on its side and tracing the contour on a piece of paper, see Figure 66. Digitize the traced contour by scanning it. Use image processing software to flip the image and adjust the contrast, resulting in Figure 67.

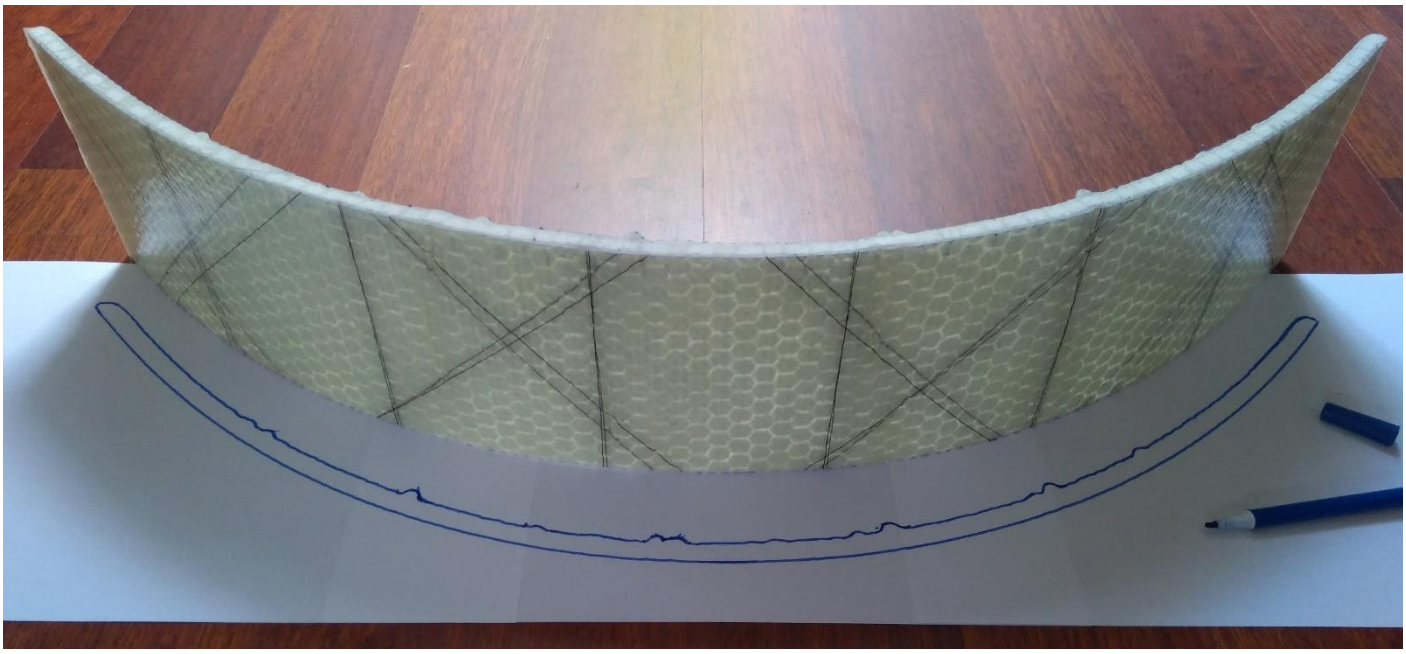

Figure 66: Traced contour of the side view

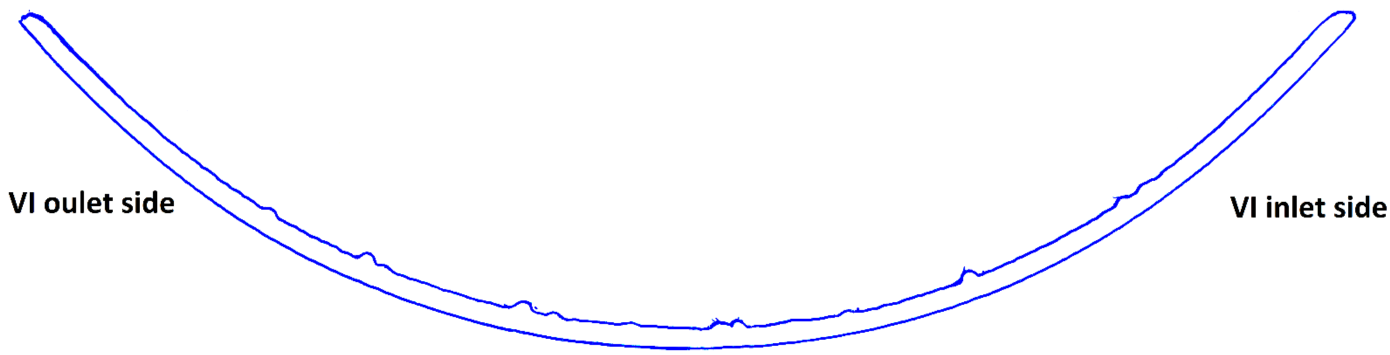

Figure 67: Final side view contour

The results are presented in section 4.1.

Close-up pictures

Close-up pictures along the cut line are taken to obtain a good view of the local geometry. The pictures are made with a “ZEISS SteREO Discovery.V8” stereomicroscope at the faculty of Aerospace Engineering in Delft, see Figure 68.

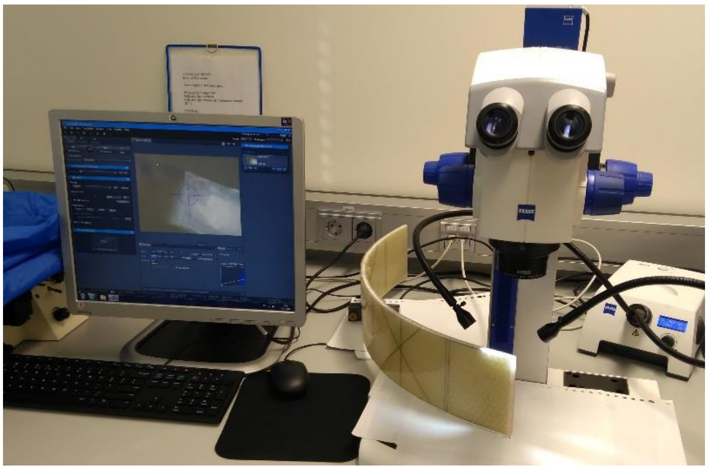

Figure 68: Taking close up pictures with the stereomicroscope

Procedure used to fully capture local geometry along the cutline:

1. Place the panel underneath the microscope and adjust the focus and illumination to obtain a clear image
2. A series of overlapping pictures is taken along the cutline.

Overlap of pictures allows for merging them with image processing software. In many cases wrinkles are not captured by a single picture, and merging is needed. An example of merging pictures to obtain the geometry of a wrinkle is shown in Figure 69.

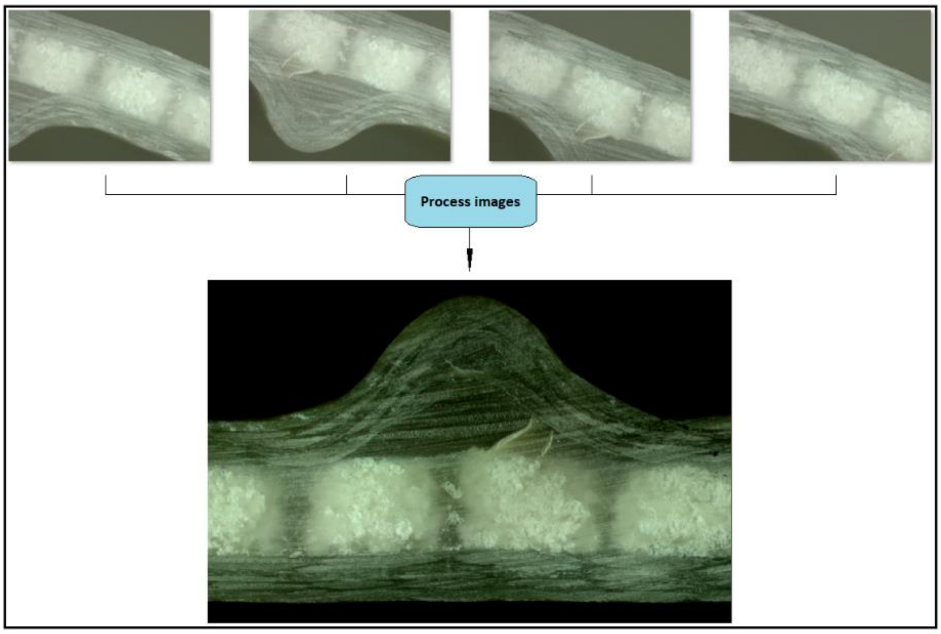

Figure 69: Close-up pictures of a panel are merged together to form a close-up wrinkle image

The results are presented in appendix A.

Radius of curvature:

The radius of curvature for the processed samples can be determined. This is done with the formula for the radius of a segment of a circle. The full derivation is provided in appendix B.

$$R = \frac{H}{2} + \frac{W^2}{8H} \qquad \text{Eq. 19}$$

The meaning of H and W is depicted in Figure 70.

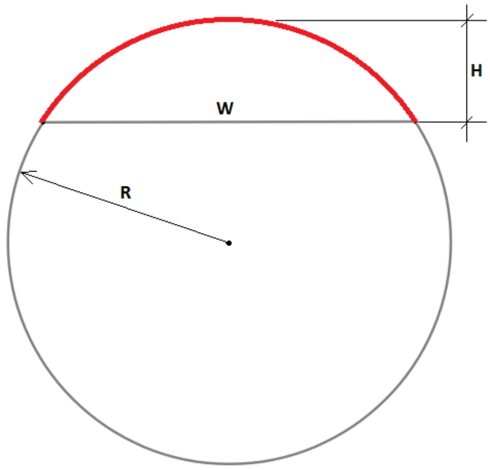

Figure 70: The red line represents the curved part of the panel looking at it from the side

To get the values for H and W all one needs to do is to place the processed specimens on a flat piece of paper and mark the line of which the radius of curvature is of interest. The side of contact with the mould surface will be used as this surface was intended to have a radius of curvature of 40cm. This side is also with very little to no wrinkling for all the panels, thus providing a smooth surface to trace the arc on a piece of paper. Now connect two points of that arc with each other and determine the maximum H with a ruler which can be held orthogonal to the chord of length W. With H and W known, R can now be computed.

The results are presented in section 4.1.

Average thickness at non-wrinkled regions:

The thickness of the panels is measured at non-wrinkled sections with a calliper at each of the 6 measurement locations. In some cases, a wrinkle is present at a measurement location and a location close to it is chosen. The average thickness is calculated and presented in section 4.1.

Difference in length of top layer, caused by wrinkling:

The two lengths defined in Figure 71 are used to determine the difference in length for wrinkle ΔW_i. The total difference in length over the top facing of a panel measured from wrinkles, is defined to be the sum the difference for each individual wrinkle:

$$\Delta W_{TOT} = \sum_{i=1}^{n} \Delta W_i = \sum_{i=1}^{n} L_{Wrinkle,i} - L_{Base,i} \qquad \text{Eq. 20}$$

Where n stands for the nth wrinkle on the top surface of a panel along the cut line.

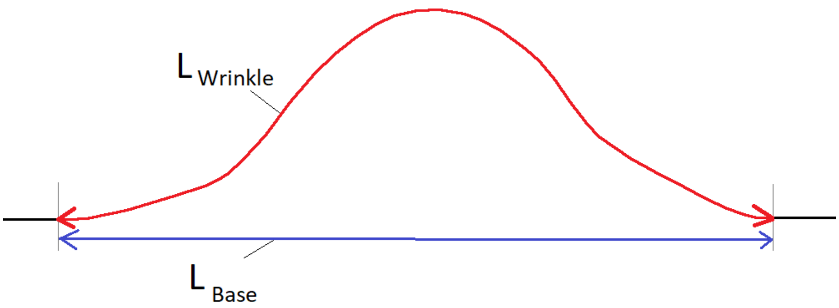

Figure 71: Definition for the lengths between two points on the top surface. $L_{Wrinkle}$ is the length along the wrinkle between two points. L_{base} is the shortest distance in between the same two points.

The results are presented in section 4.1.

4 Results and Analysis

The results of the experiments are presented in section 4.1, followed by an analysis and discussion in section 4.2. Section 4.3 will review the hypotheses as stated in section 3.1 based on the newly acquired knowledge from the analysis.

4.1 Results

Results: Side view contours

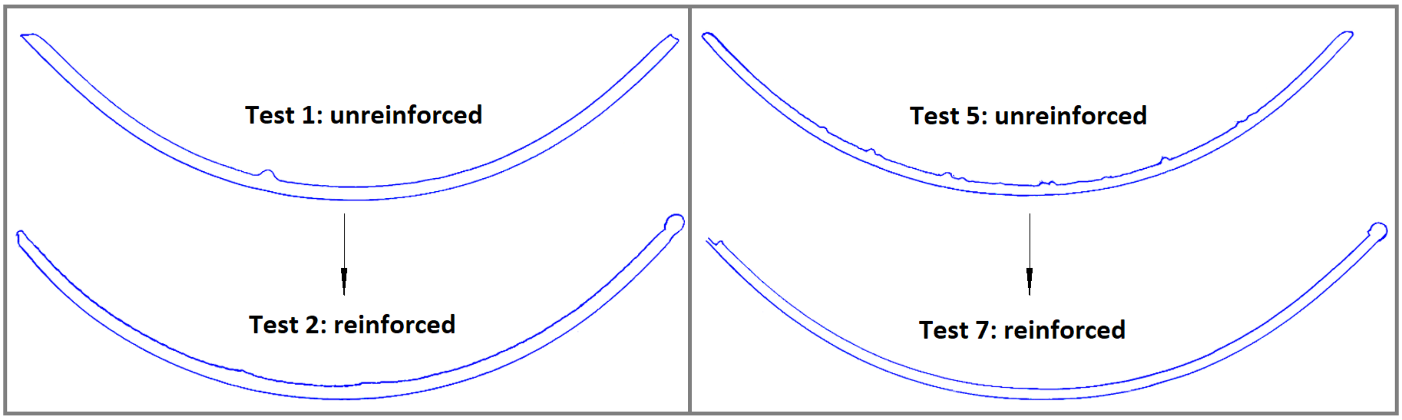

Figure 72: Comparison of similar conditions forming tests, with and without a reinforcement on top of the package. A reduction in out-of-plane displacement when using a reinforcement is clearly visible. Tests 1 and 2 had a thicker facing material and a less stiff reinforcement compared to tests 5 and 7. Tests 2 still has some light wrinkling, whereas test 7 has none (at least not visible)

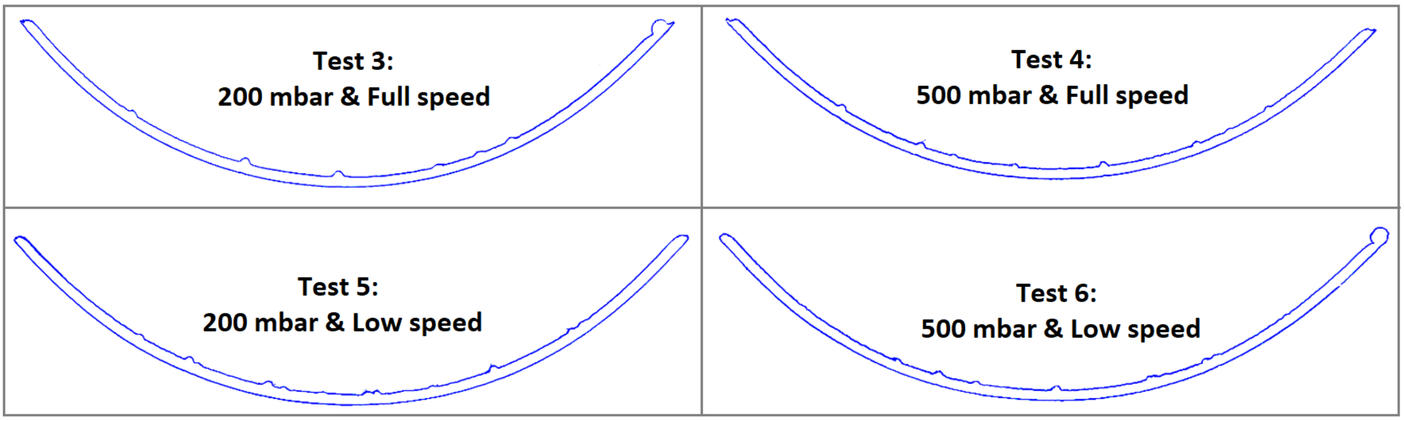

Figure 73: Comparison of forming tests with same materials and without reinforcement, but with different combinations of pressure and forming speed. Out-of-plane displacement appears to be very similar for tests 3, 4, 5, and 6.

Results: Top view contour

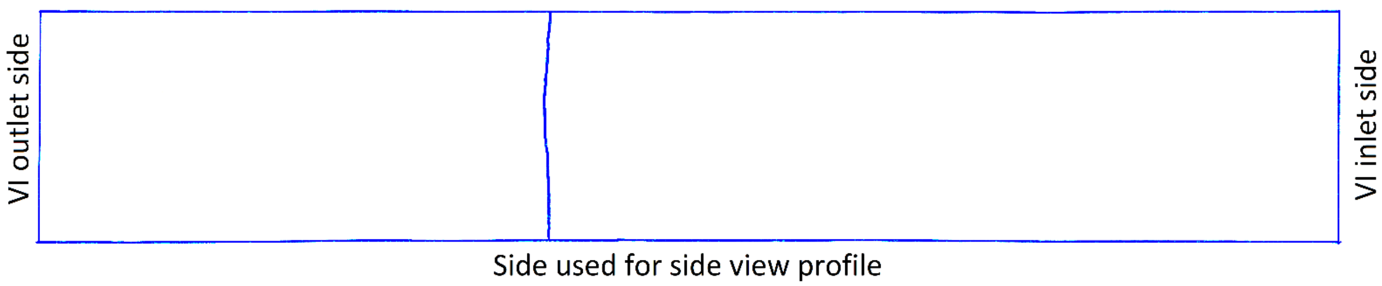

Figure 74: Test 1 top view contour. A single wrinkle region is visible.

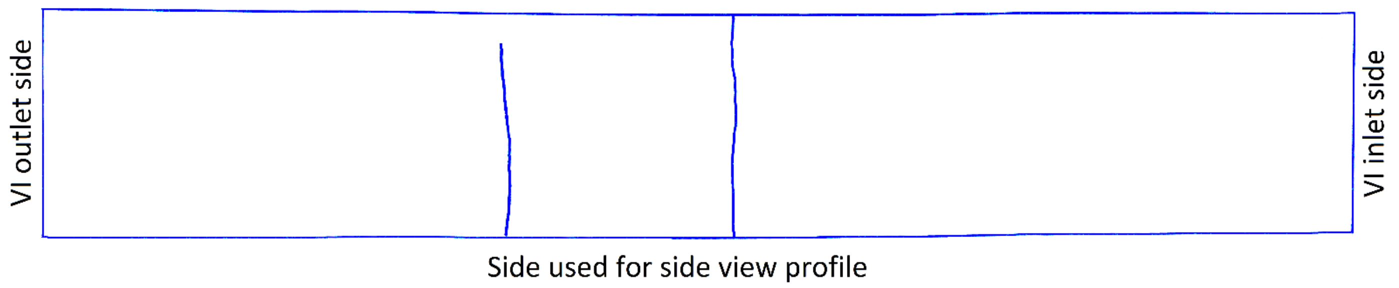

Figure 75: Test 2 top view contour. Two wrinkle regions are visible.

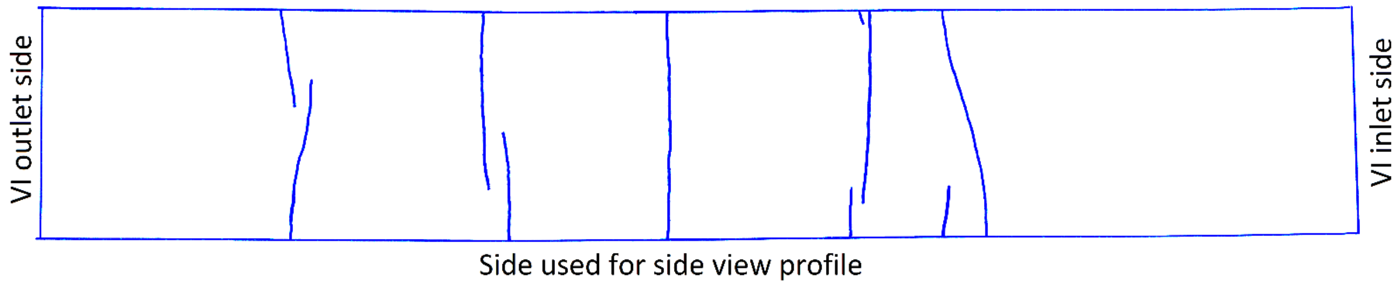

Figure 76: Test 3 top view contour. Five wrinkle regions are visible.

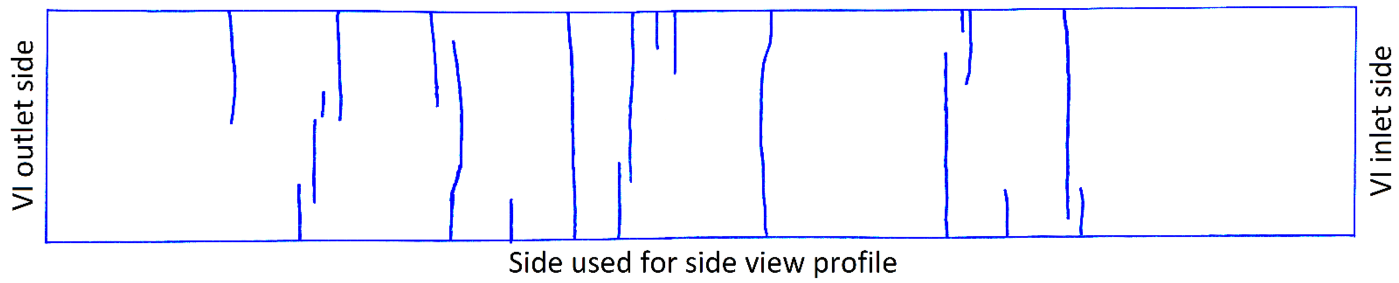

Figure 77: Test 4 top view contour. Approximately 6 wrinkle regions are visible.

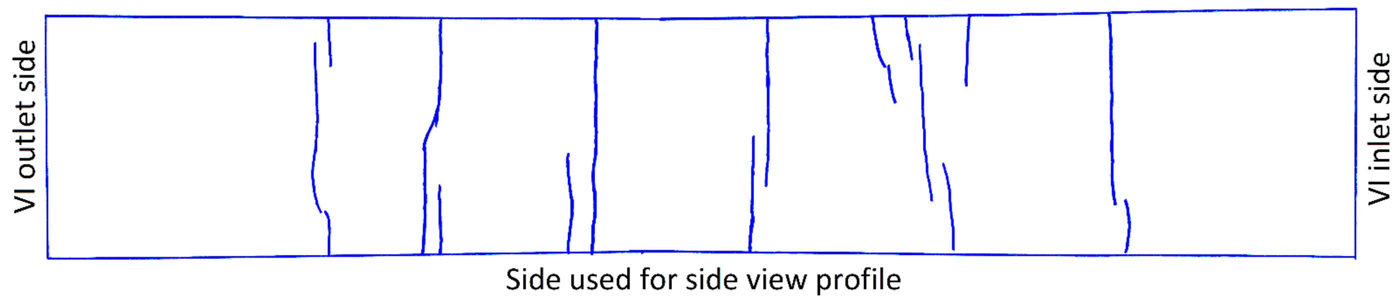

Figure 78: Test 5 top view contour. Approximately 6 wrinkle regions are visible.

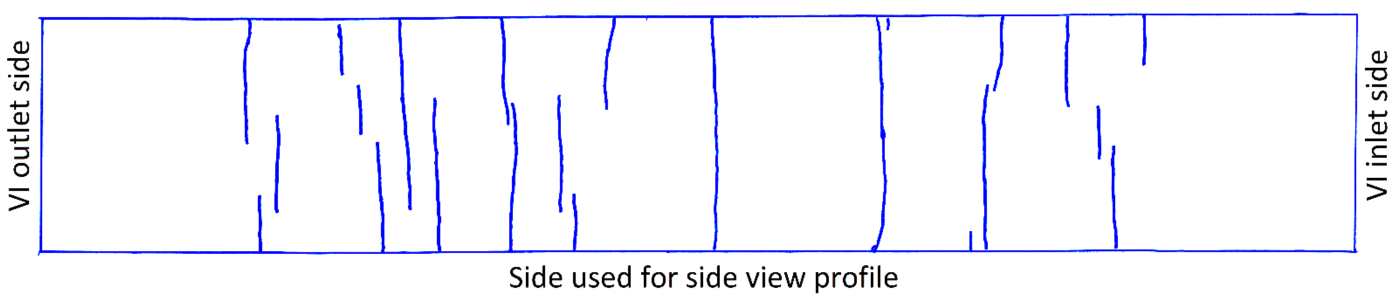

Figure 79: Test 6 top view contour. Approximately 7 wrinkle regions are visible.

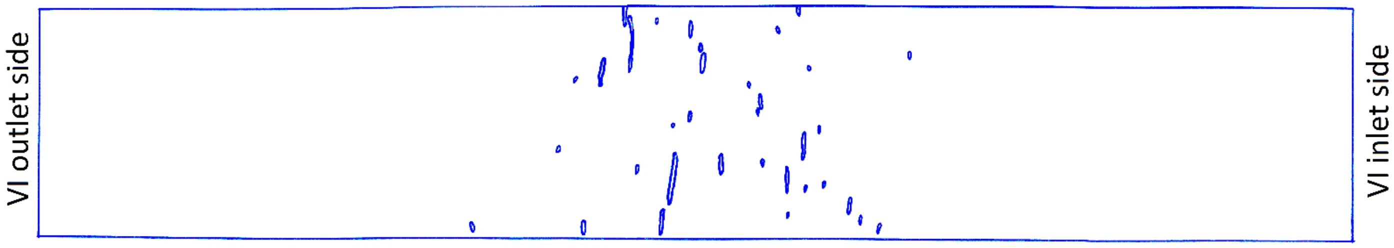

Figure 80: Test 7 top view contour. No wrinkle regions are observed like in all other tests. Small indented regions around the center of the panel are identified, i.e. no out-of-plane displacement. This can either be the result from trapped air between the top diaphragm and reinforcement, and/or very small wrinkling.

Results: Radius of curvature at bottom of panel & average thickness at non-wrinkled regions

Table 7: Average thickness at non-wrinkled regions and radius of curvature at bottom of panel

Test #	*T_{avg} [mm]*	*Radius of curvature [cm]*
1	11.55	39.39
2	11.75	39.28
3	8.98	38.86
4	8.82	39.42
5	8.87	37.91
6	8.78	38.90
7	9.1	40.21

Tests 1 and 2 have a different facing material compared to tests 3, 4, 5, 6, and 7, having a direct effect on T_{avg}. Therefore, these sets are treated separately. Differences between reinforced and unreinforced tests give some interesting results.

Unreinforced test 1 Vs. Reinforced test 2:
Reinforced test 2 is approximately 1.7% thicker at non-wrinkled regions compared to unreinforced test 1. Also, Reinforced test 2 has a 0.28% smaller radius of curvature at the bottom of the panel compared to test 1.

Unreinforced tests 3, 4, 5, 6 Vs. Reinforced test 7:
For the average thickness at non-wrinkled regions of tests 3, 4, 5, and 6, some distribution parameters are determined. The mean $(\overline{x})$ is 8.8625mm, sample standard deviation (SSD) is 0.0875mm, and percent SSD is 1%. Reinforced test 7 is approximately 2.7% thicker than the mean of the unreinforced tests and therefore considered significant if compared to percent SSD of 1%.

For the radius of curvature at the bottom of the tests 3, 4, 5, and 6, also some distribution parameters are determined. The mean $(\overline{x})$ is 38.7725mm, sample standard deviation (SSD) is 0.6390mm, and percent SSD is 1.6%. Reinforced test 7 has a 3.7% larger radius of curvature than the mean of the unreinforced tests and therefore considered significant if compared to percent SSD of 1.6%.

Results: Total difference in length caused by wrinkling

Table 8: Total difference in length caused by wrinkling.

Test #	ΔW_{TOT} *[mm]*
1	~5.5
2	~2
3	~15
4	~15
5	~15
6	~15
7	0

Results: Displacement data

The displacement data and the derived slip distributions are presented.

Table 9: Displacement data for test 1. Layer numbering is displayed on the left. Measurement locations are indicated in the top, as well as the before, after, and difference at those locations in [mm]. Layer 7 is used as a reference, hence 0 by default in all cases.

Test 1	@ Loc. 1			@ Loc. 2			@ Loc. 3			@ Loc. 4			@ Loc. 5			@ Loc. 6		
Layer #	B[mm]	A[mm]	Δ[mm]	B[mm]	A[mm]	Δ[mm]	B[mm]	A[mm]	Δ[mm]	B[mm]	A[mm]	Δ[mm]	B[mm]	A[mm]	Δ[mm]	B[mm]	A[mm]	Δ[mm]
7	0	0	0	0	0	0	0	0	0	0	0	0	0	0	0	0	0	0
6	2.7	1.9	-0.8	-8.5	-8.9	-0.4	1.2	0.8	-0.4	-0.8	-1.1	-0.3	-6.1	-6.2	-0.1	-2.9	-2.9	0
CORE																		
3	-2.9	-3.1	-0.2	-4.3	-5.6	-1.3	-5	-2.2	2.8	-5.2	-3.2	2	-7.1	-6.2	0.9	-8.1	-8	0.1
2	4.8	4	-0.8	-3.1	-5.2	-2.1	2.7	5	2.3	1.8	3	1.2	-6.9	-6.8	0.1	-1.6	-1.9	-0.3

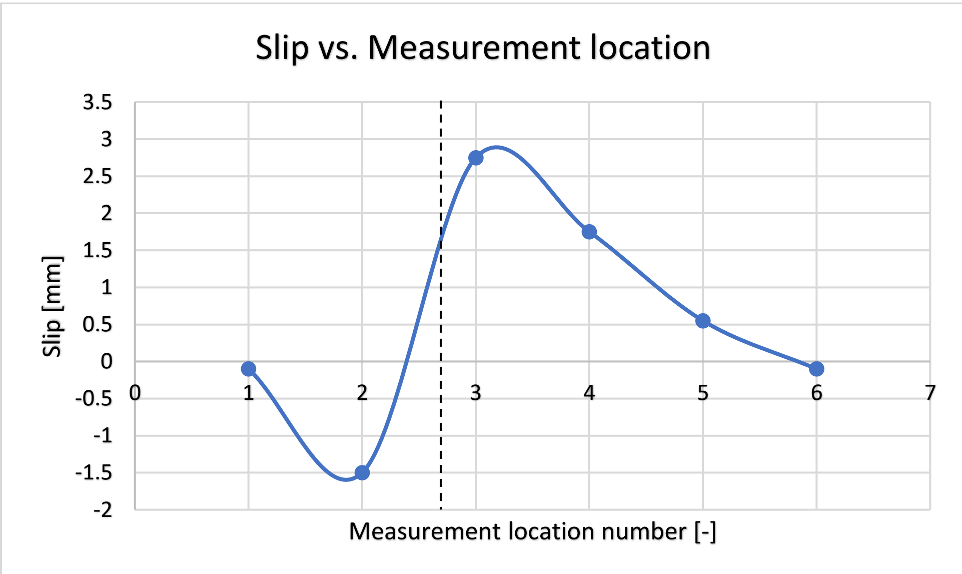

Figure 81: Slip distribution for test 1 where the top facing slips towards the wrinkle region and where the panel edges seem to be constrained. The horizontal axis shows the *measurement location numbers* defined in section 3.5.2. The amount of slip of the bottom facing w.r.t. the top facing at each measurement location is shown on the vertical axis. The sign convention for the slip is such that it is positive when the bottom layer moves to the right w.r.t. the top layer. A dashed vertical line represents the approximate location of the only wrinkle in this test panel. Two peaks of slip are observed, a negative peak at location 2 and a positive peak at location 3. Between those peaks the sign of slip flips and it is also the region of the wrinkle. From location 2 to 1 and from 3 to 6, slip reduces to approximately zero.

Table 10: Displacement data for test 2. Layer numbering is displayed on the left. Measurement locations are indicated in the top, as well as the before, after, and difference at those locations in [mm]. Layer 7 is used as a reference, hence 0 by default in all cases.

Test 2	@ Loc. 1			@ Loc. 2			@ Loc. 3			@ Loc. 4			@ Loc. 5			@ Loc. 6		
Layer #	B[mm]	A[mm]	Δ[mm]	B[mm]	A[mm]	Δ[mm]	B[mm]	A[mm]	Δ[mm]	B[mm]	A[mm]	Δ[mm]	B[mm]	A[mm]	Δ[mm]	B[mm]	A[mm]	Δ[mm]
7	0	0	0	0	0	0	0	0	0	0	0	0	0	0	0	0	0	0
6	0	0	0	-6.8	-6.5	0.3	-2	-2	0	-0.8	-0.5	0.3	-7.8	-7.2	0.6	-2.1	-1.8	0.32
CORE																		
3	3	2.9	-0.1	0.9	0	-0.9	0.3	0.3	0	1.1	2.3	1.2	-2.4	-2	0.4	-3.8	-3.9	-0.11
2	7.3	6.9	-0.4	-1.2	-2.8	-1.6	3.2	3	-0.2	3.3	4.3	1	-5.5	-4.9	0.6	-0.6	-0.9	-0.29

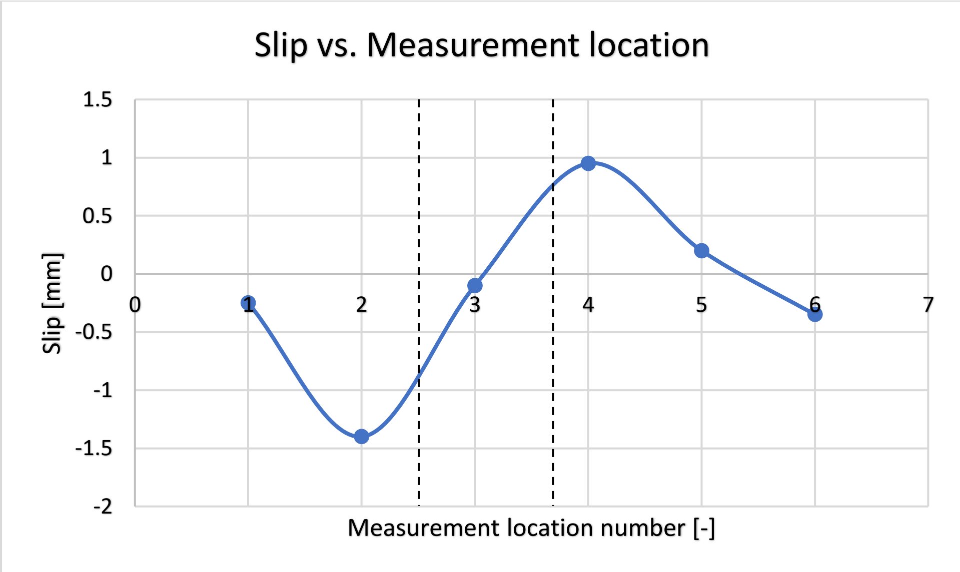

Figure 82: Slip distribution for test 2 where the top facing slips towards the wrinkle region and where the panel edges seem to be constrained. The horizontal axis shows the *measurement location numbers* defined in section 3.5.2. The amount of slip of the bottom facing w.r.t. the top facing at each measurement location is shown on the vertical axis. The sign convention for the slip is such that it is positive when the bottom layer moves to the right w.r.t. the top layer. Two dashed vertical lines represent the approximate locations of the wrinkles in this test panel. Two peaks of slip are observed, a negative peak at location 2 and a positive peak at location 4. Between those peaks the sign of slip flips and it is also the region of the wrinkles. From location 2 to 1 and from 4 to 6, slip reduces to approximately zero.

Table 11: Displacement data for test 3. Layer numbering is displayed on the left. Measurement locations are indicated in the top, as well as the before, after, and difference at those locations in [mm]. Layer 7 is used as a reference, hence 0 by default in all cases. A capital red "W" stands for: not measured due to the presence of a wrinkle.

Test 3	@ Loc. 1			@ Loc. 2			@ Loc. 3			@ Loc. 4			@ Loc. 5			@ Loc. 6		
Layer #	B[mm]	A[mm]	Δ[mm]	B[mm]	A[mm]	Δ[mm]	B[mm]	A[mm]	Δ[mm]	B[mm]	A[mm]	Δ[mm]	B[mm]	A[mm]	Δ[mm]	B[mm]	A[mm]	Δ[mm]
7	0	0	0	0	0	0	0	0	0	0	0	0	W	W	W	0	0	0
6	1.5	1.1	-0.4	-1.5	-1.9	-0.4	-1.5	-1.6	-0.1	0.8	0.8	0	W	W	W	-2	-2	0
CORE																		
3	1.4	-1.5	-2.9	0.9	-1	-1.9	-0.5	-1	-0.5	-1.4	-0.5	0.9	W	W	W	-3.4	-1.3	2.1
2	6.6	3.9	-2.7	2.8	0.9	-1.9	2	1.6	-0.4	0.6	1.6	1	W	W	W	-1.7	0.6	2.3

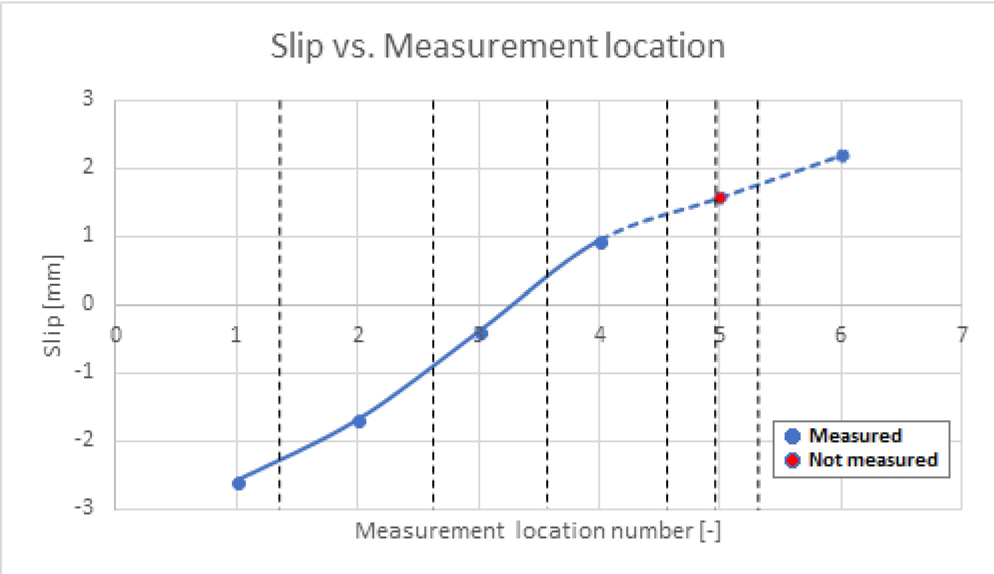

Figure 83: Slip distribution for test 3 where the top facing slips towards the wrinkle region. The horizontal axis shows the *measurement location numbers* defined in section 3.5.2. The amount of slip of the bottom facing w.r.t. the top facing at each measurement location is shown on the vertical axis. The sign convention for the slip is such that it is positive when the bottom layer moves to the right w.r.t. the top layer. Slip at measurement location 5 cannot be measured as the location is wrinkled, a linearly interpolated result is used instead. Six dashed vertical lines represent the approximate locations of the wrinkles in this test panel. The slip distribution varies approximately linear from location 1 to 6.

Table 12: Displacement data for test 4. Layer numbering is displayed on the left. Measurement locations are indicated in the top, as well as the before, after, and difference at those locations in [mm]. Layer 7 is used as a reference, hence 0 by default in all cases. A capital red "W" stands for: not measured due to the presence of a wrinkle.

Test 4	@ Loc. 1			@ Loc. 2			@ Loc. 3			@ Loc. 4			@ Loc. 5			@ Loc. 6		
Layer #	B[mm]	A[mm]	Δ[mm]	B[mm]	A[mm]	Δ[mm]	B[mm]	A[mm]	Δ[mm]	B[mm]	A[mm]	Δ[mm]	B[mm]	A[mm]	Δ[mm]	B[mm]	A[mm]	Δ[mm]
7	0	0	0	0	0	0	0	0	0	W	W	W	W	W	W	0	0	0
6	-1.9	-2	-0.1	-0.8	-0.9	-0.1	-3.7	-3.8	-0.1	W	W	W	W	W	W	-1.9	-2	-0.1
CORE																		
3	-0.8	-3.8	-3	-0.8	-2.8	-2	-5.5	-6.5	-1	W	W	W	W	W	W	-6.2	-3.6	2.6
2	-0.4	-3.3	-2.9	2.5	0.6	-1.9	0.2	-1.1	-1.3	W	W	W	W	W	W	-2.4	0.3	2.7

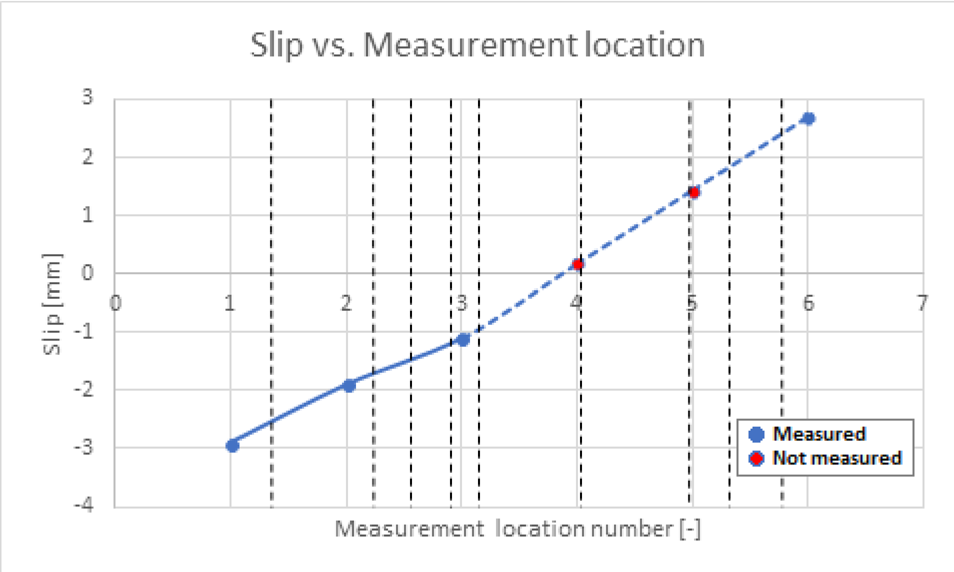

Figure 84: Slip distribution for test 4 where the top facing slips towards the wrinkle region. The horizontal axis shows the *measurement location numbers* defined in section 3.5.2. The amount of slip of the bottom facing w.r.t. the top facing at each measurement location is shown on the vertical axis. The sign convention for the slip is such that it is positive when the bottom layer moves to the right w.r.t. the top layer. Slip at measurement locations 4 and 5 cannot be measured as the locations are wrinkled. A linearly interpolated result is used instead. Nine dashed vertical lines represent the approximate locations of the wrinkles in this test panel. The slip distribution varies approximately linear from location 1 to 6.

Table 13: Displacement data for test 5. Layer numbering is displayed on the left. Measurement locations are indicated in the top, as well as the before, after, and difference at those locations in [mm]. Layer 7 is used as a reference, hence 0 by default in all cases. A capital red "W" stands for: not measured due to the presence of a wrinkle.

Test 5	@ Loc. 1			@ Loc. 2			@ Loc. 3			@ Loc. 4			@ Loc. 5			@ Loc. 6		
Layer #	B[mm]	A[mm]	Δ[mm]	B[mm]	A[mm]	Δ[mm]	B[mm]	A[mm]	Δ[mm]	B[mm]	A[mm]	Δ[mm]	B[mm]	A[mm]	Δ[mm]	B[mm]	A[mm]	Δ[mm]
7	0	0	0	W	W	W	0	0	0	0	0	0	0	0	0	0	0	0
6	-1.4	-1.4	0	W	W	W	-0.8	-0.8	0	-0.9	-1	-0.1	-1.2	-1.1	0.1	-1.5	-1.4	0.1
CORE																		
3	-0.6	-3	-2.4	W	W	W	2.6	2.8	0.2	-1.7	-0.6	1.1	-1.5	1	2.5	-6.3	-3.2	3.1
2	1.4	-1.2	-2.6	W	W	W	4.1	4.3	0.2	0	1.1	1.1	0.2	2.8	2.6	-1.1	2	3.1

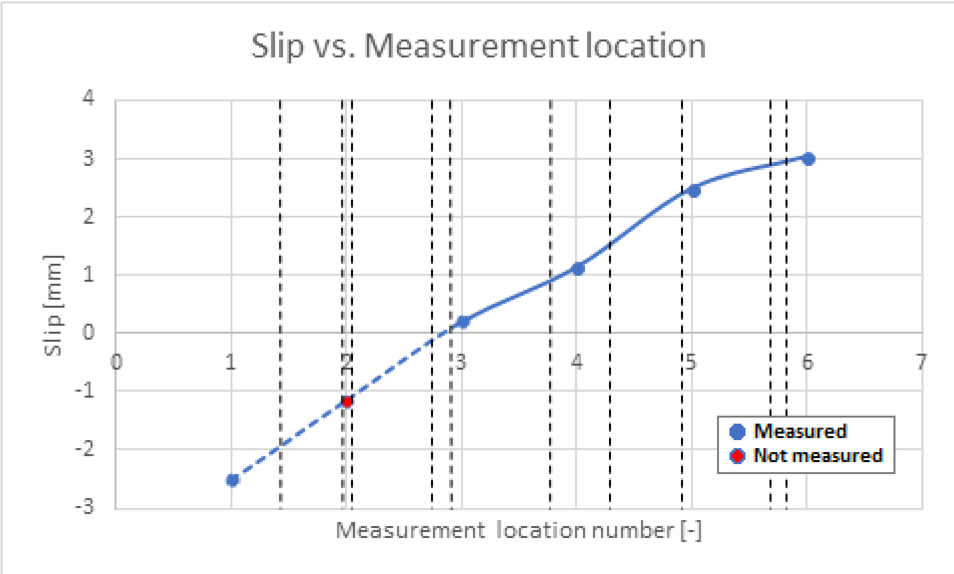

Figure 85: Slip distribution for test 5 where the top facing slips towards the wrinkle region. The horizontal axis shows the *measurement location numbers* defined in section 3.5.2. The amount of slip of the bottom facing w.r.t. the top facing at each measurement location is shown on the vertical axis. The sign convention for the slip is such that it is positive when the bottom layer moves to the right w.r.t. the top layer. Slip at measurement location 2 cannot be measured as the location is wrinkled, a linearly interpolated result is used instead. Ten dashed vertical lines represent the approximate locations of the wrinkles in this test panel. The slip distribution varies approximately linear from location 1 to 6.

Table 14: Displacement data for test 6. Layer numbering is displayed on the left. Measurement locations are indicated in the top, as well as the before, after, and difference at those locations in [mm]. Layer 7 is used as a reference, hence 0 by default in all cases. A capital red "W" stands for: not measured due to the presence of a wrinkle.

Test 6	@ Loc. 1			@ Loc. 2			@ Loc. 3			@ Loc. 4			@ Loc. 5			@ Loc. 6		
Layer #	B[mm]	A[mm]	Δ[mm]	B[mm]	A[mm]	Δ[mm]	B[mm]	A[mm]	Δ[mm]	B[mm]	A[mm]	Δ[mm]	B[mm]	A[mm]	Δ[mm]	B[mm]	A[mm]	Δ[mm]
7	0	0	0	W	W	W	0	0	0	0	0	0	W	W	W	0	0	0
6	1.8	1.8	0	W	W	W	0.6	0.4	-0.2	0.8	0.7	-0.1	W	W	W	-0.3	-0.3	0
CORE																		
3	4.1	1.3	-2.8	W	W	W	-1.7	-2.3	-0.6	-2.3	-1.8	0.5	W	W	W	-1.2	1.2	2.4
2	7.5	4.8	-2.7	W	W	W	1.2	0.8	-0.4	0.2	0.6	0.4	W	W	W	-0.2	2.5	2.7

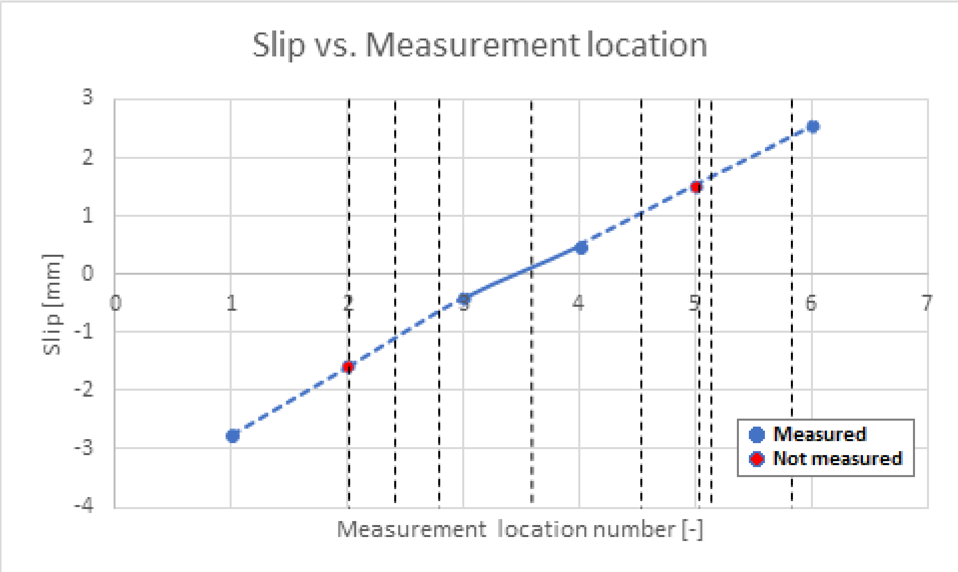

Figure 86: Slip distribution for test 6 where the top facing slips towards the wrinkle region. The horizontal axis shows the *measurement location numbers* defined in section 3.5.2. The amount of slip of the bottom facing w.r.t. the top facing at each measurement location is shown on the vertical axis. The sign convention for the slip is such that it is positive when the bottom layer moves to the right w.r.t. the top layer. Slip at measurement locations 2 and 5 cannot be measured as the locations are wrinkled. A linearly interpolated result is used instead. Eight dashed vertical lines represent the approximate locations of the wrinkles in this test panel. The slip distribution varies approximately linear from location 1 to 6.

Table 15: Displacement data for test 7. Layer numbering is displayed on the left. Measurement locations are indicated in the top, as well as the before, after, and difference at those locations in [mm]. Layer 7 is used as a reference, hence 0 by default in all cases.

Test 7	@ Loc. 1			@ Loc. 2			@ Loc. 3			@ Loc. 4			@ Loc. 5			@ Loc. 6		
Layer #	B[mm]	A[mm]	Δ[mm]	B[mm]	A[mm]	Δ[mm]	B[mm]	A[mm]	Δ[mm]	B[mm]	A[mm]	Δ[mm]	B[mm]	A[mm]	Δ[mm]	B[mm]	A[mm]	Δ[mm]
7	0	0	0	0	0	0	0	0	0	0	0	0	0	0	0	0	0	0
6	-0.2	-0.2	0	0.5	0.4	-0.1	0.2	0.2	0	-0.1	-0.1	0	1.2	1.1	-0.1	3.1	3	-0.1
CORE																		
3	3.8	2.8	-1	3	2	-1	3.1	2.7	-0.4	1.2	1.9	0.7	1.4	2	0.6	-0.8	0.2	1
2	2.6	1.9	-0.7	6	5.2	-0.8	4.9	4.5	-0.4	3.6	4.6	1	3.9	5	1.1	1.5	2.7	1.2

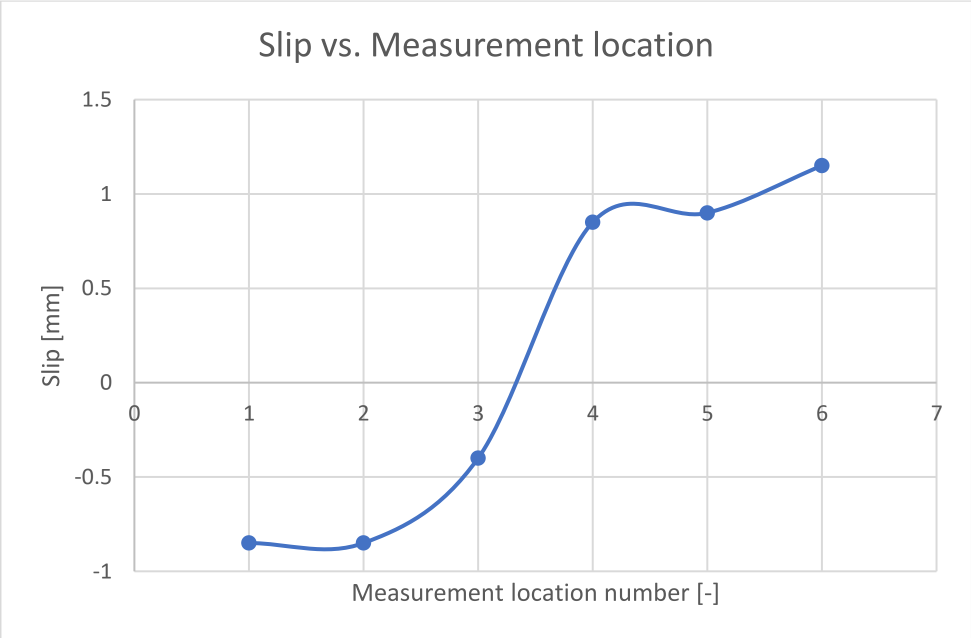

Figure 87: Slip distribution for test 7 where the top facing slips towards the wrinkle region. The horizontal axis shows the *measurement location numbers* defined in section 3.5.2. The amount of slip of the bottom facing w.r.t. the top facing at each measurement location is shown on the vertical axis. The sign convention for the slip is such that it is positive when the bottom layer moves to the right w.r.t. the top layer. The slip seems level from points 1 to 2 and from points 4 to 6. From point 2 to 4 the slip distribution varies approximately linear.

4.2 Analysis and Discussion

4.2.1 Effect of a reinforcement

The effect of a reinforcement on wrinkles is shown in Figure 88. This is based on the reduction of out-of-plane displacement shown in Figure 72, where test 7 has a reinforcement with a higher flexural rigidity compared to test 2. The widening of wrinkle regions is based on the top view contour of reinforced test 2 (Figure 75) compared to that of unreinforced test 1 (Figure 74) in combination with close up pictures of the wrinkle regions (appendix A). The widening of wrinkle regions is also confirmed by a comparison of the top view contour of reinforced test 7 (Figure 80) w.r.t. that of unreinforced test 5 (Figure 78) in combination with close up pictures of the wrinkle regions (appendix A).

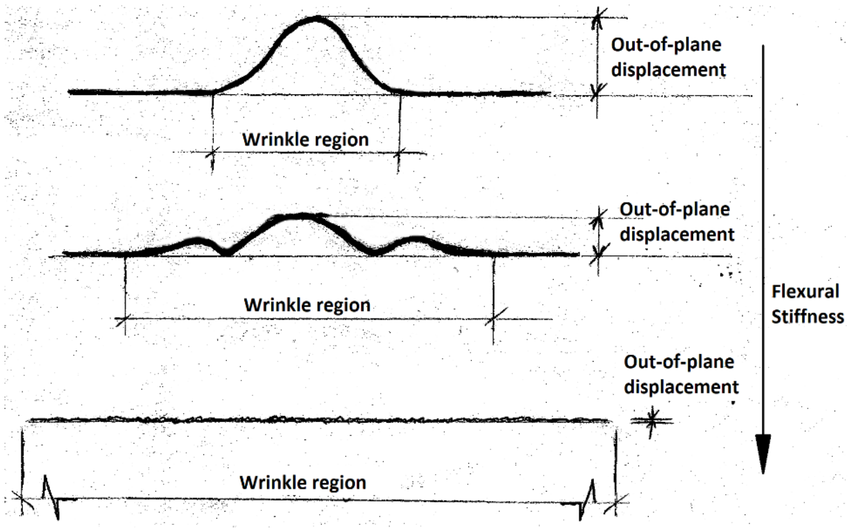

Figure 88: Effect of a reinforcement on wrinkles. An increase in flexural stiffness of a reinforcement will decrease out-of-plane displacement, widen the wrinkle region, and increase the number of wrinkles.

When wrinkles are "smeared out" by the introduction of a reinforcement, the amount of slip of the top facing w.r.t. the bottom facing decreases. This is clearly shown by comparing the slip distribution of reinforced test 2 (Figure 82) with unreinforced test 1 (Figure 81), both distributions are shown here in Figure 89. The formation of wrinkles can be seen as a way for the panel to release compressive stresses. This release of compressive stresses is also observed by the gradually decreasing slip from a maximum towards 0 at the outer measurement locations. A decrease in the amount of slip is therefore considered to increase compressive stresses and/or result in an increase of other deformation modes. Similar results can be found by comparing the slip distribution of reinforced test 7 (Figure 87) with unreinforced test 5 (Figure 85), both distributions are shown together in Figure 90.

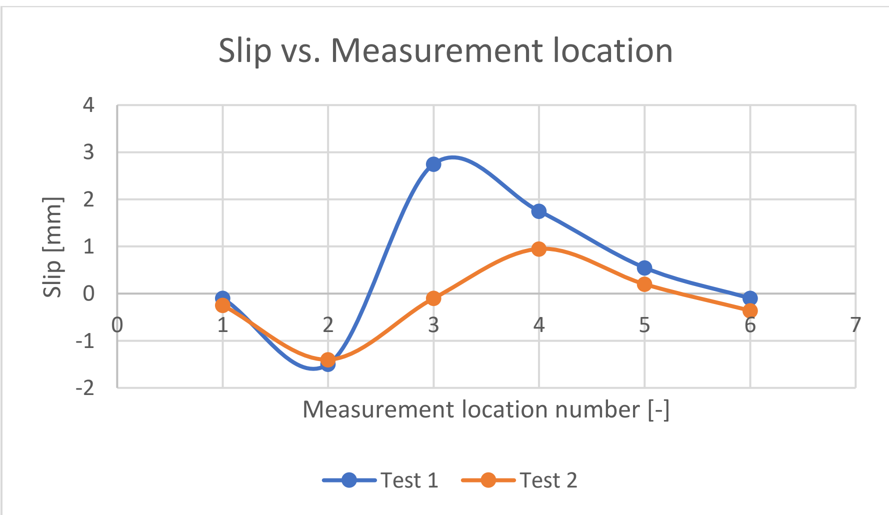

Figure 89: Comparison of slip distributions for unreinforced test 1 and reinforced test 2

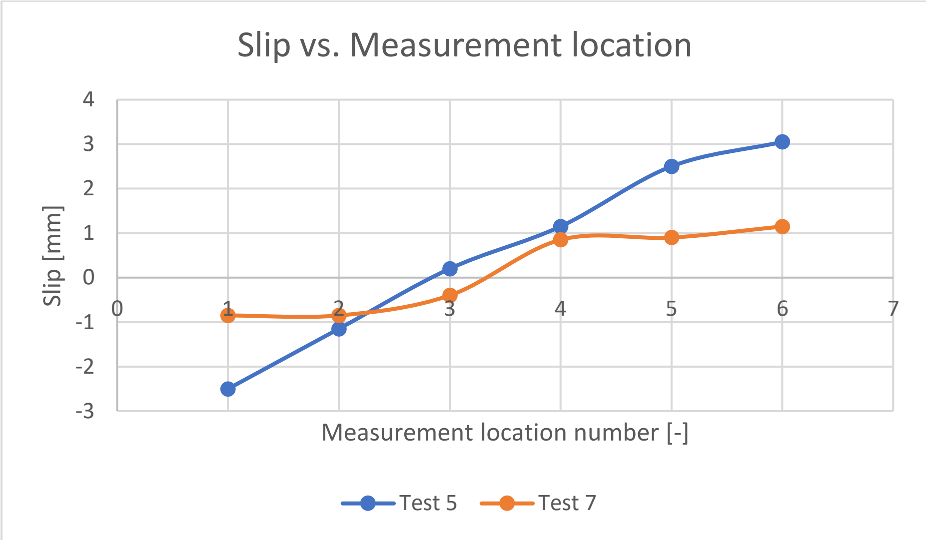

Figure 90: Comparison of slip distributions for unreinforced test 5 and reinforced test 7

It is believed that a reinforcement can lead to an increase in thickness. This can be substantiated by inspecting the values for the average thickness at non-wrinkled regions. Reinforced test 2 is approximately 1.7% thicker at non-wrinkled regions compared to unreinforced test 1. Also, reinforced test 7 is approximately 2.7% thicker than the mean of the unreinforced tests 3, 4, 5, and 6. Since the percent SSD is 1%, this increase is considered to be significant.

A full reduction of visible wrinkles by a reinforcement can lead to an increase in the radius of curvature after removing a panel from the tool surface. Reinforced test 7 showed a 3.7% larger radius of curvature than the mean of the unreinforced tests 3, 4, 5, and 6. Since the percent SSD is 1.6%, this increase is considered to be significant. The difference in radius of curvature between reinforced test 2 and unreinforced test 1 is insignificantly small. This is believed to be because the reinforcement was not stiff enough to fully suppress wrinkles.

The change in radius of curvature between reinforced test 7 and the mean of the unreinforced tests 3, 4, 5, and 6, is believed to be because of residual stresses caused by wrinkle reduction. As the panel of test 7 was removed from the tool surface it was able to release those stresses. An estimation of the distribution of the residual stresses appears to be complex. If one assumes only normal stresses in the top and bottom facing, an estimation for the compressive stress in the top facing could be made by computing the total slip over the length of the top facing, resulting in strain, and finding the stress with Hooke's law by assuming linear elastic behaviour. The bottom facing is more difficult. If it is in tension, it would be hard to detect as the strain would be very low. Also, looking at close-up pictures of tests 3, 4, 5, and 6, it could be possible that the bottom facing is in compression. It might be possible to estimate the bending moment resulting from the residual stress. The approach would be to determine the pure bending moment needed to change the curvature with the use of a curved sandwich bending theory, or with FEM calculations.

4.2.2 Effect of pressure and forming speed

The effect of pressure and forming speed on wrinkles seem to be insignificant under the testing conditions of the experiments. This is clearly seen in the side view contours of tests 3, 4, 5, and 6 (Figure 73). Close-up pictures (appendix A) of wrinkle regions for tests 3, 4, 5, and 6, show that the top facing wrinkles. Also, some wrinkling of the core and bottom facing is observed.

Reason for the bottom facing and core to be lightly wrinkled is at least partially because the top surface of the tool lightly wrinkled. This behaviour of the tool surface can be the result of insufficient vacuum underneath the protective layer of the tool surface. Another reason might be that the protective layer of the tool surface is under compression itself. It is unclear where the neutral line of the tool surface lies during forming.

Top view contours for tests 3, 4, 5, and 6 (Figure 76 up to and including Figure 79) show little variation in the amount of wrinkling. The variation in radii of curvature and average thicknesses of unwrinkled areas between tests 3 ,4, 5, and

6 is considered to be insignificantly small. The slip distributions for tests 3, 4, 5, and 6 (Figure 83 up to and including Figure 86) are also very similar in both shape and magnitude, Figure 91.

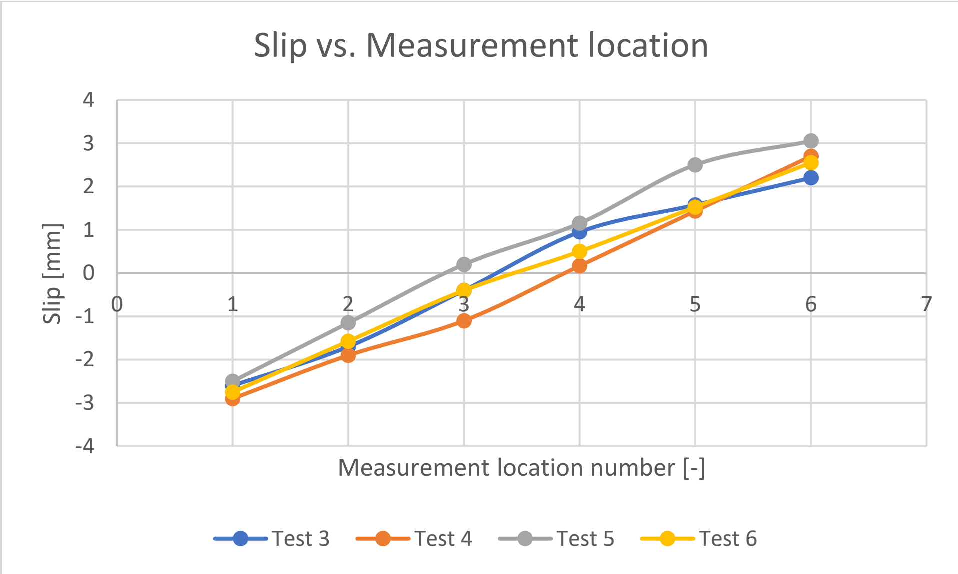

Figure 91: Comparison of slip distributions for tests 3, 4, 5, and 6

4.2.3 Comparison of model for slip, wrinkle lengths, and slip distributions

The 2d assumption for the geometrical model of slip is supported by the observation that wrinkle regions spread over the width of the panel (Figure 74 up to and including Figure 79).

The total amount of slip (S_{TOT}) according to the geometrical model (defined by Eq. 18) shows that it is able to approximately predict the amount of potential slip. This is substantiated by comparing it with the total difference in length, caused by wrinkling (ΔW_{TOT}) as defined in Eq. 20. A comparison of S_{TOT} and ΔW_{TOT} for the tests that showed wrinkles is made:

- Unreinforced tests 3, 4, 5, and 6 all have a $\Delta W_{TOT} \approx 15mm$. The total amount of theoretically desired slip for tests 3, 4, 5, and 6 is $S_{TOT} \approx 14mm$. This shows that the actual measured difference in length caused by wrinkling in the top facing is approximately 7% larger than the estimation of the potential slip based on the geometrical model. This indicates that the wrinkles are likely to have relieved any compressive stress that was built up.
- Comparing unreinforced test 1 with its theoretical counterpart, a different behaviour is observed. $\Delta W_{TOT} \approx 5.5mm$ and $S_{TOT} \approx 15.5mm$, indicating that the wrinkling in the top facing is approximately 65% smaller:
    - A possible explanation is that test 1 still had compressive stresses that were not relieved by wrinkle formation. The underlying reason for this difference in the amount of wrinkling might be the fact that test 1 has a thicker facing compared to tests 3, 4, 5, and 6, i.e. increased buckling stress of that facing.
    - Other in-plane deformations might have occurred, such as increased roundness of fibre bundle shape or in-plane buckling. Fibre bundle shape seems to vary very little in test 1 and tests 3, 4, 5, and 6. In-plane buckling has not been measured. Future research should try to capture the amount of in-plane buckling. This can possibly be done with insertion of threads into the fabric.

Slip distributions for unreinforced test 1, reinforced test 2, and the theoretical desired slip are shown in Figure 92. Slip distributions for unreinforced test 5, reinforced test 7, and the theoretical desired slip are shown in Figure 93. Comparing Figure 92 and Figure 93, the difference is that for tests 1 and 2 the slip decreases towards zero towards the edges and this is not visible for tests 5 and 7. It is believed that the slip distribution for tests 5 and 7 will also go to zero outside measurement locations 1 and 6, as the wrinkle region stops at those locations. Future research should add more measurement locations near the edge to test this statement. 0 slip at the edges is an indication of constrained conditions at the edges.

Introducing a reinforcement as in test 2 decreases the slip distribution compared to unreinforced test 1. The maximum achievable result would be to fully stop the slip. The introduction of a tensile stress would further improve the result as it would force the top layers to move towards the edges, i.e. enforcing the slip distribution to become more like the theoretically desired. This can be further facilitated by decreasing the friction between layers used. The layers used in this test where not ideal for keeping friction forces low, but they were needed to enable the insertion of threads.

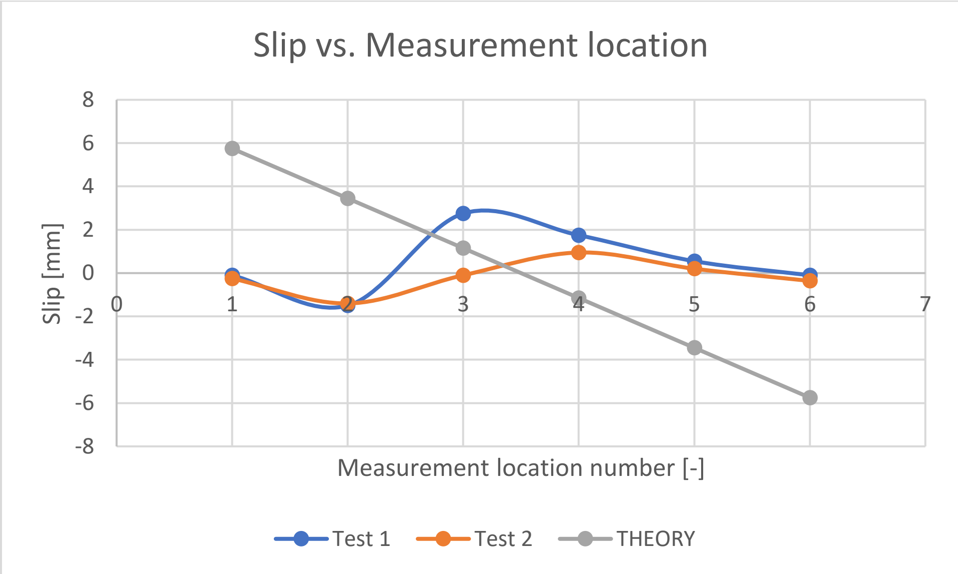

Figure 92: Comparison of slip distributions for tests 1, 2, and theoretically desired. For tests 1 and 2 the facing slips towards the region of wrinkling and also seems to be constrained near the edges. For the theoretically desired slip, the facing slips towards the edges of the panels and it has its edges free of constraints.

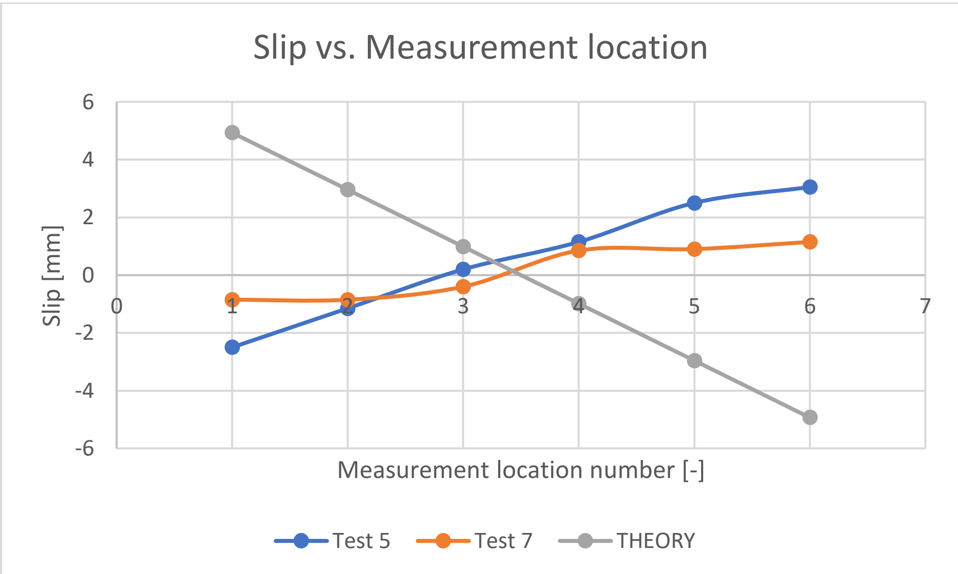

Figure 93: Comparison of slip distributions for tests 5, 7, and theoretically desired. For tests 5 and 7 the facing slips towards the region of wrinkling. For the theoretically desired slip, the facing slips towards the edges of the panels and it has its edges free of constraints.

4.3 Review of the hypotheses

The hypotheses stated in the section 3.1 are repeated here for convenience such that they can be reviewed with the help of new insights from the results and analysis in sections 4.1 and 4.2:

1. A reinforcement reduces out-of-plane wrinkles by constraining out-of-plain displacement and therefore promoting the slipping of layers
2. A reduction in pressure reduces out-of-plane wrinkles by lowering the friction between layers and therefore promoting the slipping of layers
3. A reduction in forming speed reduces out-of-plane wrinkles by lowering the friction between layers and therefore promoting the slipping of layers

Review of hypothesis 1:

- A reinforcement on top of a package does indeed reduce wrinkles by constraining out-of-plane displacement. It will also widen the wrinkle region and increase the number of wrinkles. An increase in flexural stiffness of the reinforcement will increase this effect.
- The reduction of out-of-plane displacement did not promote the slipping of layers. It actually decreased the amount of slip. As the amount of slip did not increase, other deformation modes must have occurred, such as in-plane fibre buckling, changes in fibre bundle shape. It is believed that with enough reinforcement a compressive stress is built up in the sandwich panel. Leading to residual stresses, causing changes in the radius of curvature when the panel is removed from the tool.

Review of hypotheses 2 and 3:

- Pressure and forming speed have not shown a significant effect on the out-of-plane wrinkles. It is believed that the absence of tensile stresses is a potential cause for this. Therefore, hypotheses 2 and 3 should be tested again in future research under the additional influence of tensile stresses.

5 Conclusions and Recommendations

Forming of high quality sandwich panels on a reconfigurable mould is the ultimate goal. This exploratory research is intended to serve as a starting point for further research on the quality improvement of such a process. Quality refers to sandwich panels without unwanted deformation modes. A first test series to initiate a starting point for further research has been performed. The conclusions and recommendations based on this research are presented in this chapter.

The aim of the test series, as stated in the introduction, is to investigate the underlying forming mechanisms of resin infused sandwich panels under the influence of forming speed, infusion pressure, and diaphragm reinforcement. These tests are performed only for single curved panels where the tooling surface reconfigures itself to a concave shape. Therefore, the conclusions are limited to single curved resin infused sandwich panels where the tooling reconfigures itself to a concave shape.

Very important fact to keep in mind is that the number of tests performed is relatively low. More tests are required for the validation of the preliminary conclusions provided in this chapter.

5.1 Conclusions

Conclusions concerning the reinforcement:

A reinforcement decreases the out-of-plane displacement of wrinkles while at the same time widening the wrinkle region and increasing the number of wrinkles. An increase in flexural stiffness of the reinforcement will increase this effect.

The formation of wrinkles can be seen as a way for the panel to release compressive stresses. By obstructing the out-of-plane displacement, other types of deformations were observed:

- Slipping of the facings w.r.t. each other is decreased
- Average thickness at non-wrinkled regions of the panel increased by 1.7% in reinforced test 2 compared to unreinforced test 1. Reinforced test 7 showed a 2.7% increase compared with the mean of unreinforced tests 3, 4, 5, and 6, while the percent standard deviation was only 1%
- Obstructing wrinkles to the point where they are hard to detect by eye, showed that the radius of curvature can also increase. Test 7 showed an increase of 3.7% for the radius of curvature compared with the mean of unreinforced tests 3, 4, 5, and 6, while the percent standard deviation was only 1.6%

A thicker core will lead to more potential deformation in the top facing. A thicker top facing will lead to a higher critical buckling stress and will therefore form a lower number of wrinkles compared to a thin bottom facing. A sandwich panel is valued for its high specific bending stiffness. This is achieved by having a high ratio of core thickness to facing thickness, i.e. thick core and thin facing. This indicates an inherent trade-off between design and manufacturing when forming single curved sandwich panels on a reconfigurable mould. A reinforcement adds its bending stiffness on top of the sandwich, increasing the limits of forming sandwich panels on a reconfigurable mould.

Conclusion concerning pressure and forming speed:

Pressure and forming speed have an insignificant effect under the testing conditions as described in this work. Different pressure and forming speed combinations have shown to result in very similar panels. The idea was to decrease the friction between layers such that the tendency of layers to slip was higher than the tendency to wrinkle. The opposite seems to be the case.

Conclusions concerning the geometrical model for slip:

The 2d assumption for the geometrical model of slip is supported by the observation that wrinkle regions spread over the width of the panel.

The geometrical model is able to approximately estimate the amount potential deformation in the form of the slipping of the facings w.r.t. each other. For tests with lots of wrinkles, as in tests 3, 4, 5, and 6, the total amount of slip predicted by the geometrical model was only 7% smaller than that of the directly measured differences in length caused by wrinkles. However, an overestimation of 65% was also measured in the case of test 1 which had thicker facings. From this it can be concluded that the geometrical model is useful to get a rough idea of how much deformation one can expect.

Conclusions concerning the method used for collecting displacement data:
The slip distributions that are shown in the results section are able to give an indication of the amount of slip at multiple locations with a reasonable accuracy. However, the measurement technique involves a lot of steps, making it both error-prone and time-consuming.

5.2 Recommendations

For future research it is recommended to focus on the quality improvement of single curved sandwich panels, before moving on to the ultimate goal of forming double curved sandwich panels. The reason is that double curved panels undergo the same deformation mechanisms as single curved panels, with the addition of intra-ply shear. Also, the quality of single curved panels is still not where it needs to be.

To improve the forming of single curved sandwich panels it is recommended to:

- Pursue ways of introducing tensile stresses in the sandwich to overcome compressive stresses that are built up during forming. The comparison of the theoretical slip distribution and the slip distribution from the displacement data showed that a tensile stress could further improve the slip distribution.
- If tensile stresses can be introduced, it is advised to perform a test series where pressure and forming speed vary. This could possibly reduce the forces needed.
- Investigate if the edges of the panels are indeed constrained as the slip distributions seem to go to 0 near the edges. If confirmed, explore ways to free the edges such that slipping of layers is promoted.
- In the case of using a reinforcement, investigate the relation between residual stresses after forming and the relation to a change in radius.

Recommendations concerning the method used for collecting displacement data:

- It is a method that involves a lot of steps, making it both error-prone and time-consuming. Therefore, it is not advised to use this method, unless no better options are available.
- This method can be made more effective by first performing a test without threads and observe where deformation occurs. Allowing for a better choice of the thread locations in the second test.
- The method of modifying fabric layers by inserting threads might also be suitable for the visualization of in-plane buckling.

Appendix A / Results: Close-up pictures

This appendix contains close-up pictures of wrinkles for each test. The accompanying top view and side view for each panel is provided to illustrate the approximate location of the close-up pictures.

Test 1:

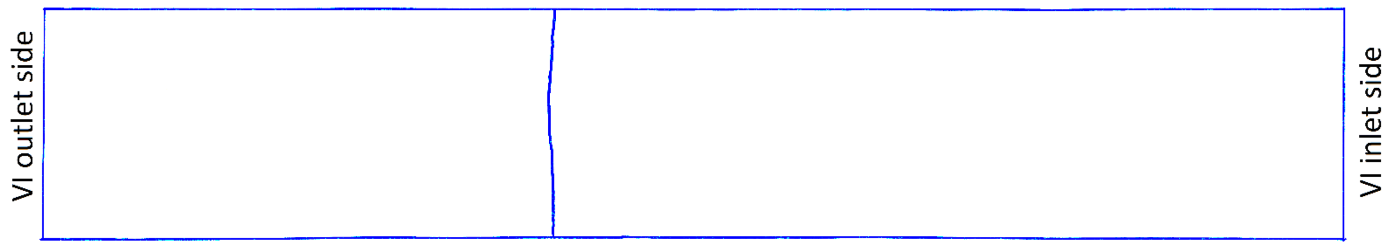

Figure A - 1: Top view test 1

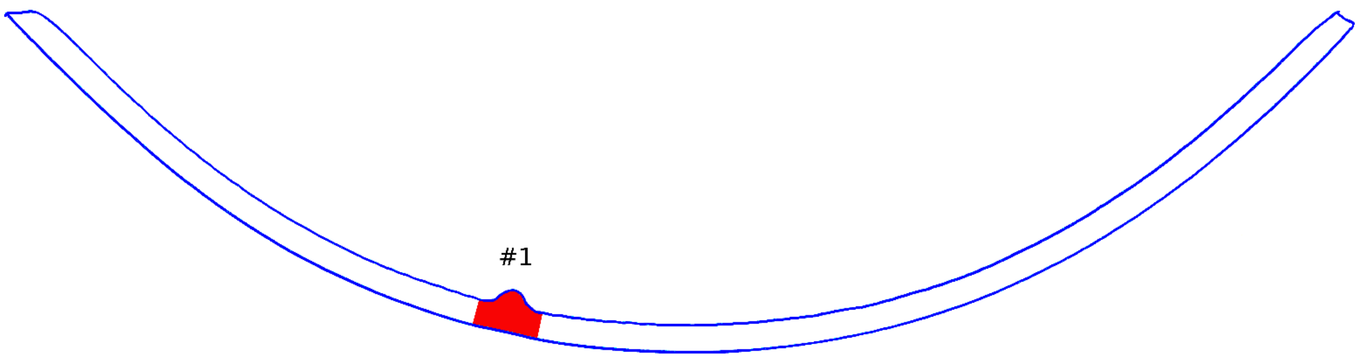

Figure A - 2: Side view test 1

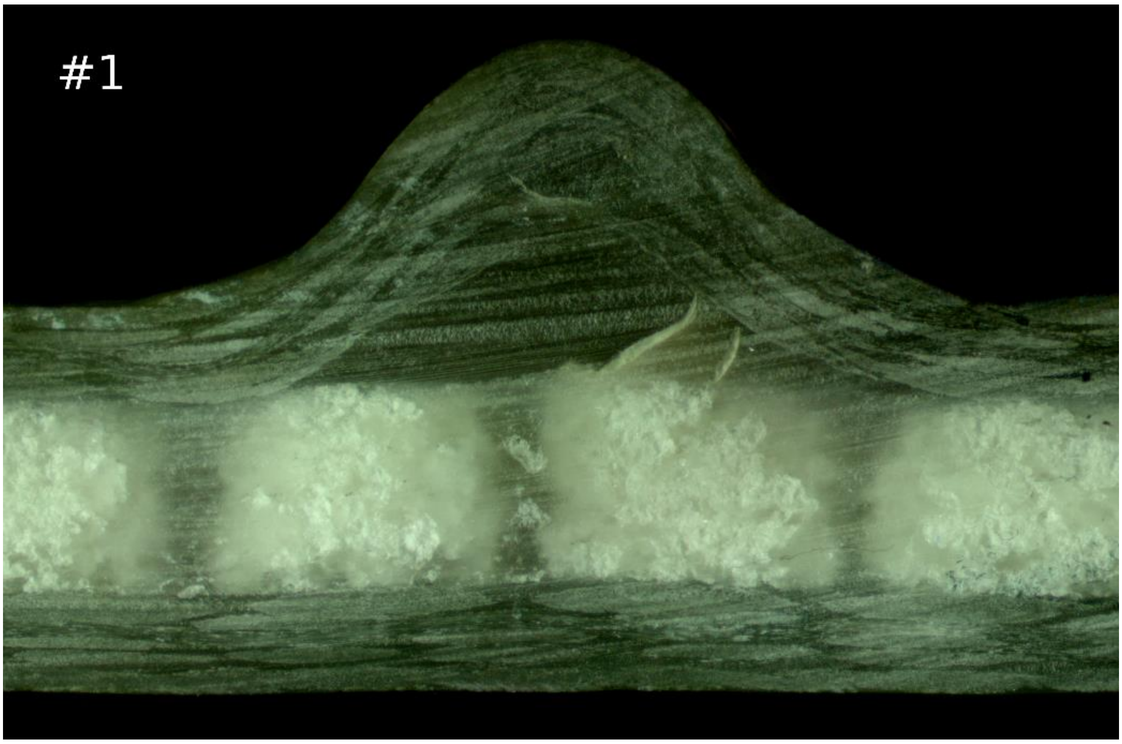

Figure A - 3: Wrinkle region #1 for test 1

Test 2:

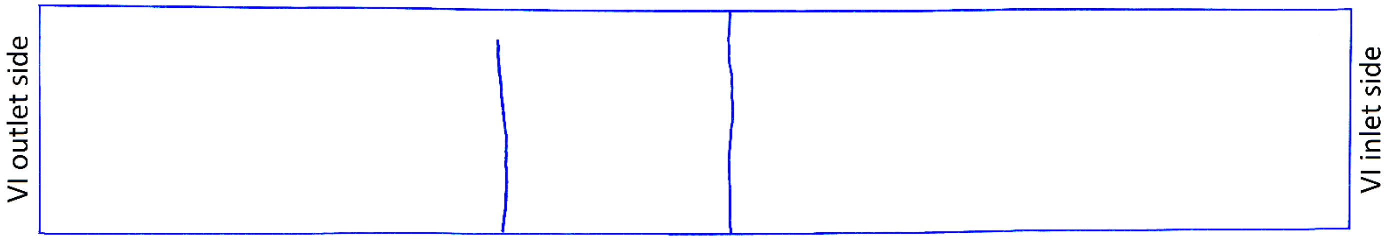

Side used for side view profile

Figure A - 4: Top view test 2

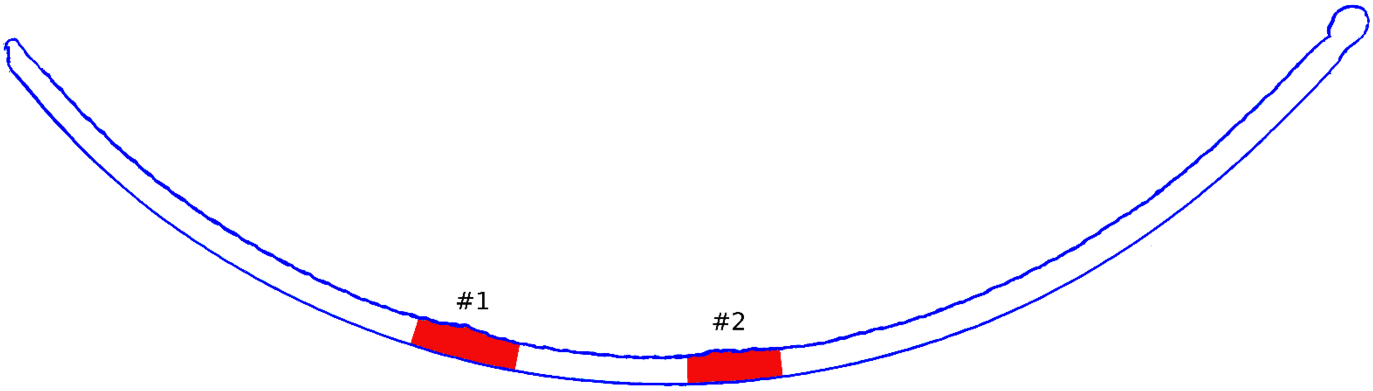

Figure A - 5: Side view test 2

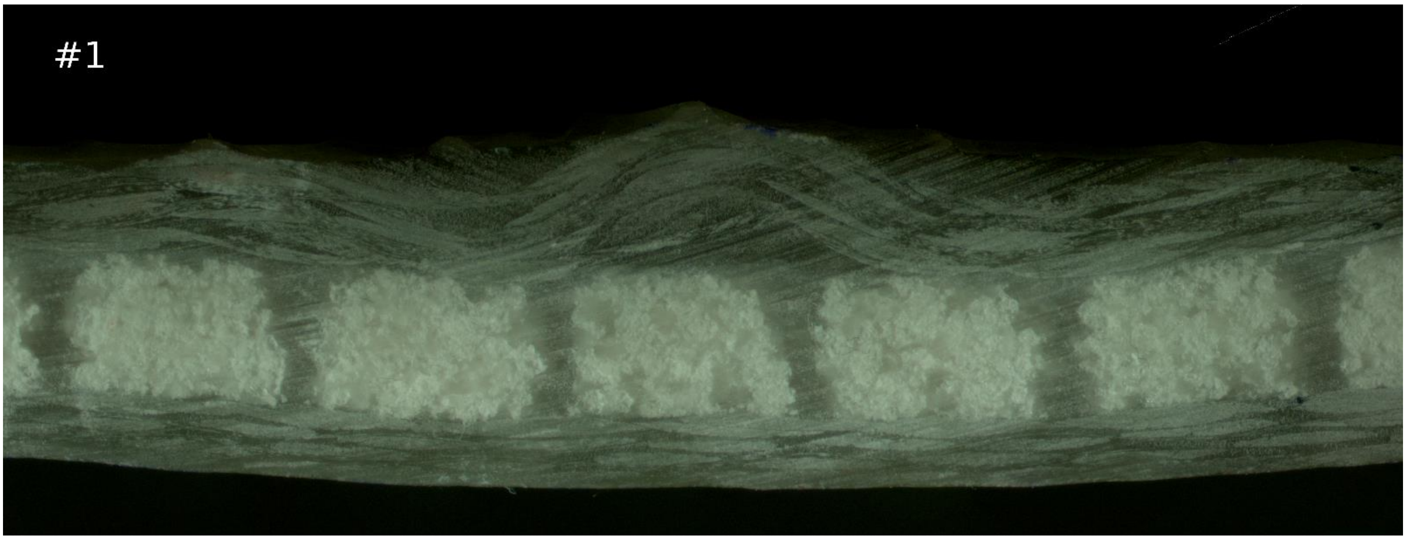

Figure A - 6: Wrinkle region #1 for test 2

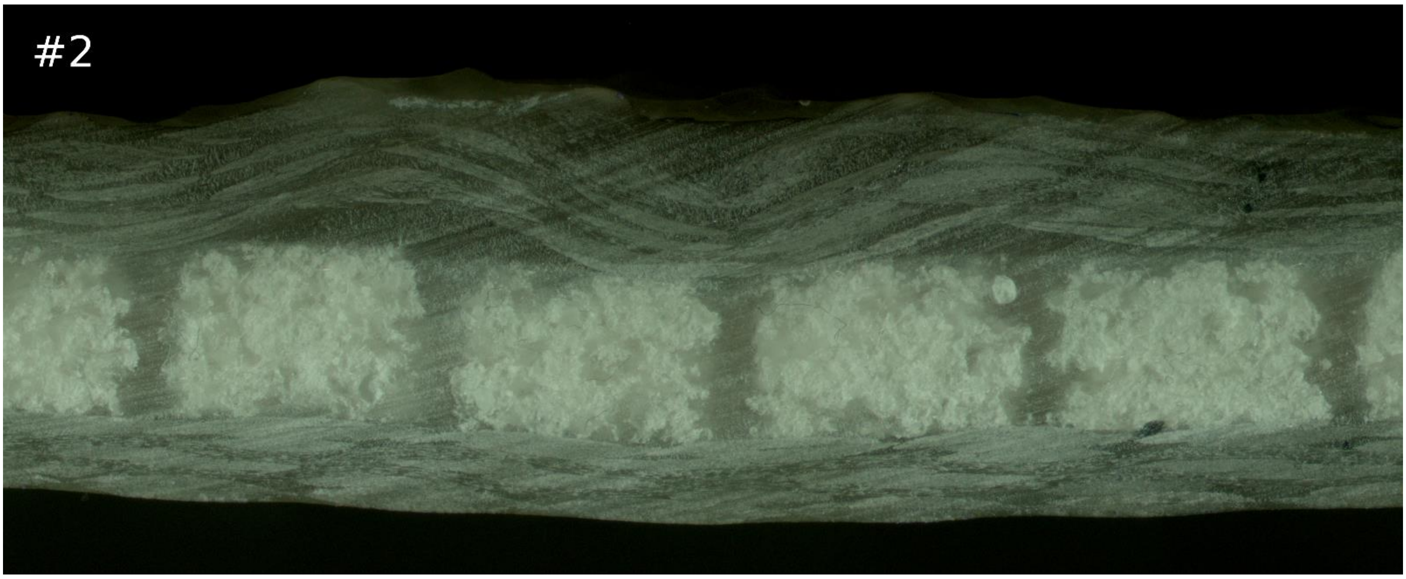

Figure A - 7: Wrinkle region #2 for test 2

Test 3:

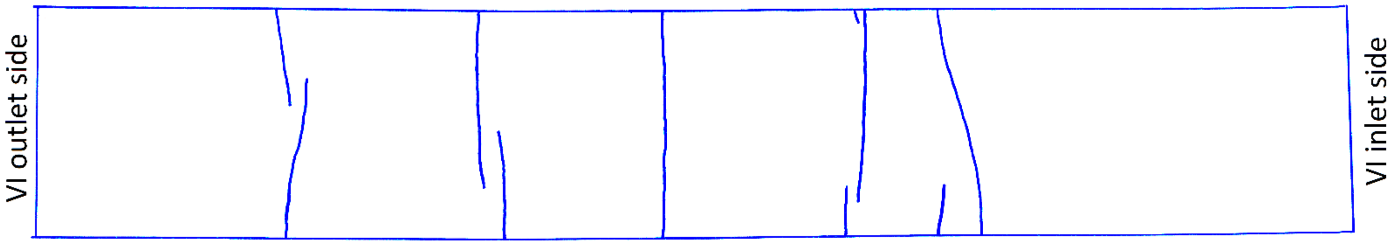

Figure A - 8: Top view test 3

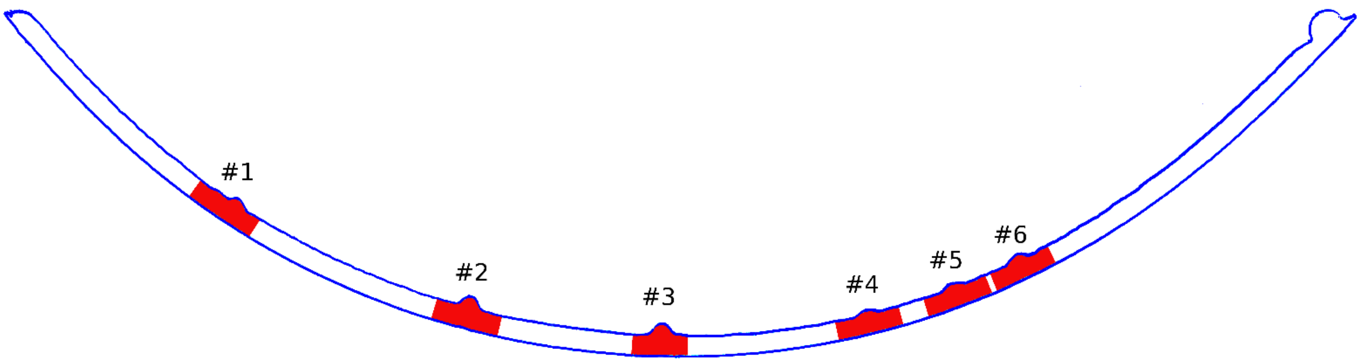

Figure A - 9: Side view test 3

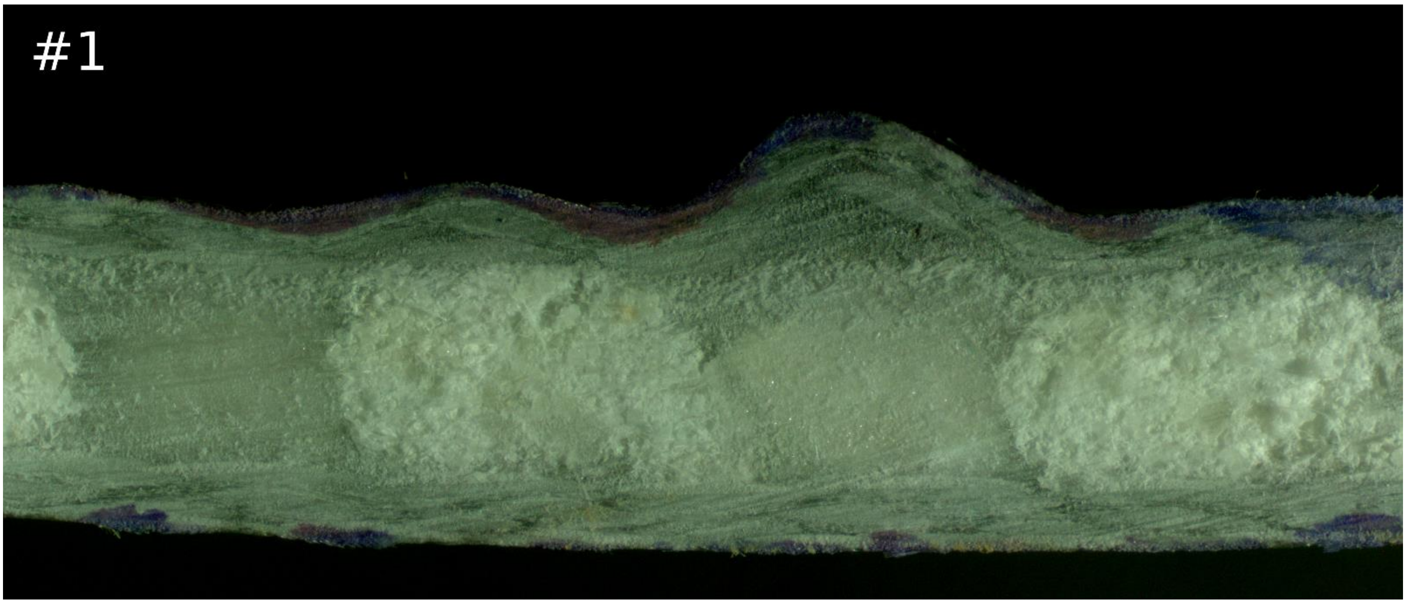

Figure A - 10: Wrinkle region #1 for test 3

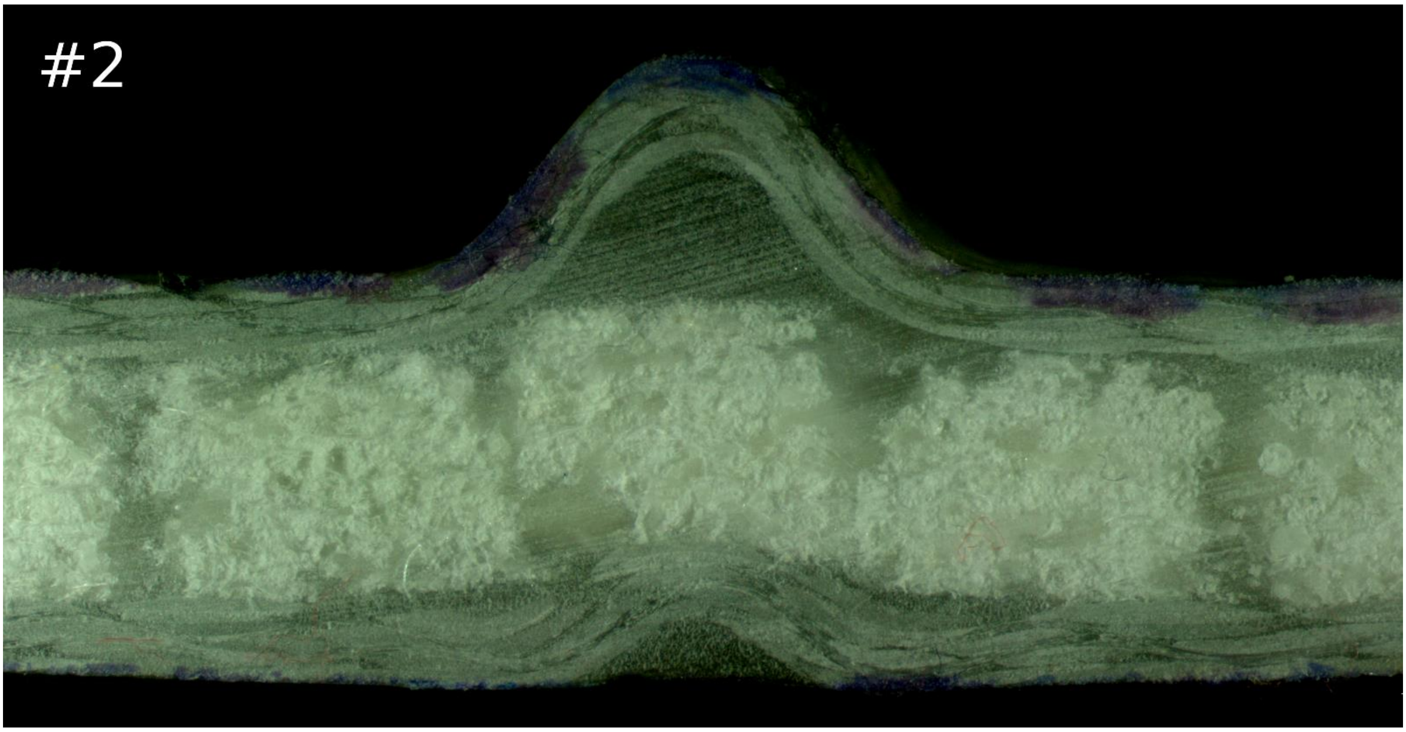

Figure A - 11: Wrinkle region #2 for test 3

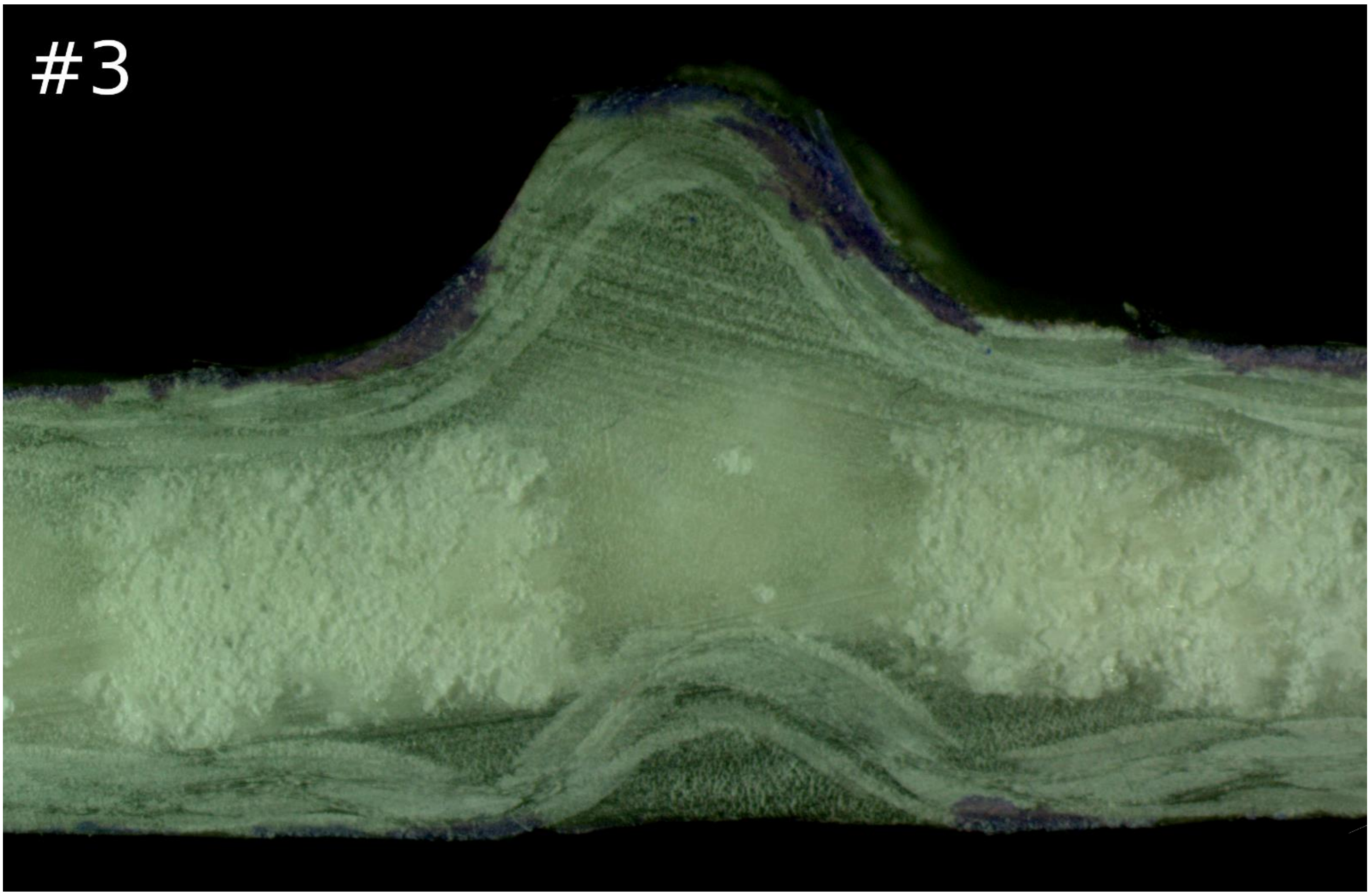

Figure A - 12: Wrinkle region #3 for test 3

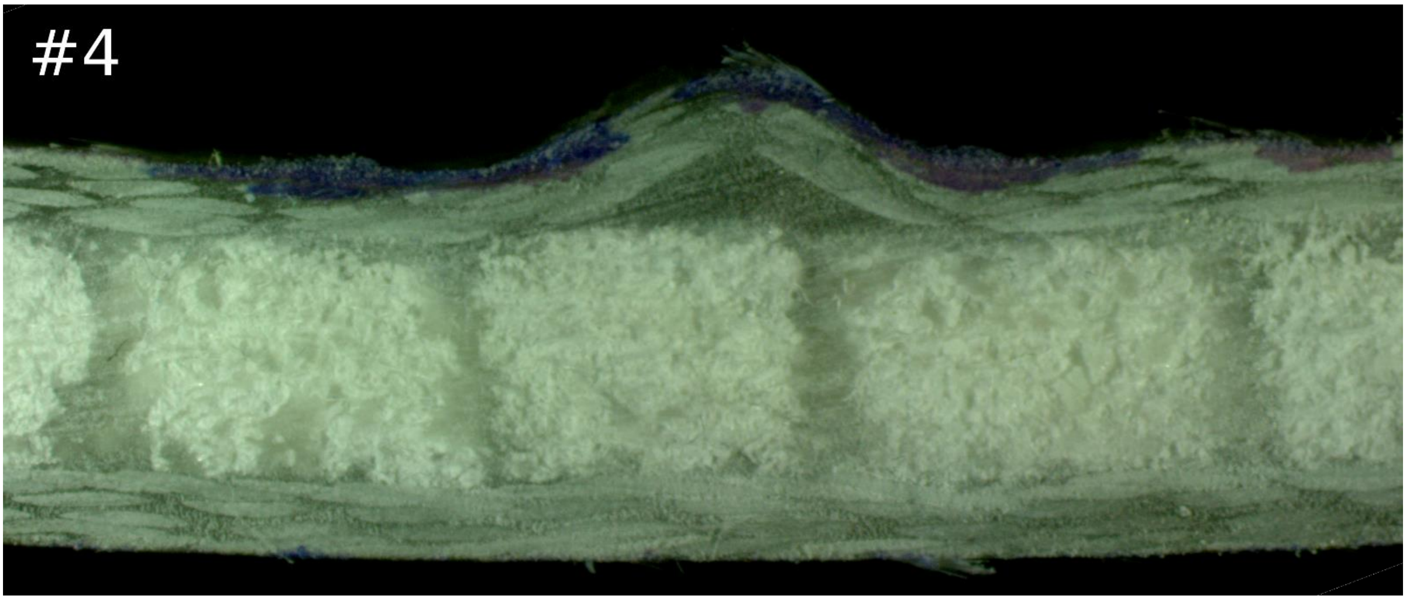

Figure A - 13: Wrinkle region #4 for test 3

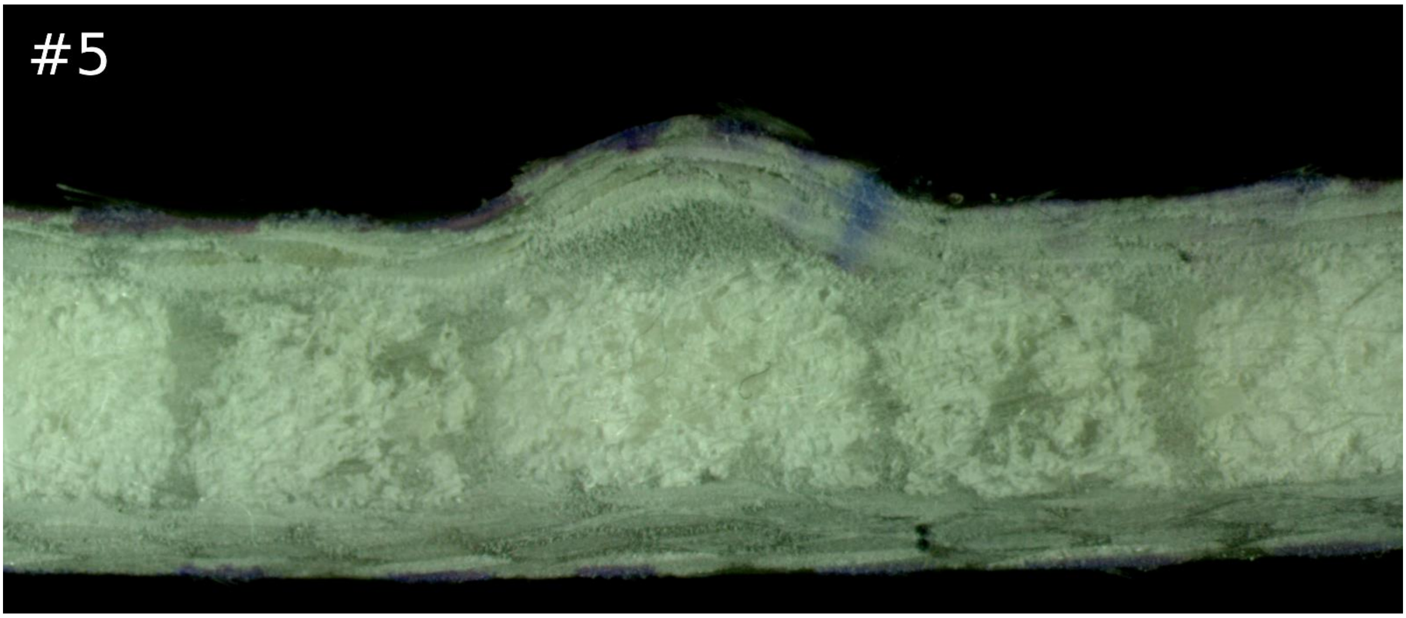

Figure A - 14: Wrinkle region #5 for test 3

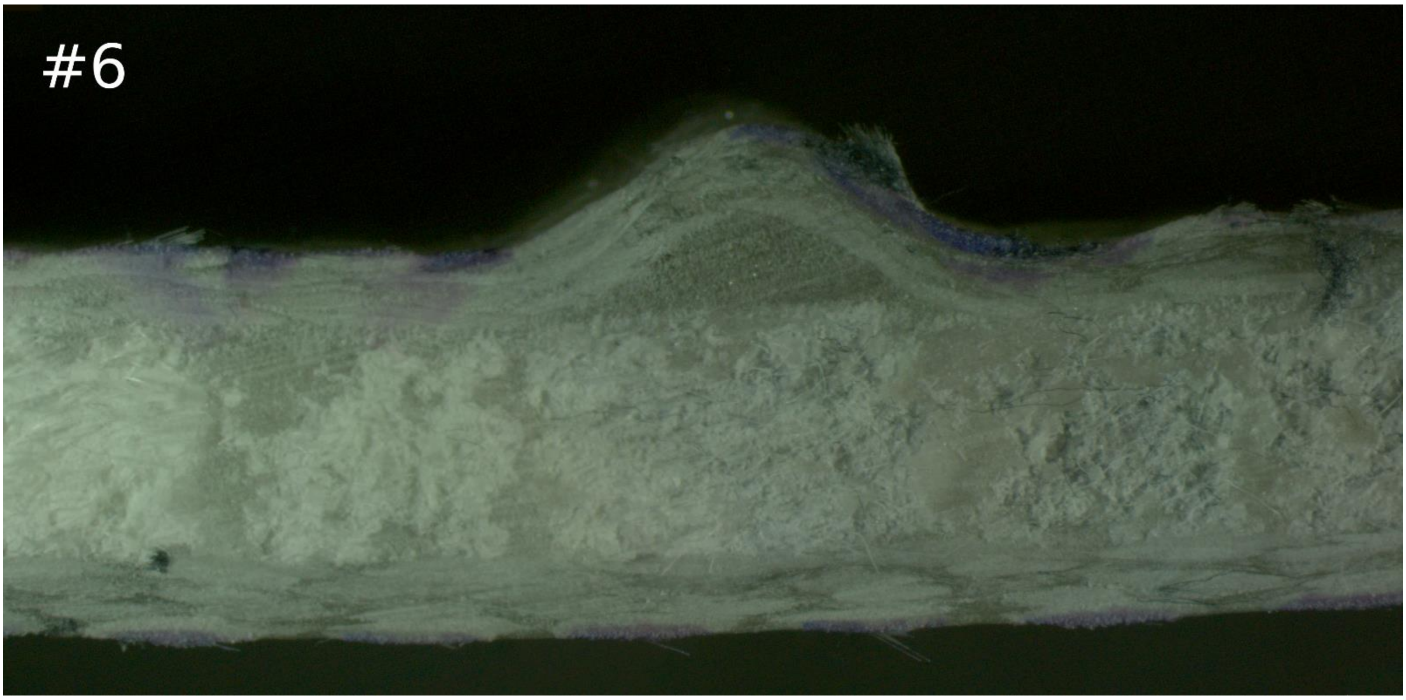

Figure A - 15: Wrinkle region #6 for test 3

Test 4:

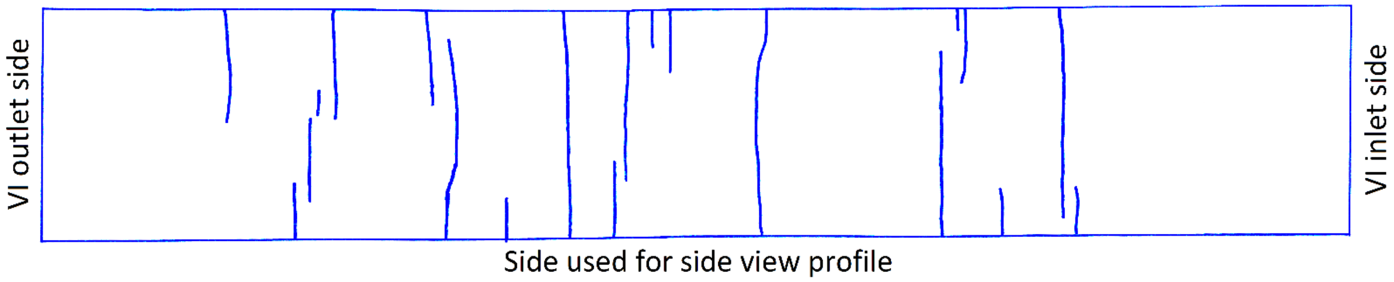

Figure A - 16: top view test 4

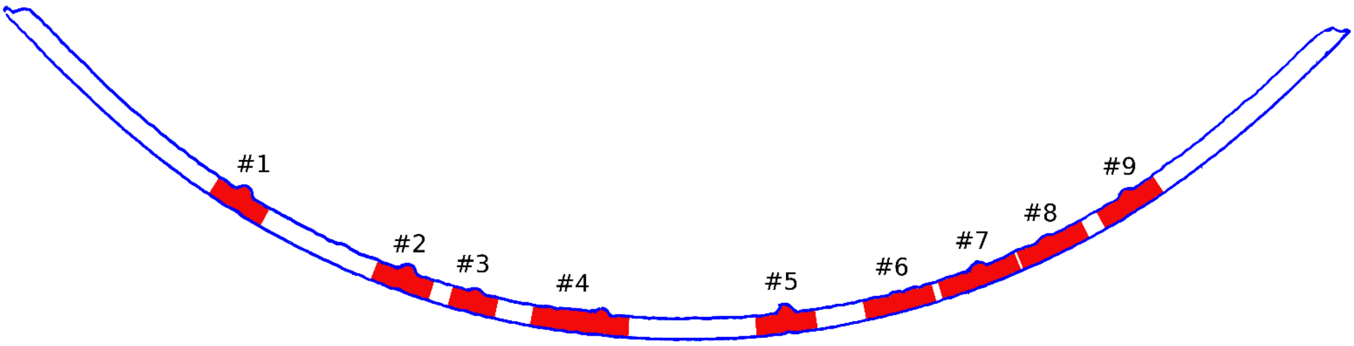

Figure A - 17: Side view test 4

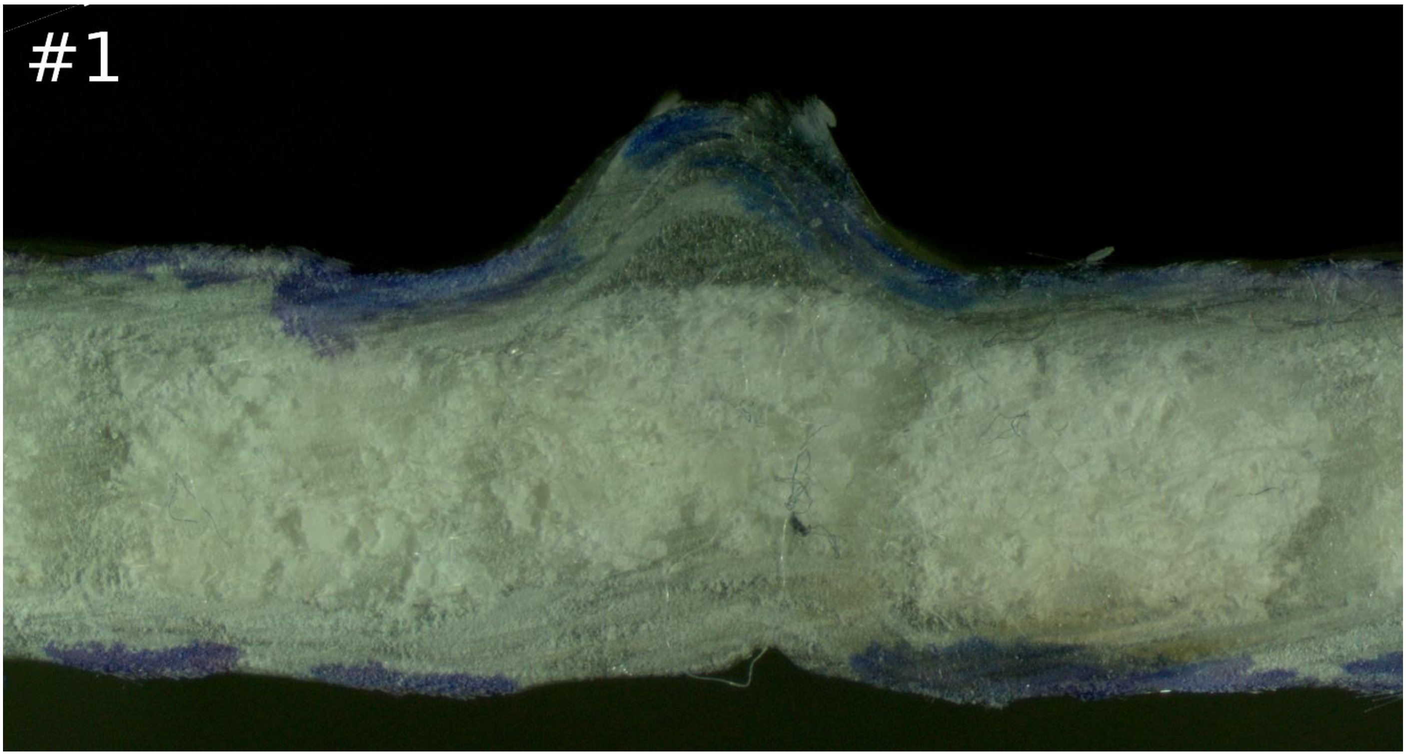

Figure A - 18: Wrinkle region #1 for test 4

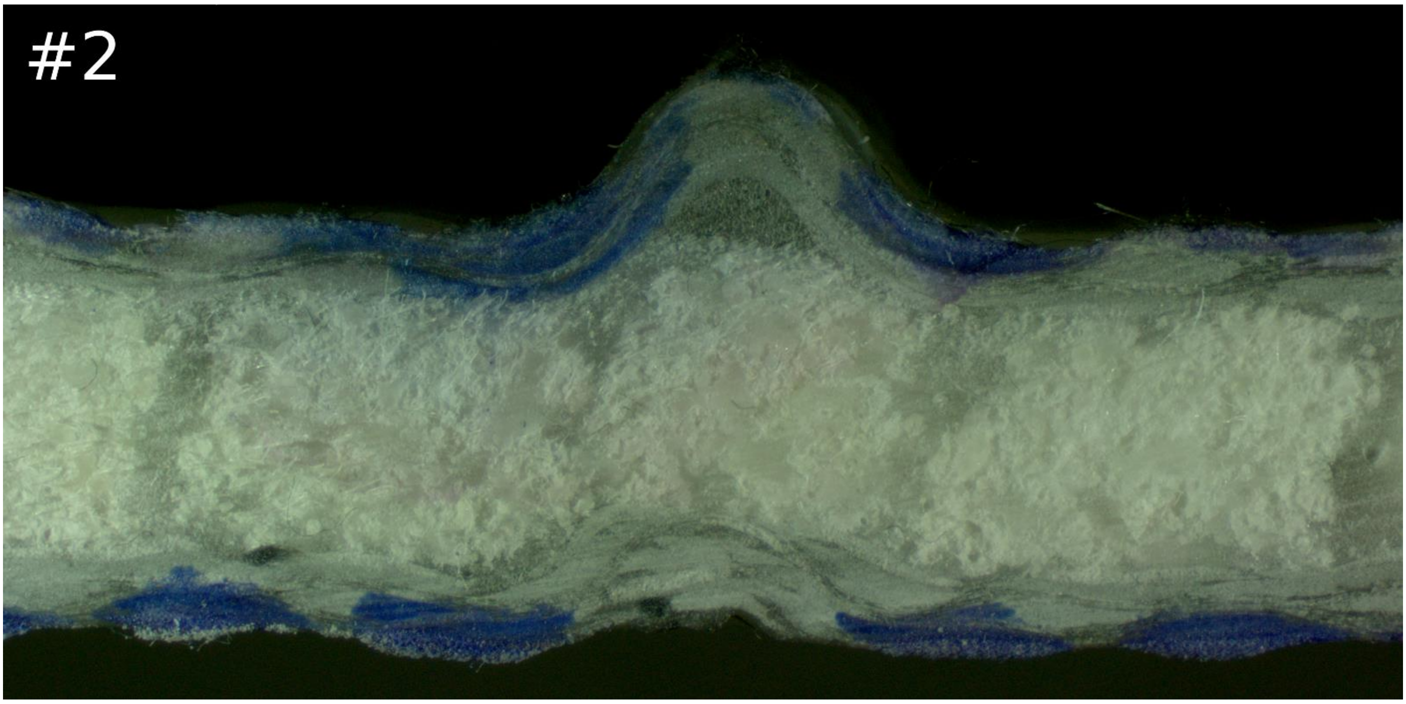

Figure A - 19: Wrinkle region #2 for test 4

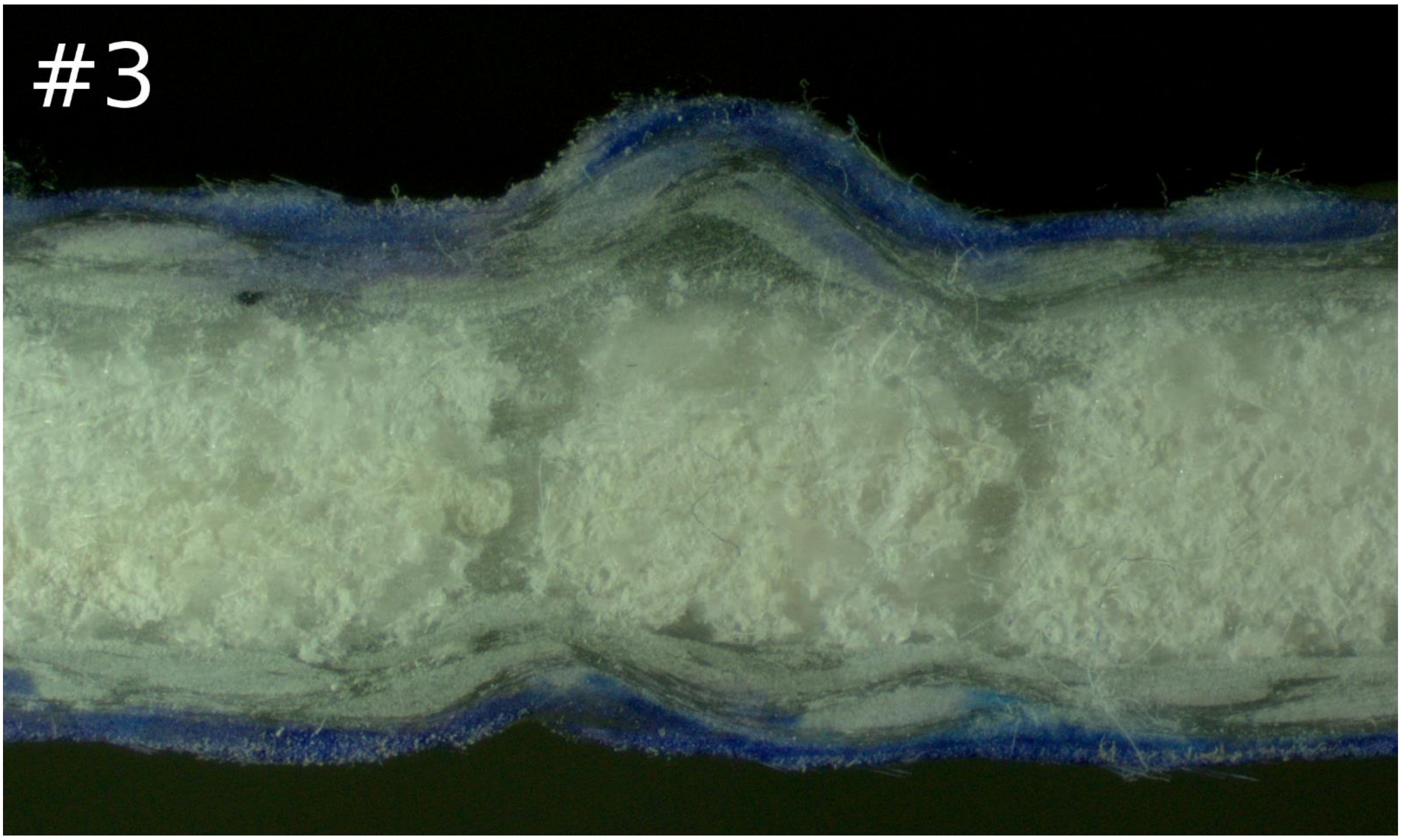

Figure A - 20: Wrinkle region #3 for test 4

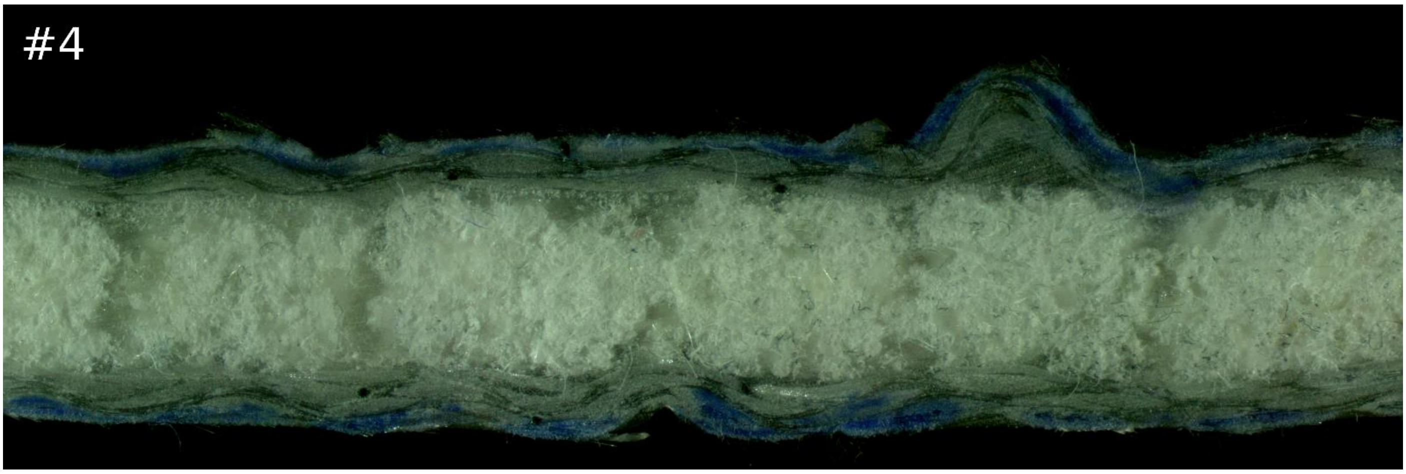

Figure A - 21: Wrinkle region #4 for test 4

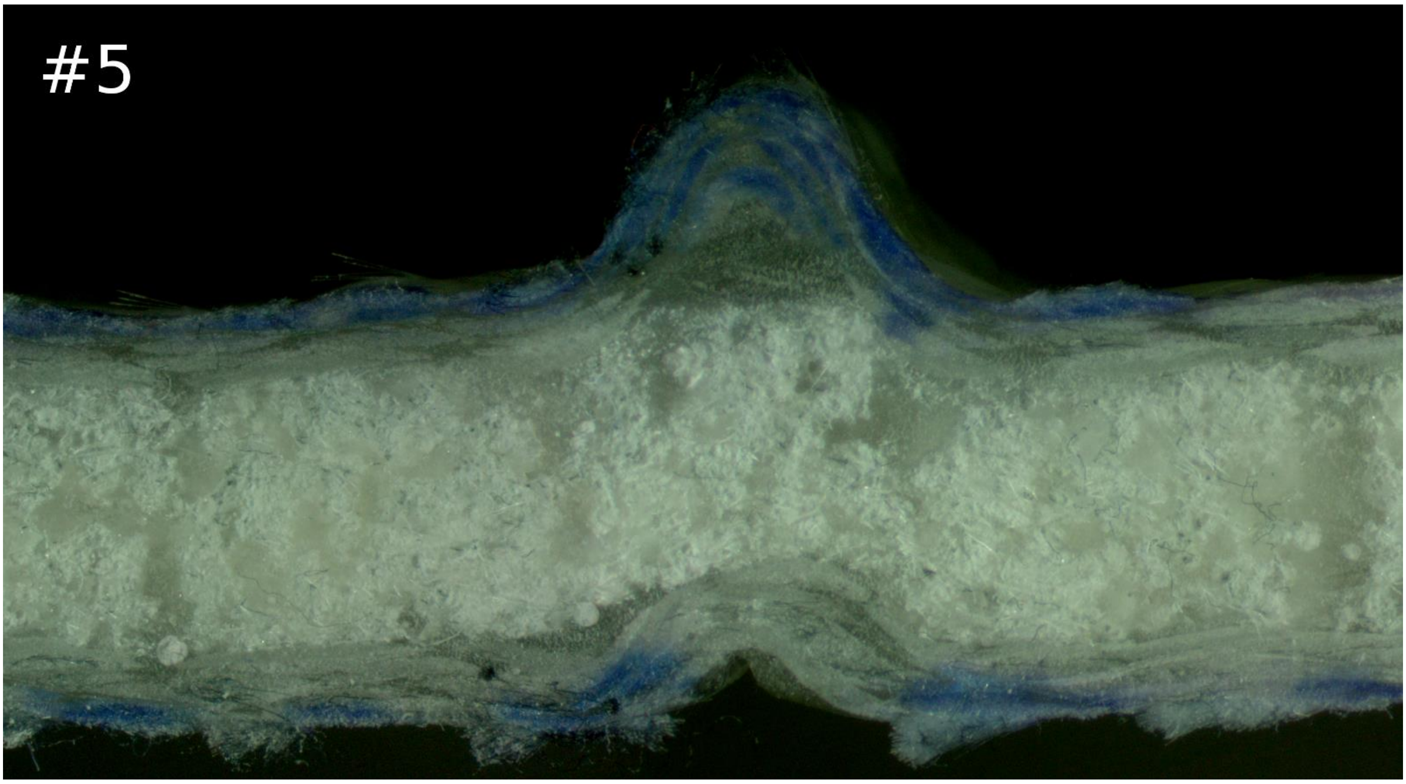

Figure A - 22: Wrinkle region #5 for test 4

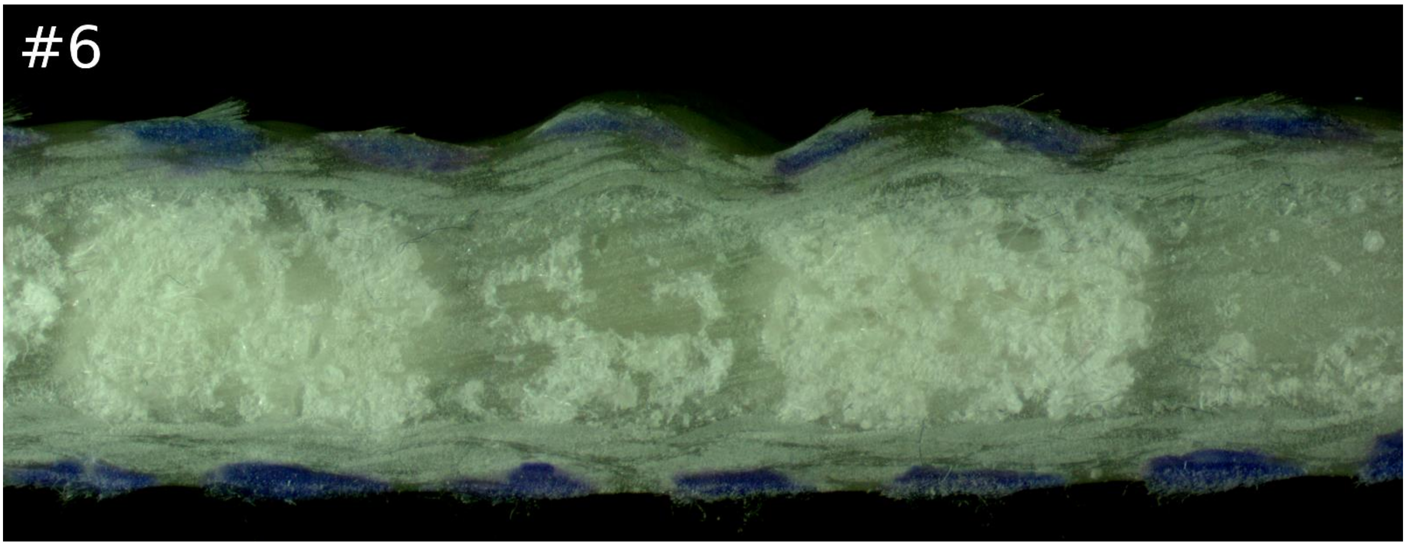

Figure A - 23: Wrinkle region #6 for test 4

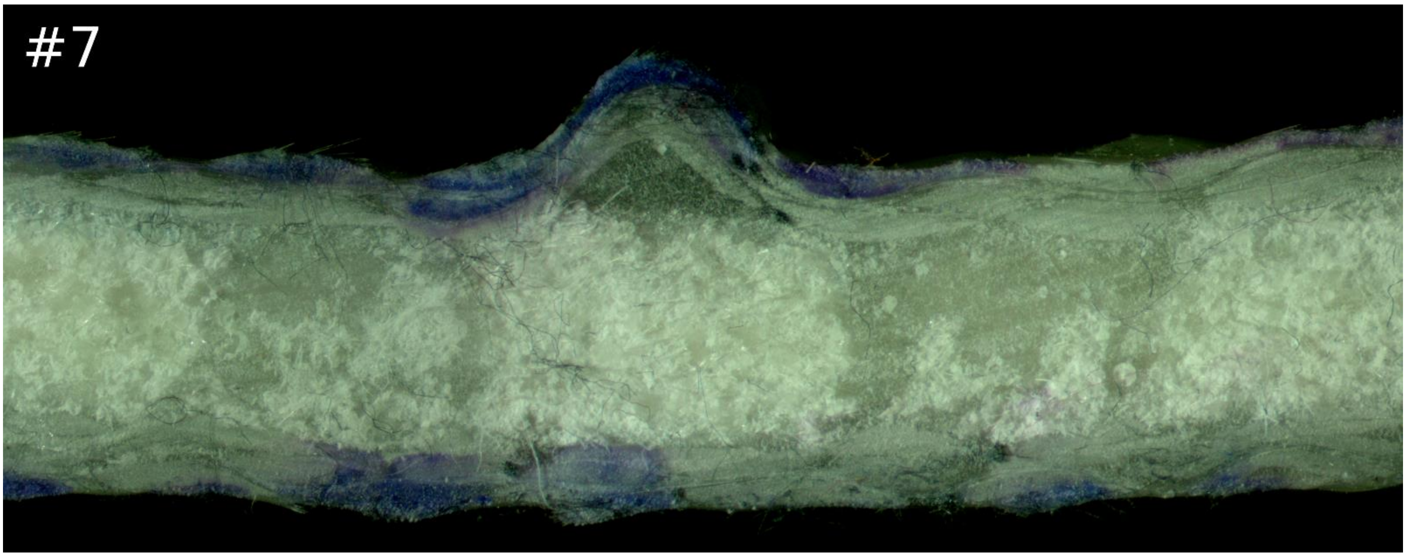

Figure A - 24: Wrinkle region #7 for test 4

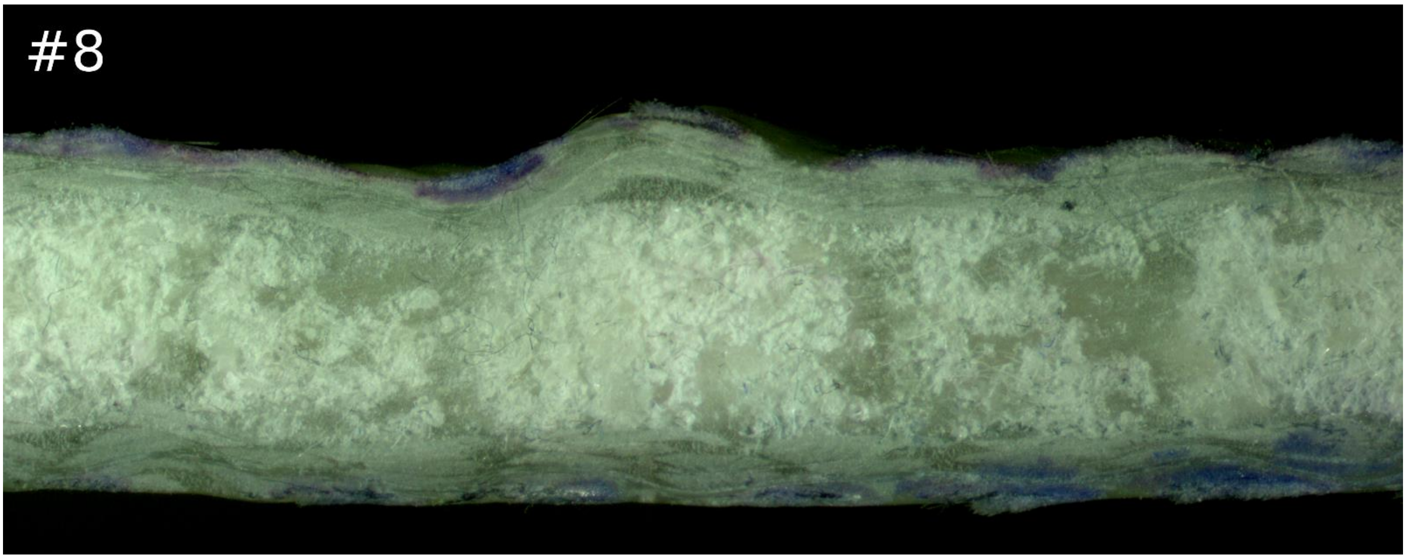

Figure A - 25: Wrinkle region #8 for test 4

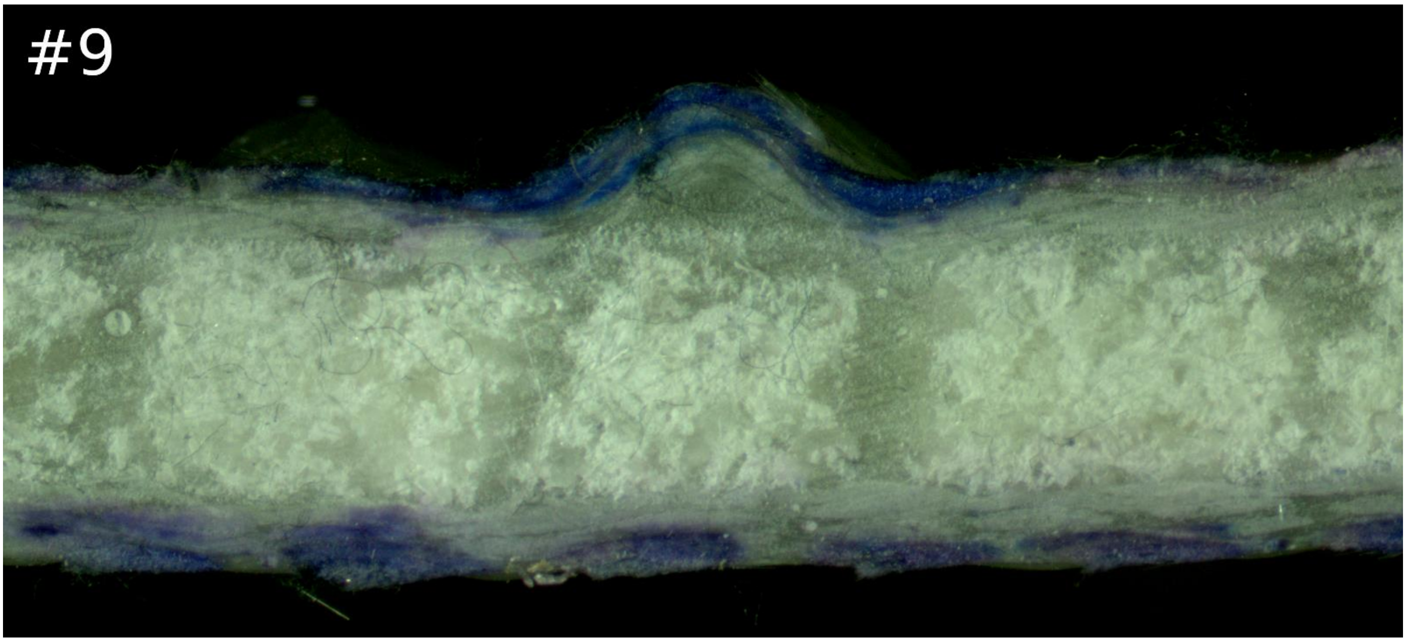

Figure A - 26: Wrinkle region #9 for test 4

Test 5:

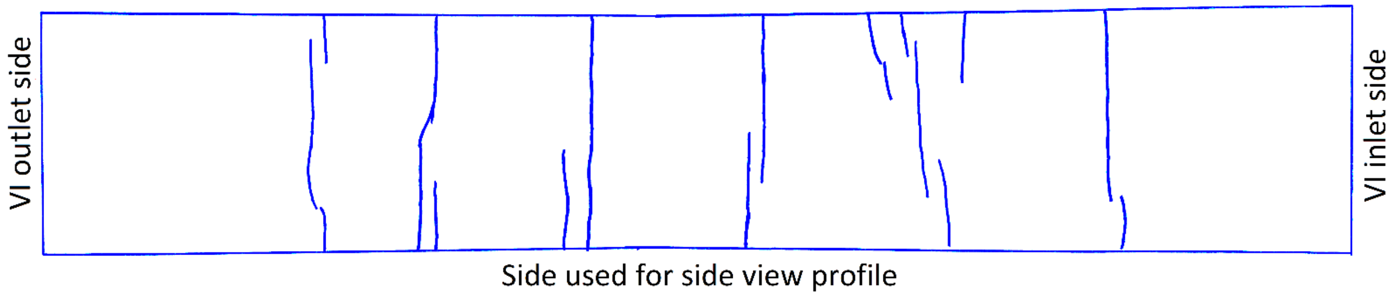

Figure A - 27: Top view test 5

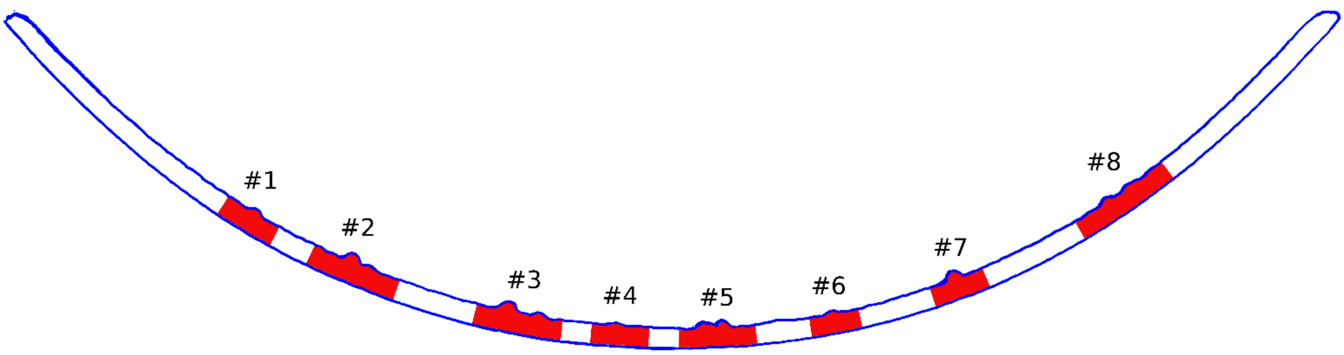

Figure A - 28: Side view test 5

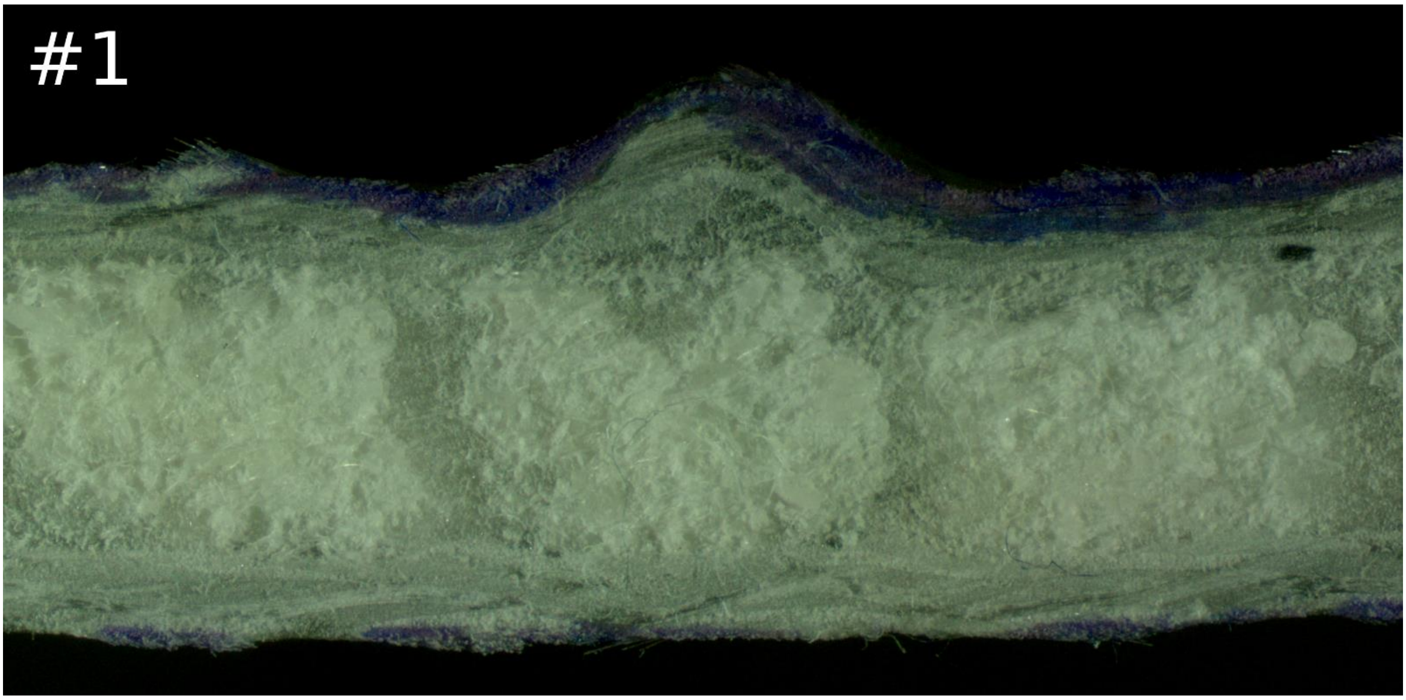

Figure A - 29: Wrinkle region #1 for test 5

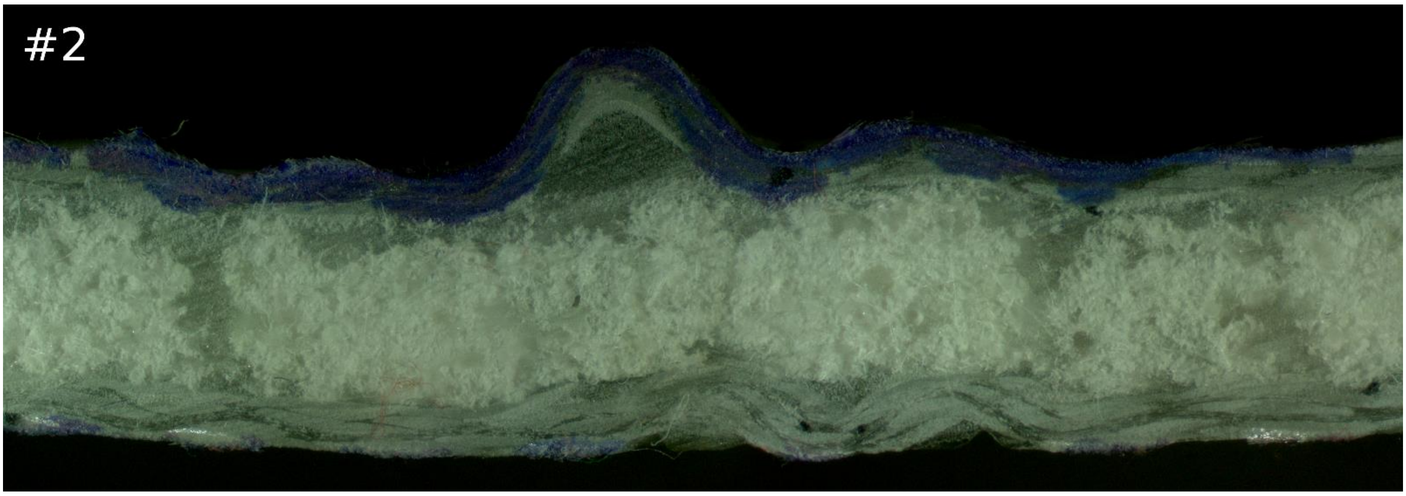

Figure A - 30: Wrinkle region #2 for test 5

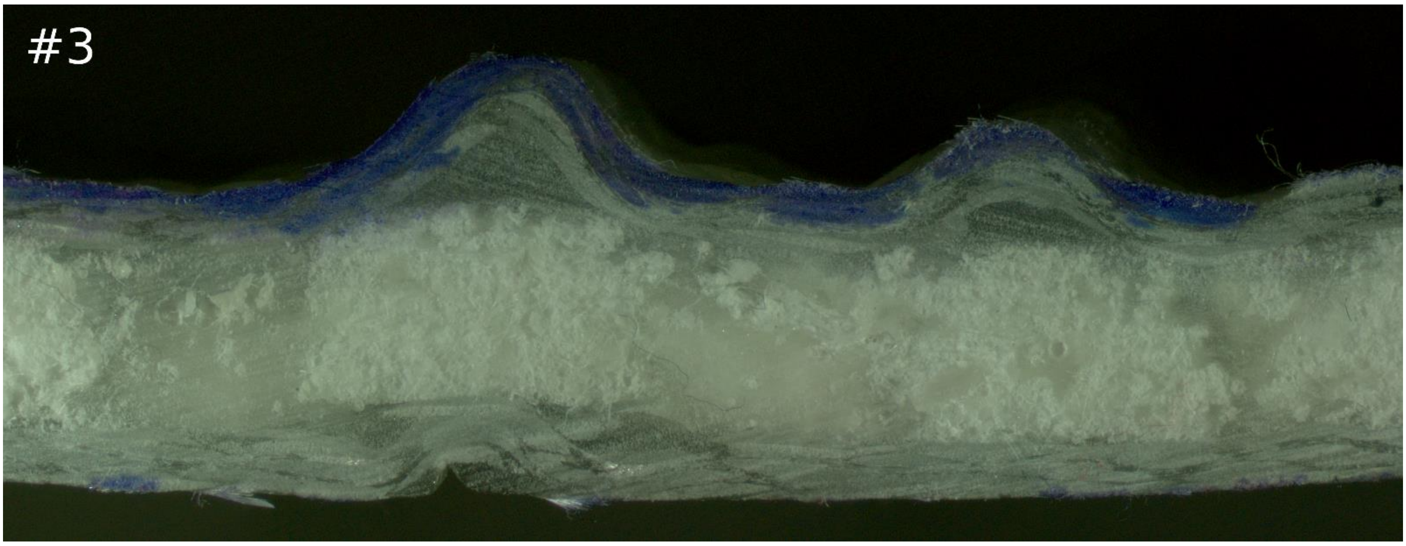

Figure A - 31: Wrinkle region #3 for test 5

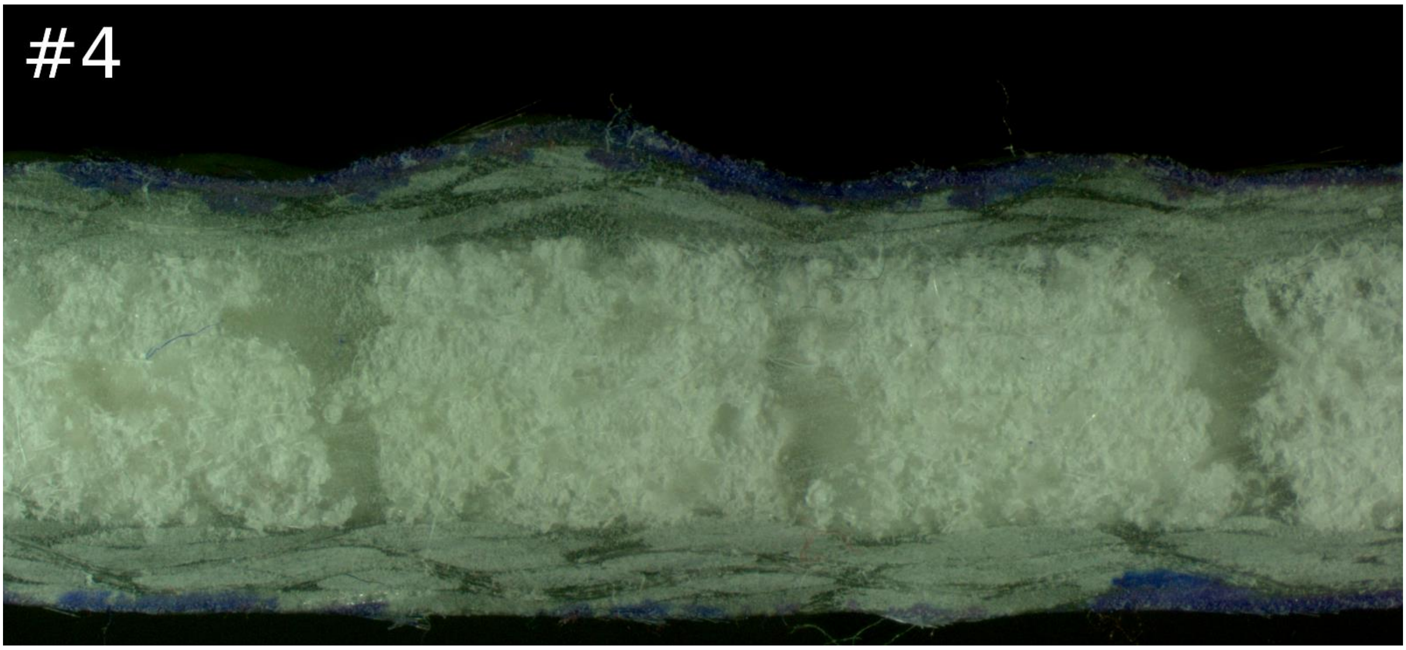

Figure A - 32: Wrinkle region #4 for test 5

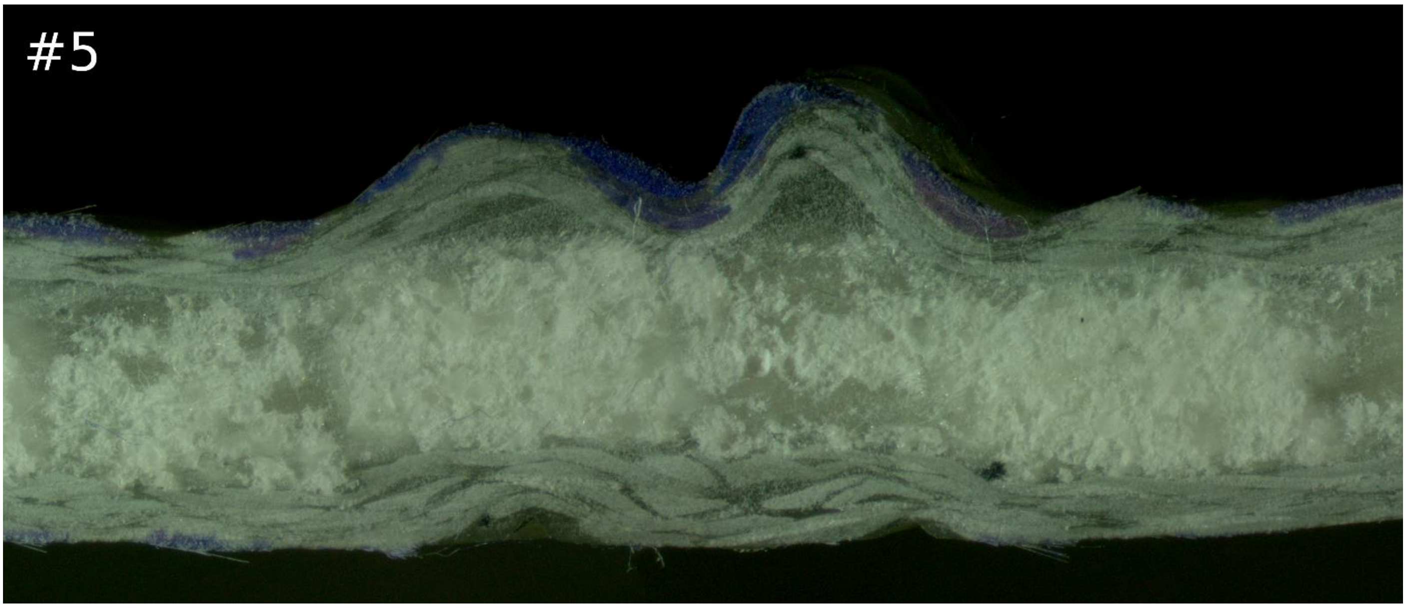

Figure A - 33: Wrinkle region #5 for test 5

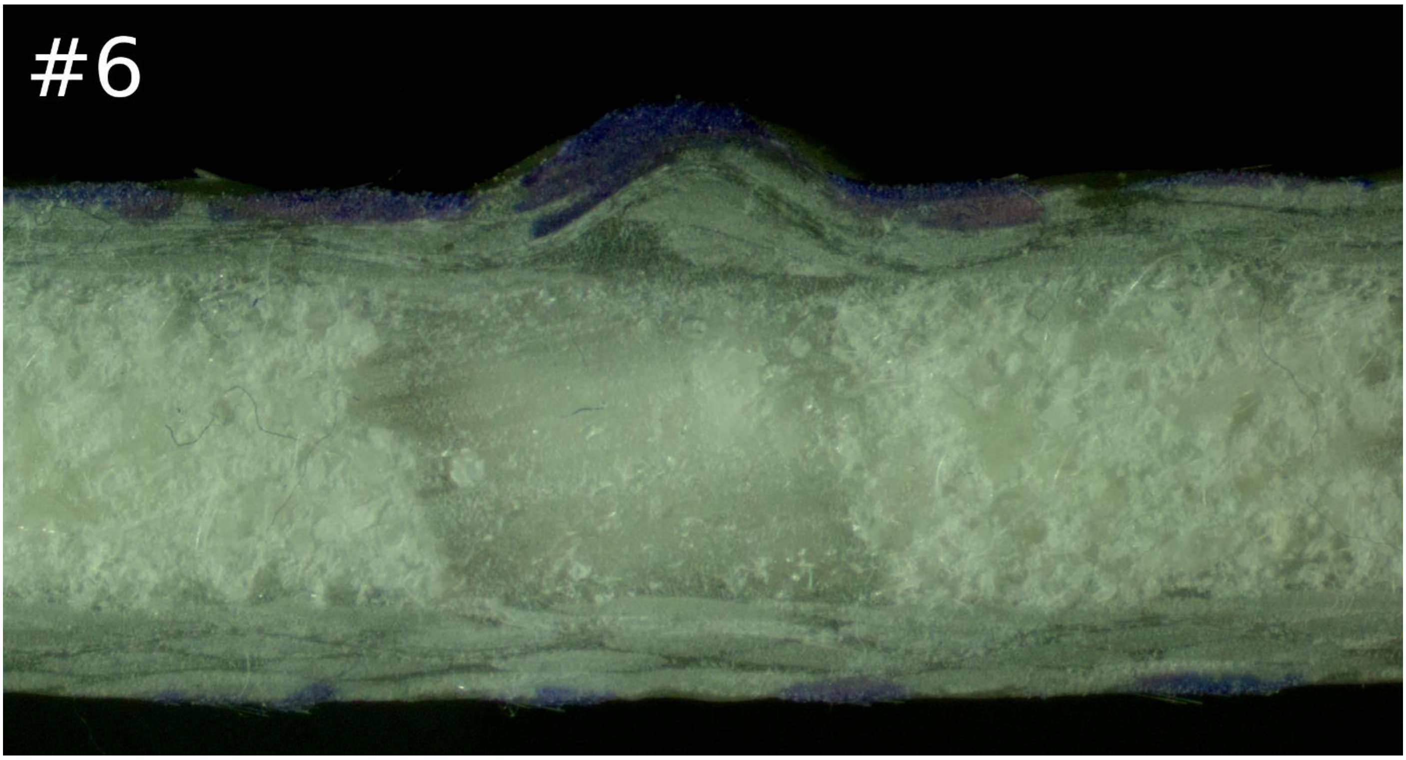

Figure A - 34: Wrinkle region #6 for test 5

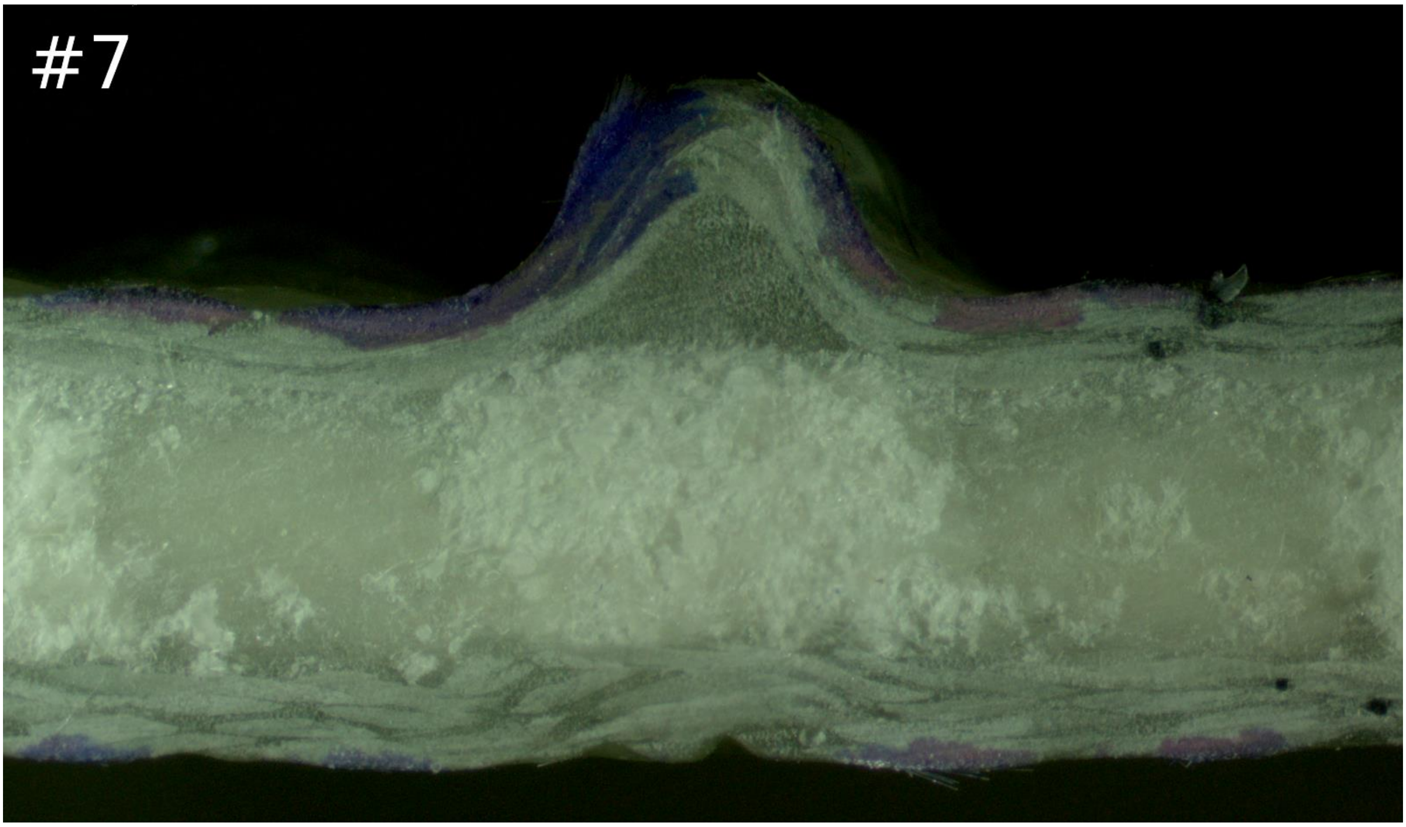

Figure A - 35: Wrinkle region #7 for test 5

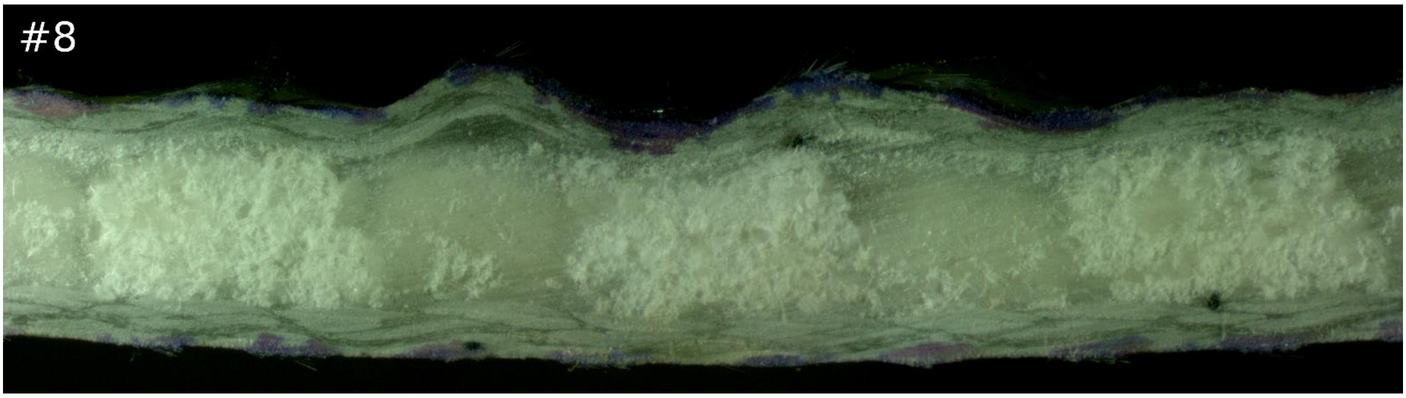

Figure A - 36: Wrinkle region #8 for test 5

Test 6:

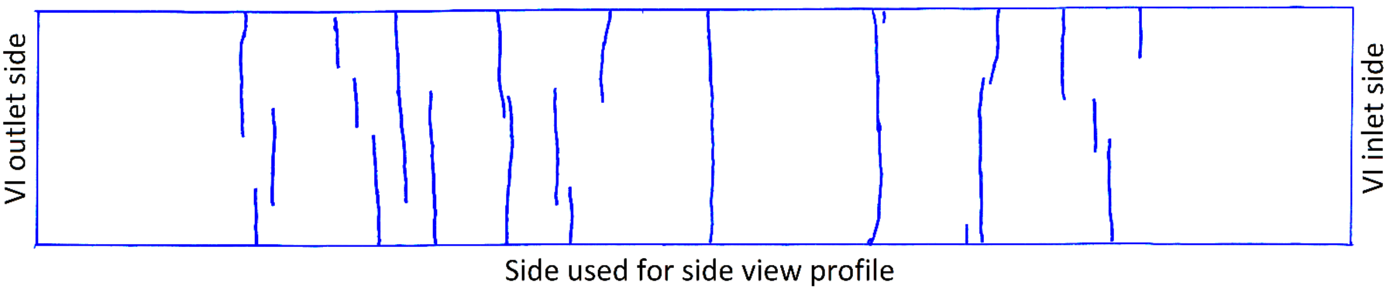

Figure A - 37: Top view test 6

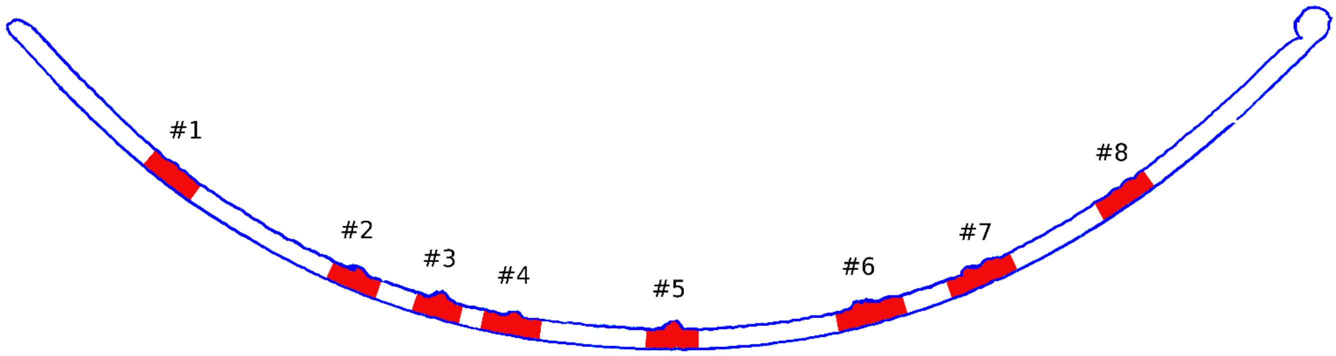

Figure A - 38: Side view test 6

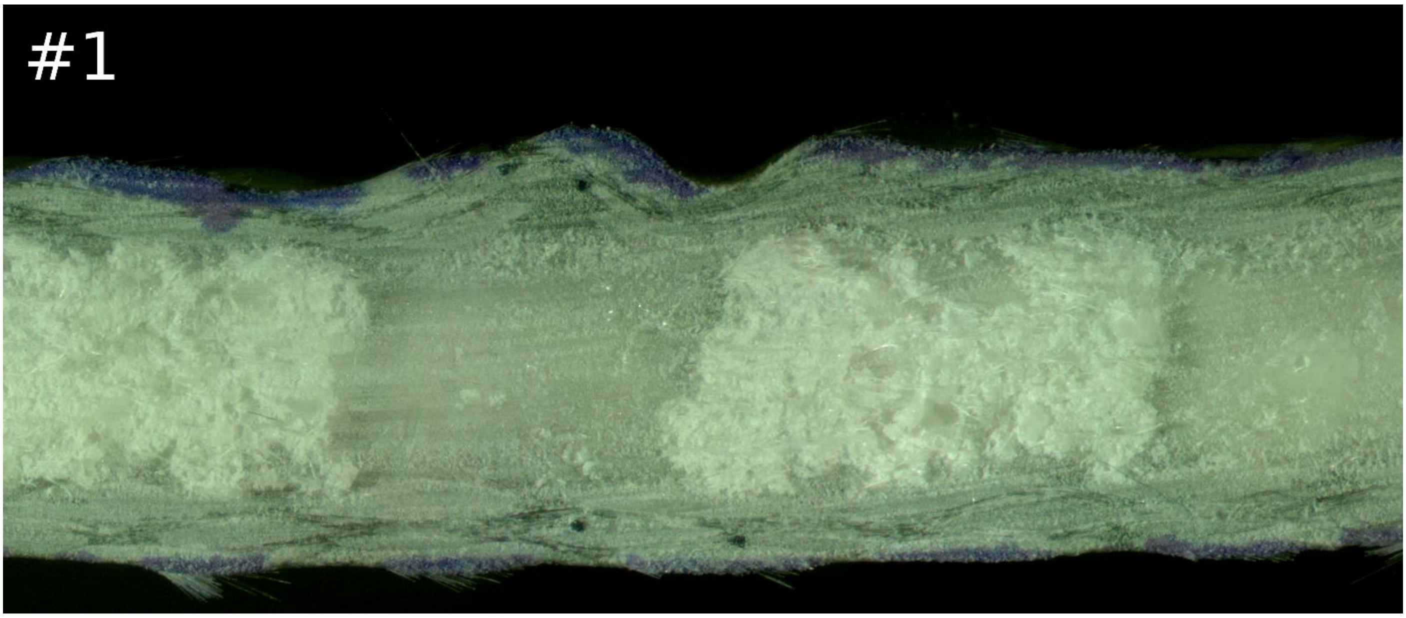

Figure A - 39: Wrinkle region #1 for test 6

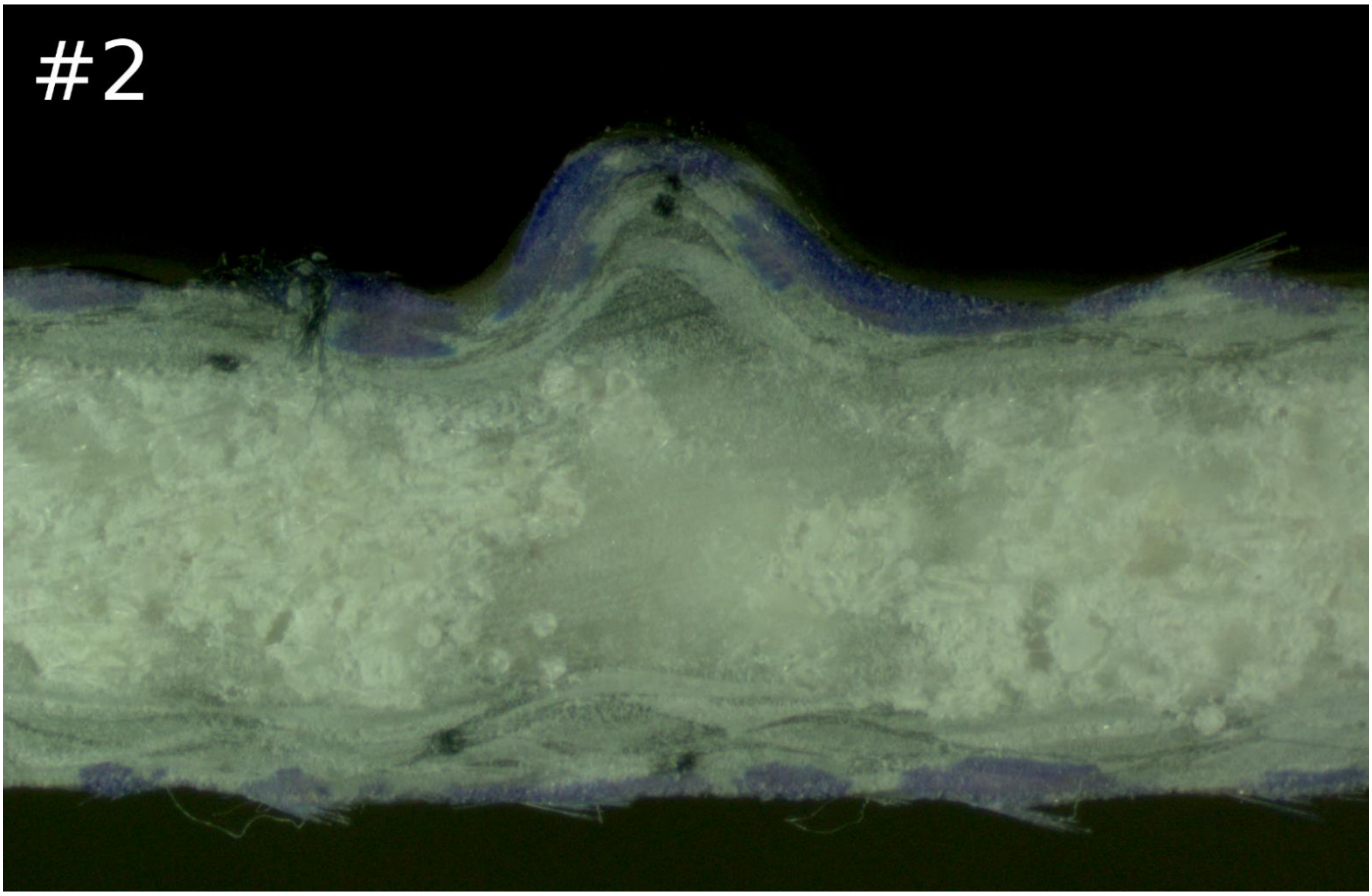

Figure A - 40: Wrinkle region #2 for test 6

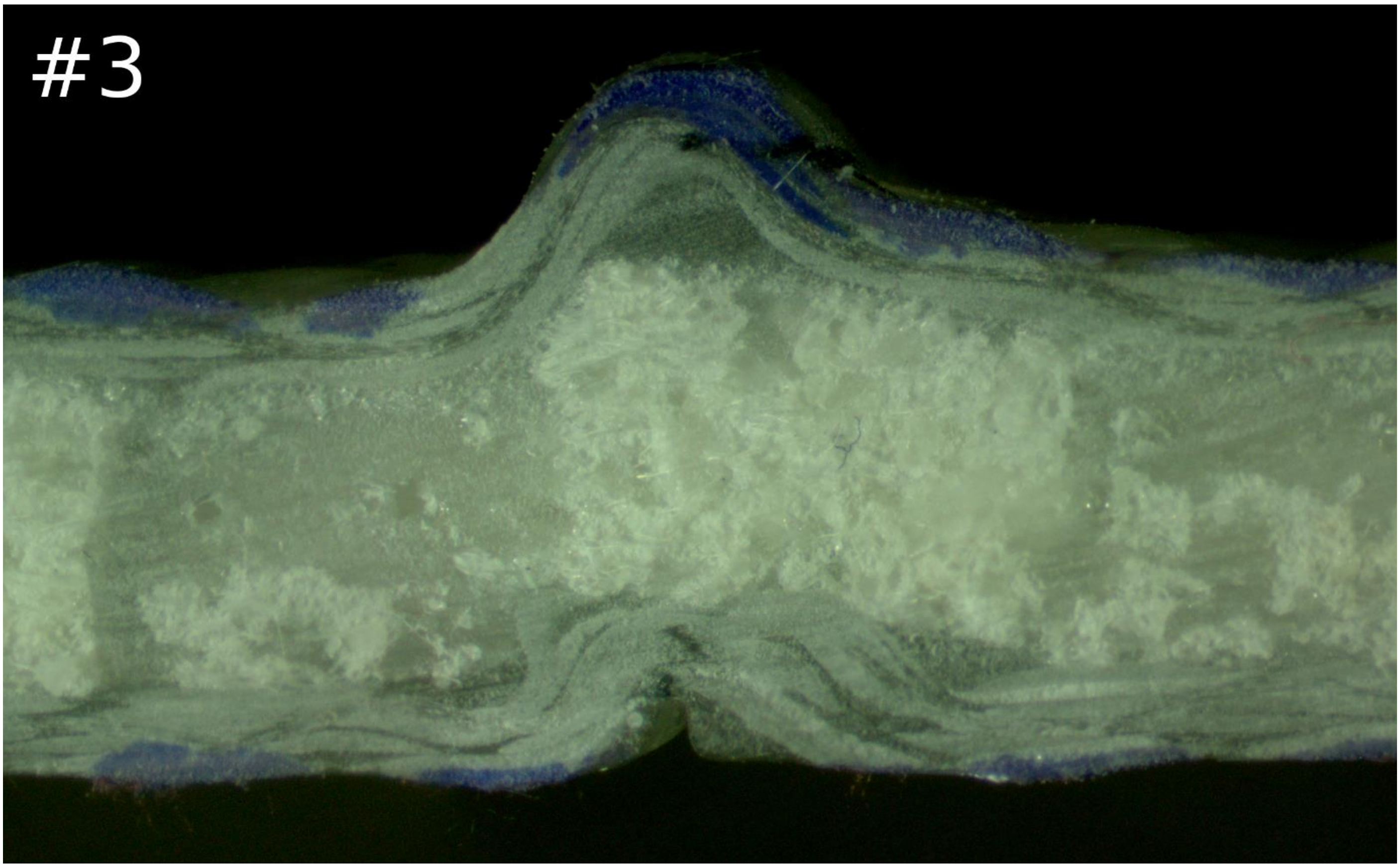

Figure A - 41: Wrinkle region #3 for test 6

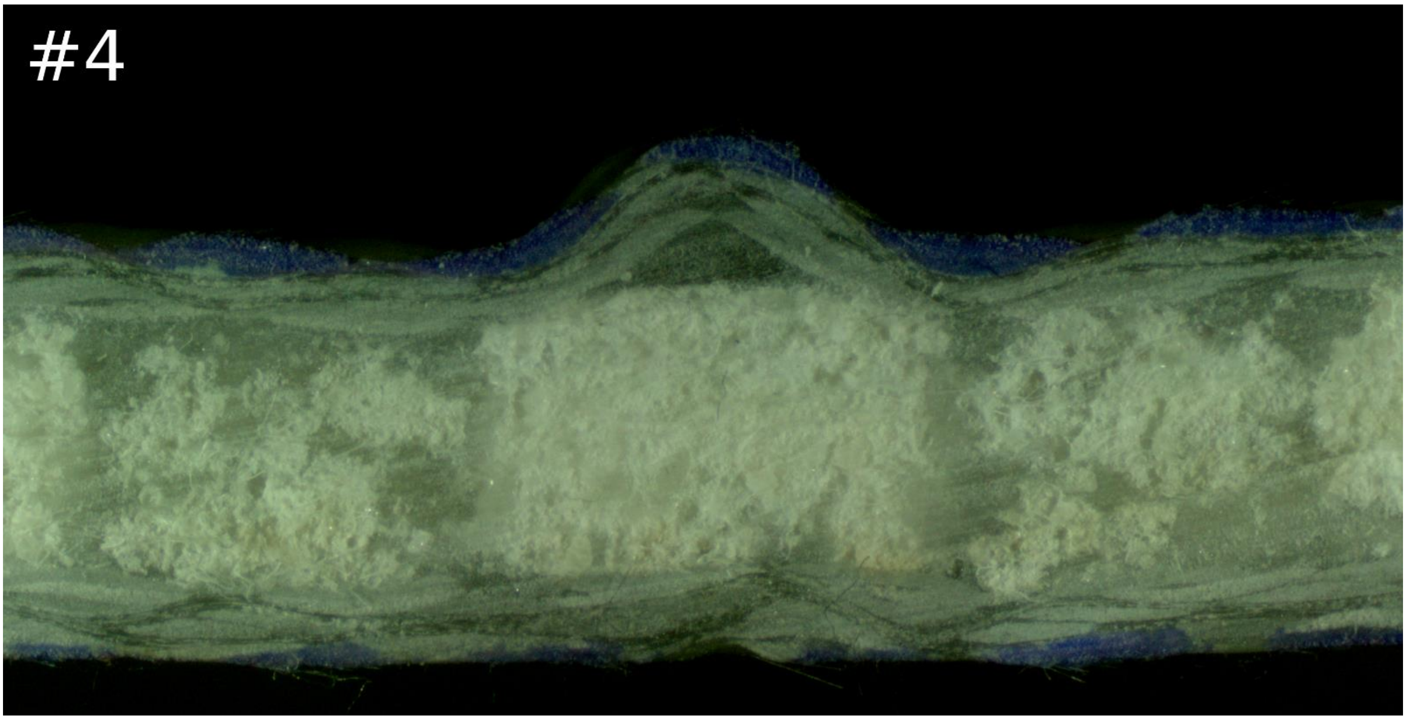

Figure A - 42: Wrinkle region #4 for test 6

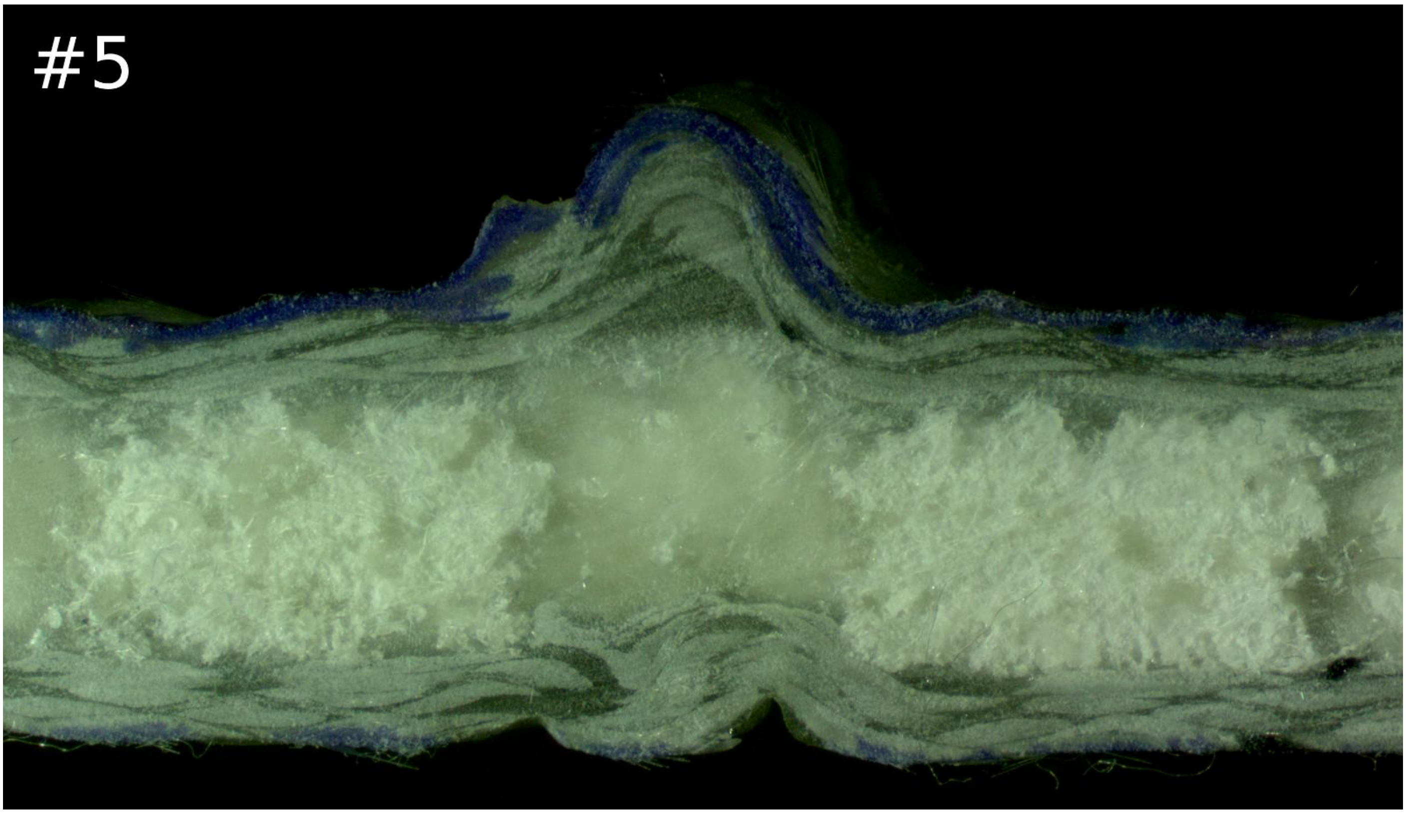

Figure A - 43: Wrinkle region #5 for test 6

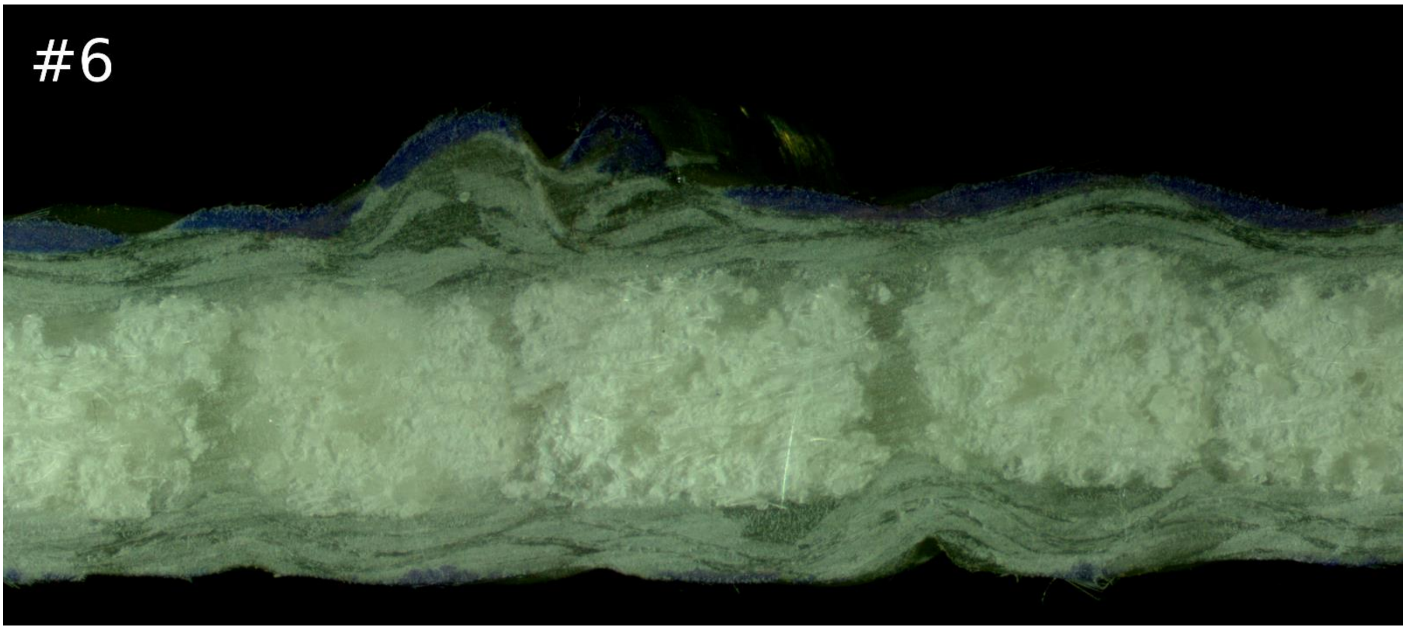

Figure A - 44: Wrinkle region #6 for test 6

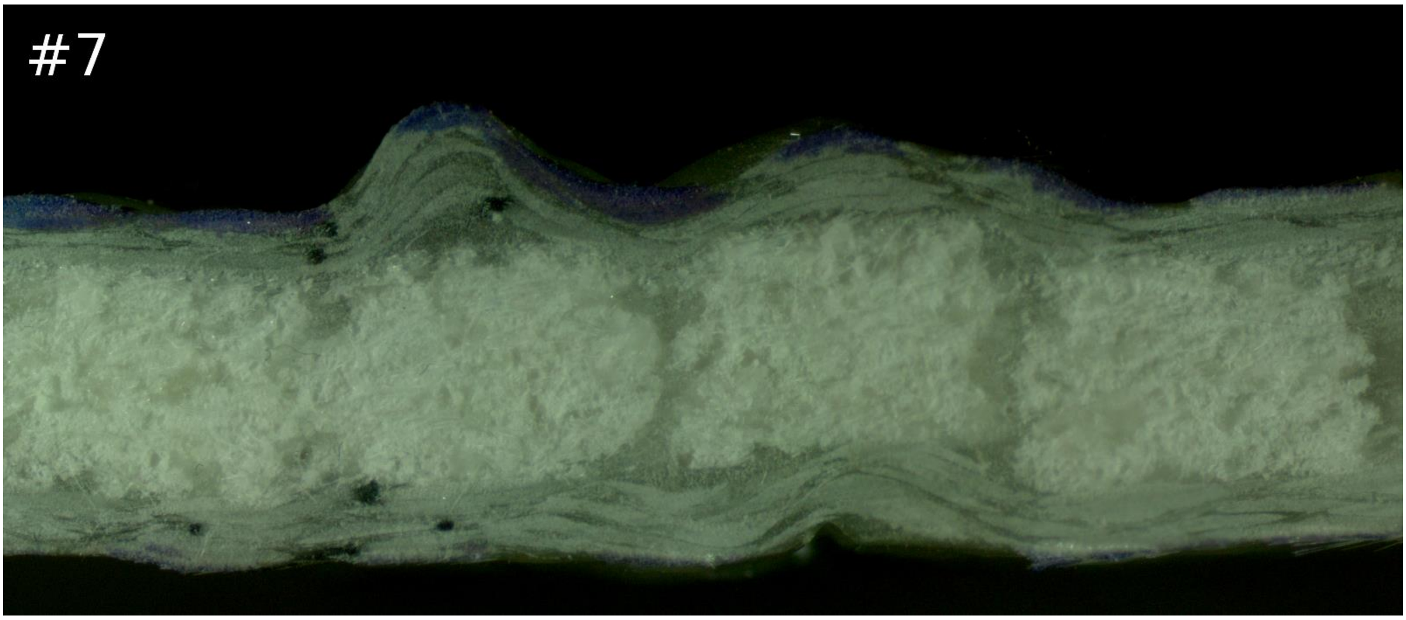

Figure A - 45: Wrinkle region #7 for test 6

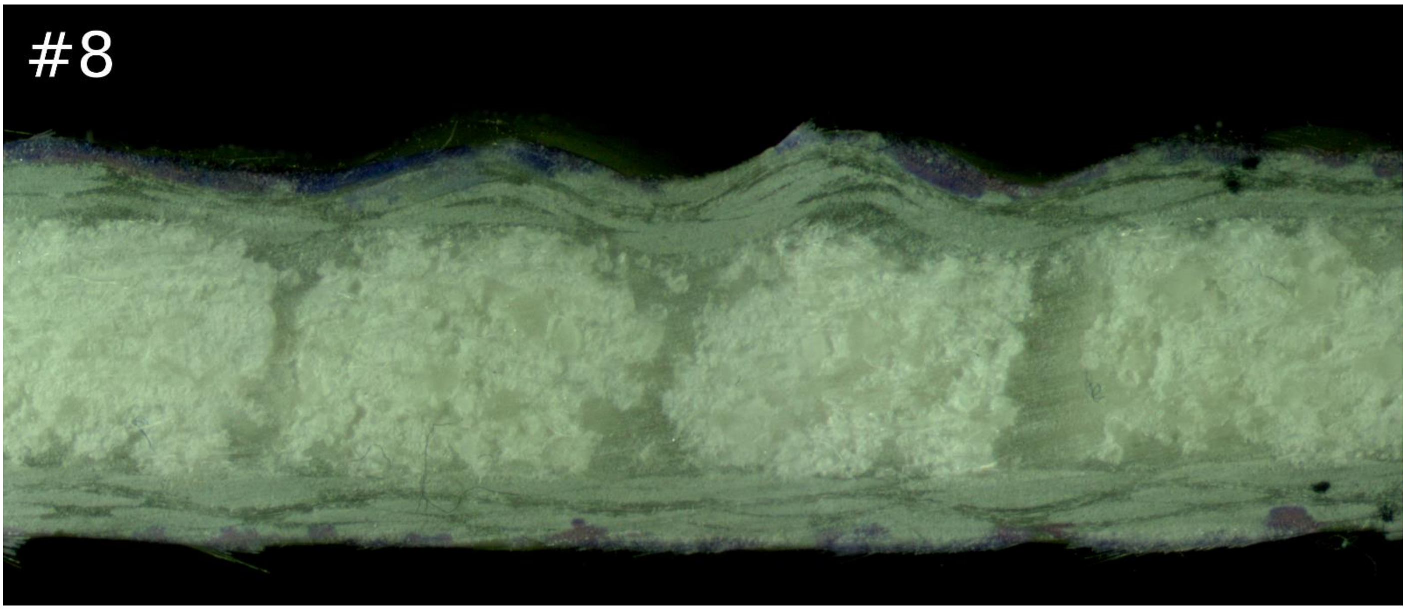

Figure A - 46: Wrinkle region #8 for test 6

Test 7:

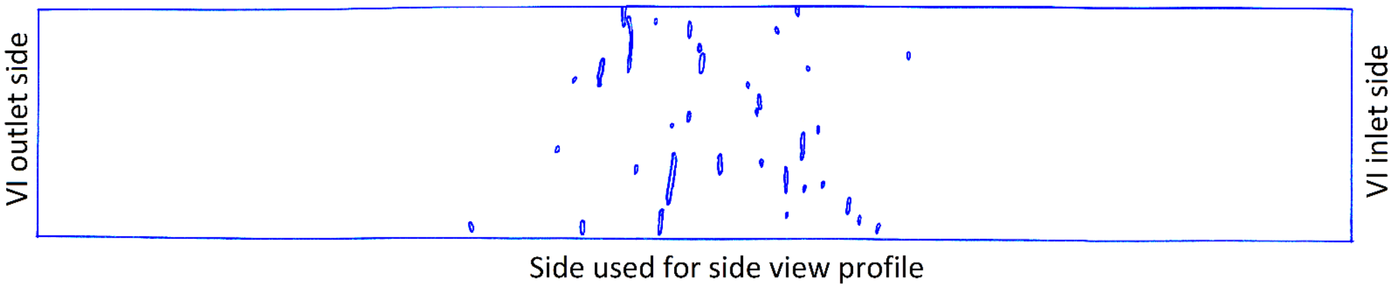

Figure A - 47: Top view test 7

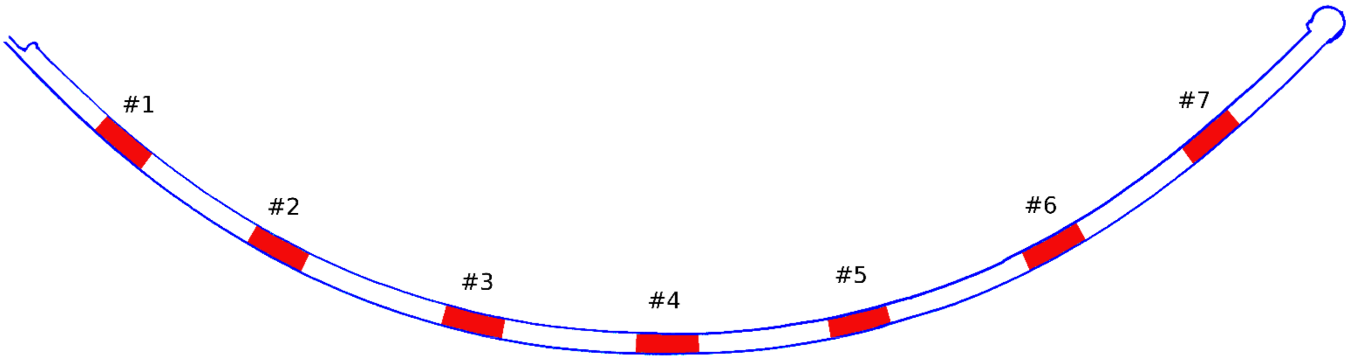

Figure A - 48: Side view test 7

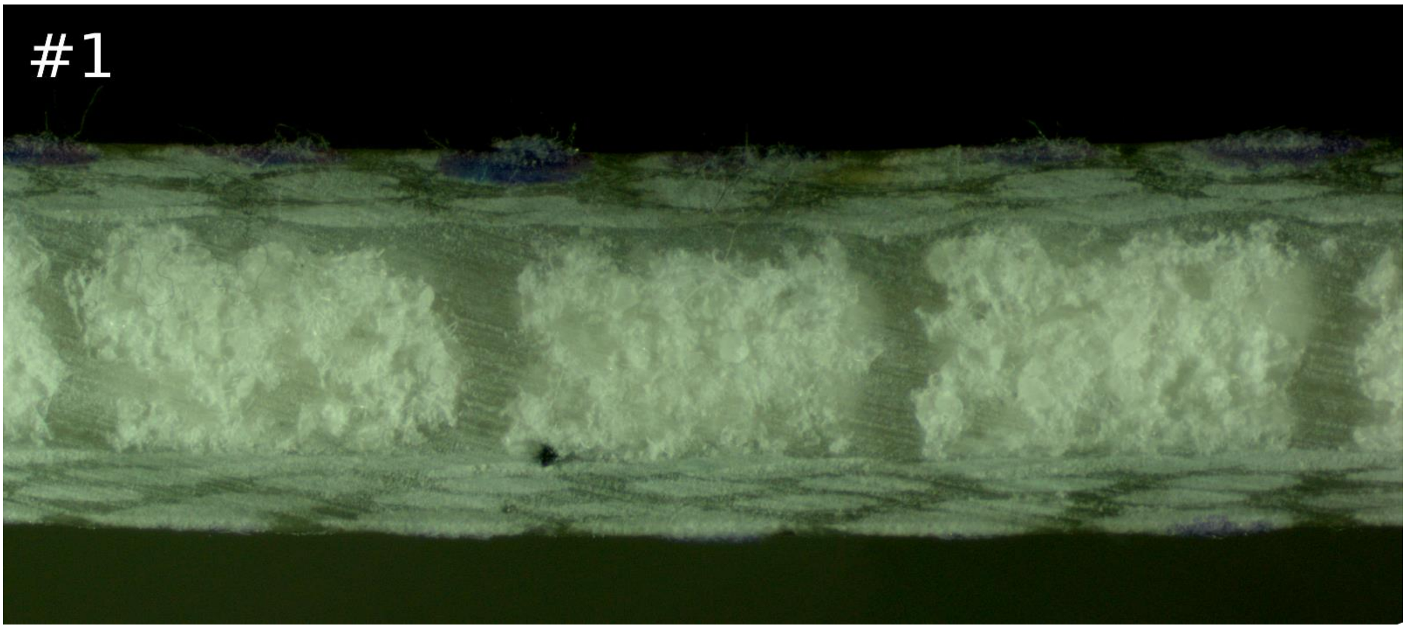

Figure A - 49: Panel region #1 for test 7

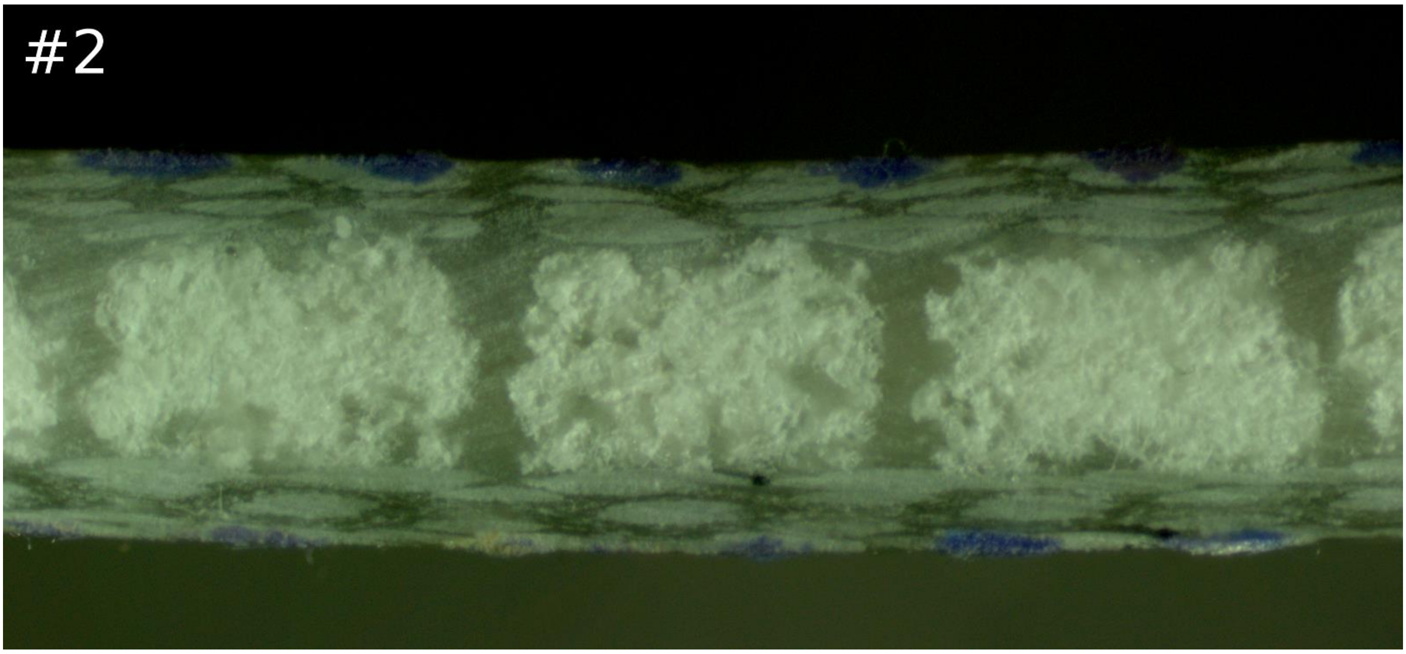

Figure A - 50: Panel region #2 for test 7

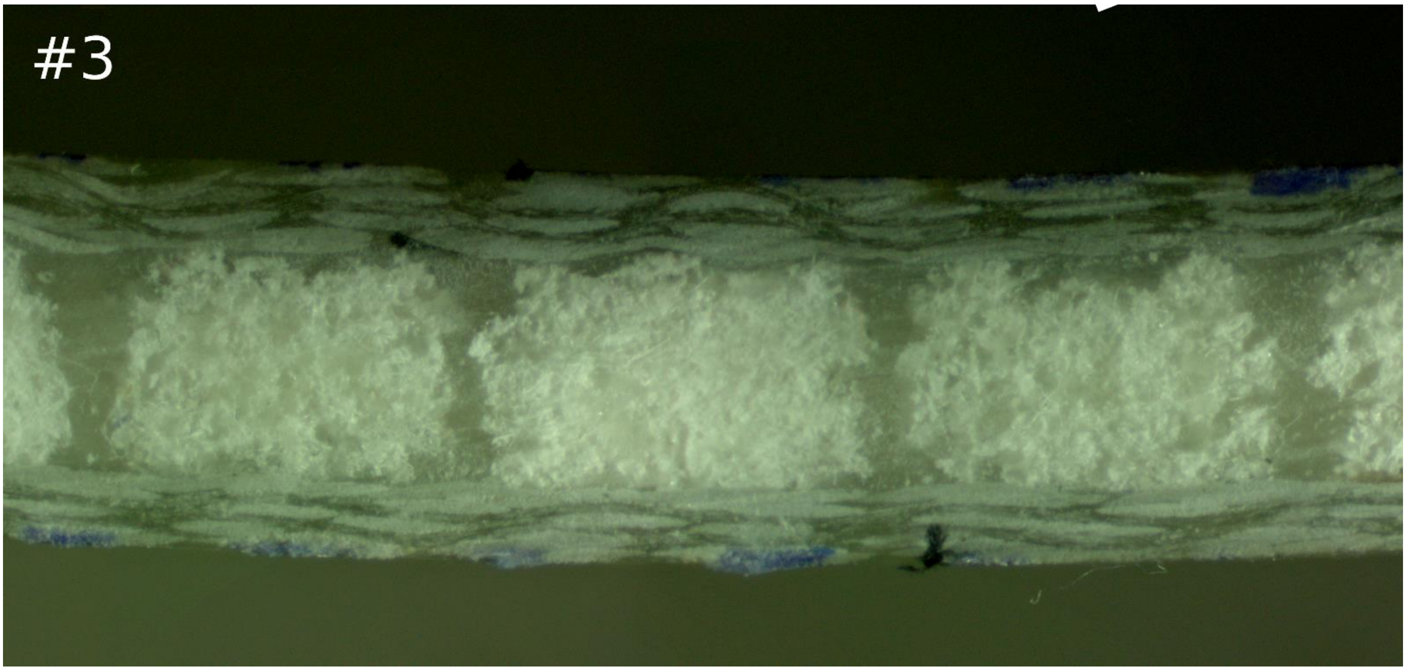

Figure A - 51: Panel region #3 for test 7

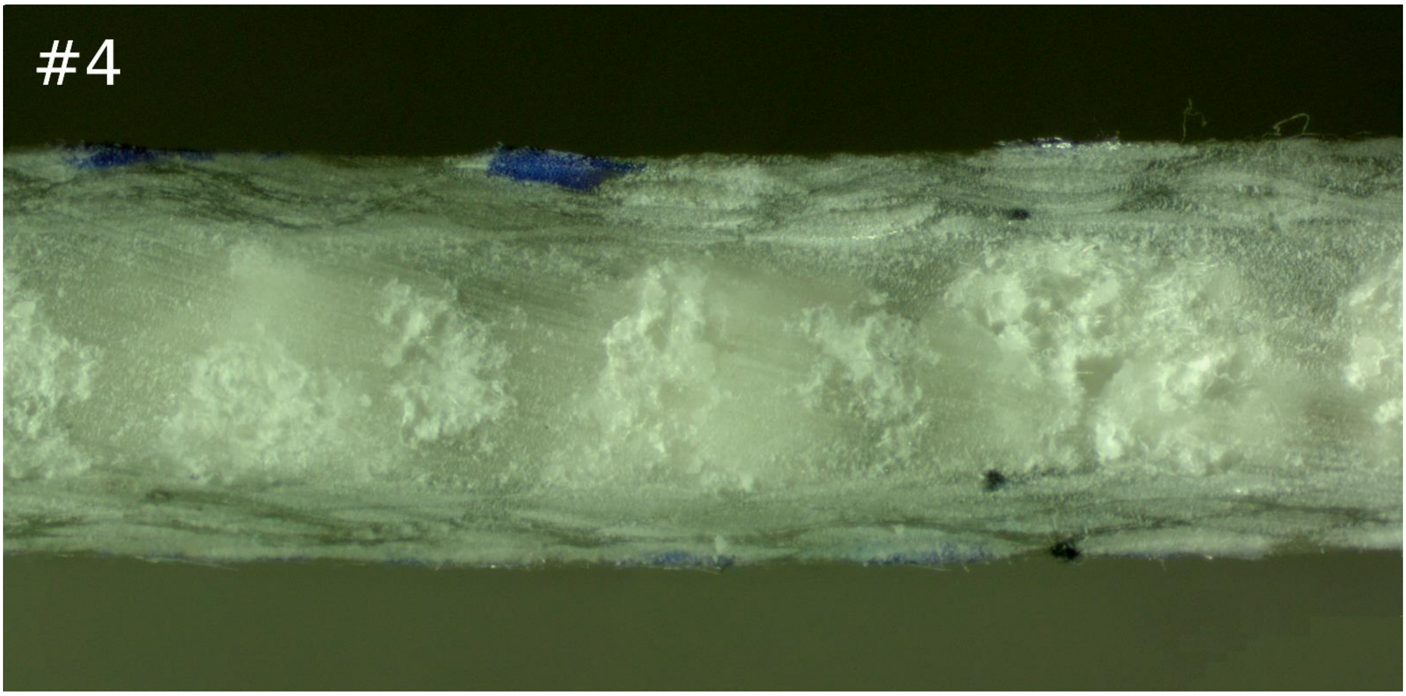

Figure A - 52: Panel region #4 for test 7

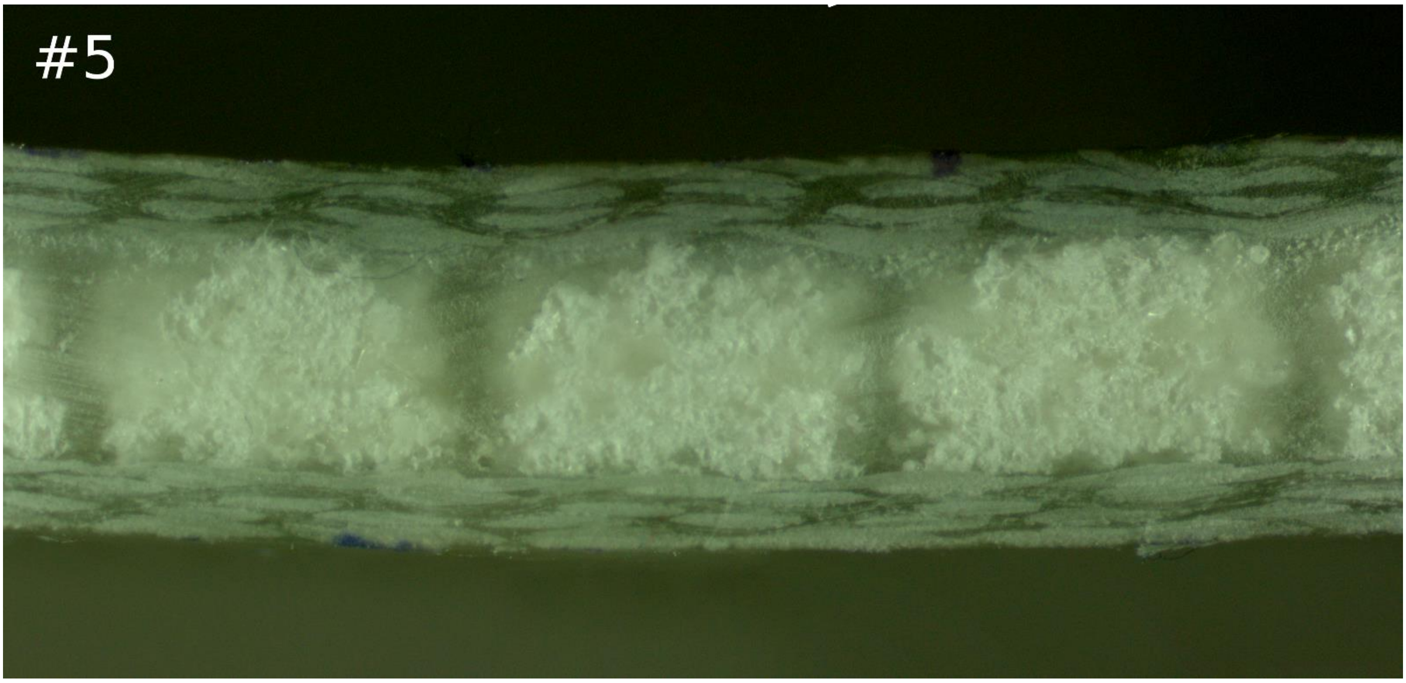

Figure A - 53: Panel region #5 for test 7

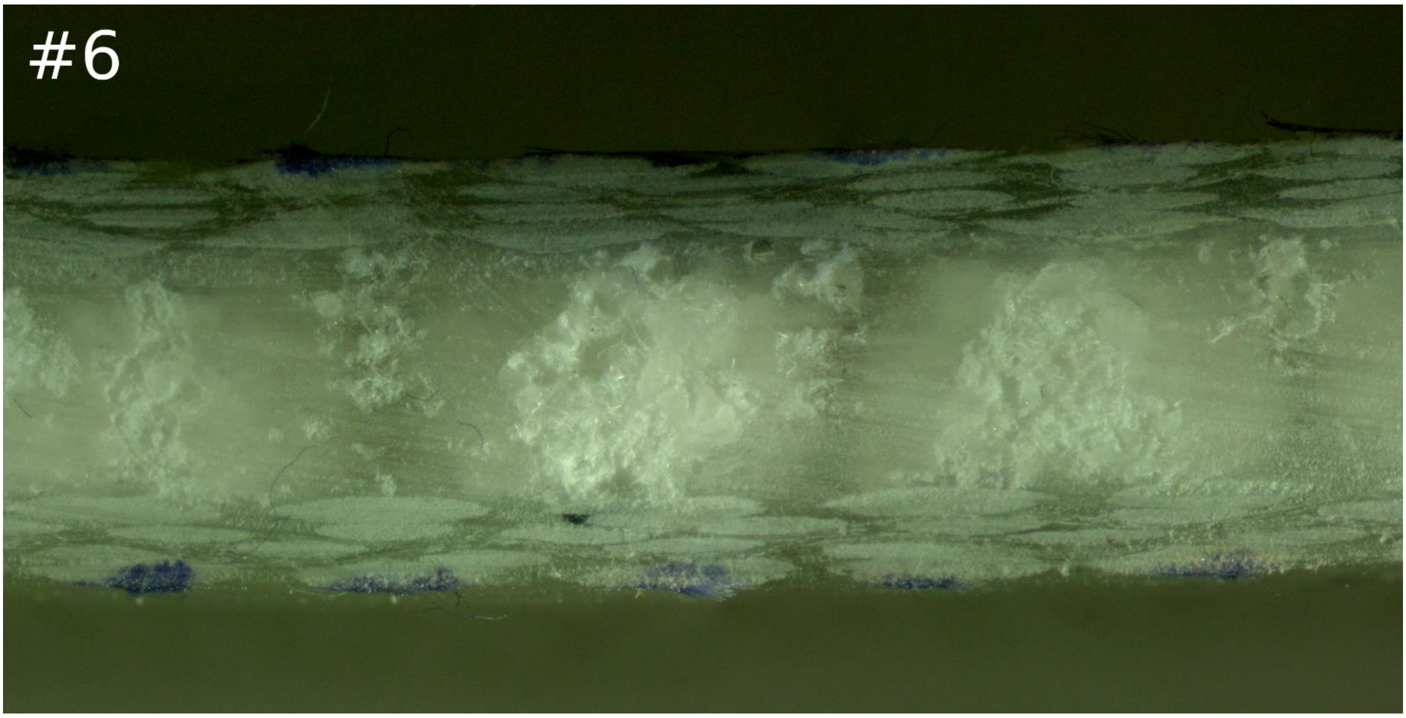

Figure A - 54: Panel region #6 for test 7

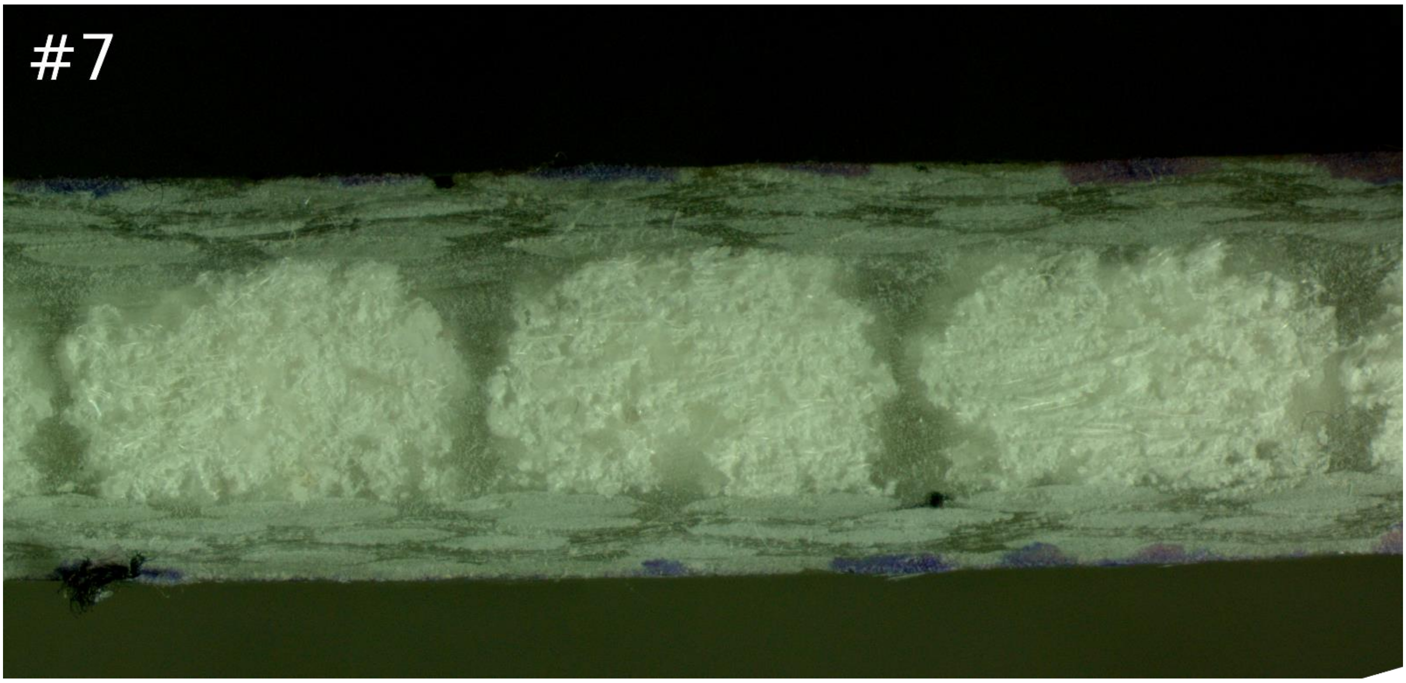

Figure A - 55: Panel region #7 for test 7

Appendix B / Radius of a circle segment

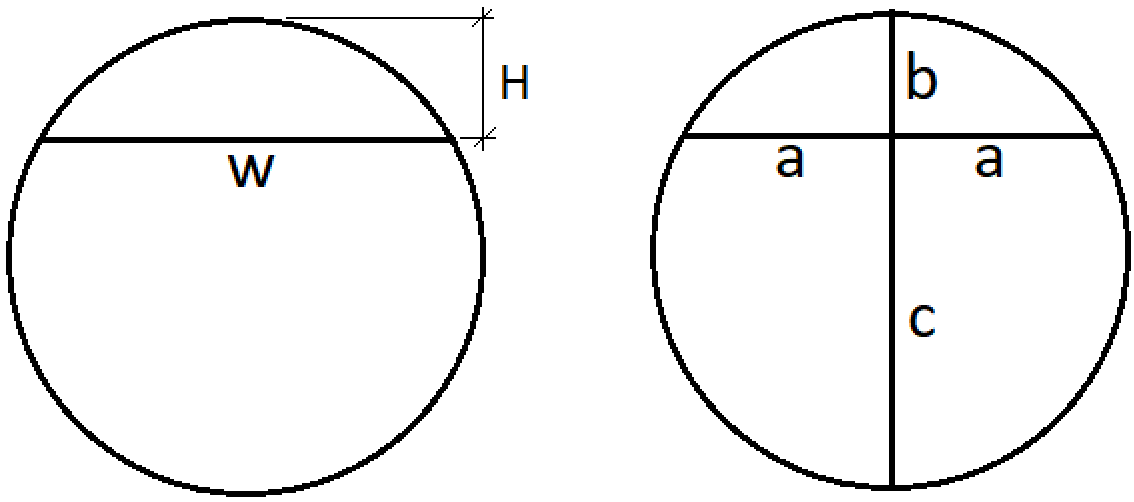

Figure B - 1: Two circles with the same radius

This appendix shows the derivation of the formula for the radius of a circle segment. The intersecting chord theorem states that:

$$a \cdot a = b \cdot c$$

Comparing both circles in Figure B - 1 it is recognized that:

$$a = \frac{W}{2},\ b = H$$

Substitute solve for c:

$$c = \frac{W^2}{4H}$$

Recognize that:

$$\text{circle diameter } = b + c = H + \frac{W^2}{4H}$$

The final result for the radius of a circle segment is:

$$\mathrm{R} = \frac{H}{2} + \frac{W^2}{8H}$$

Appendix C / Material properties

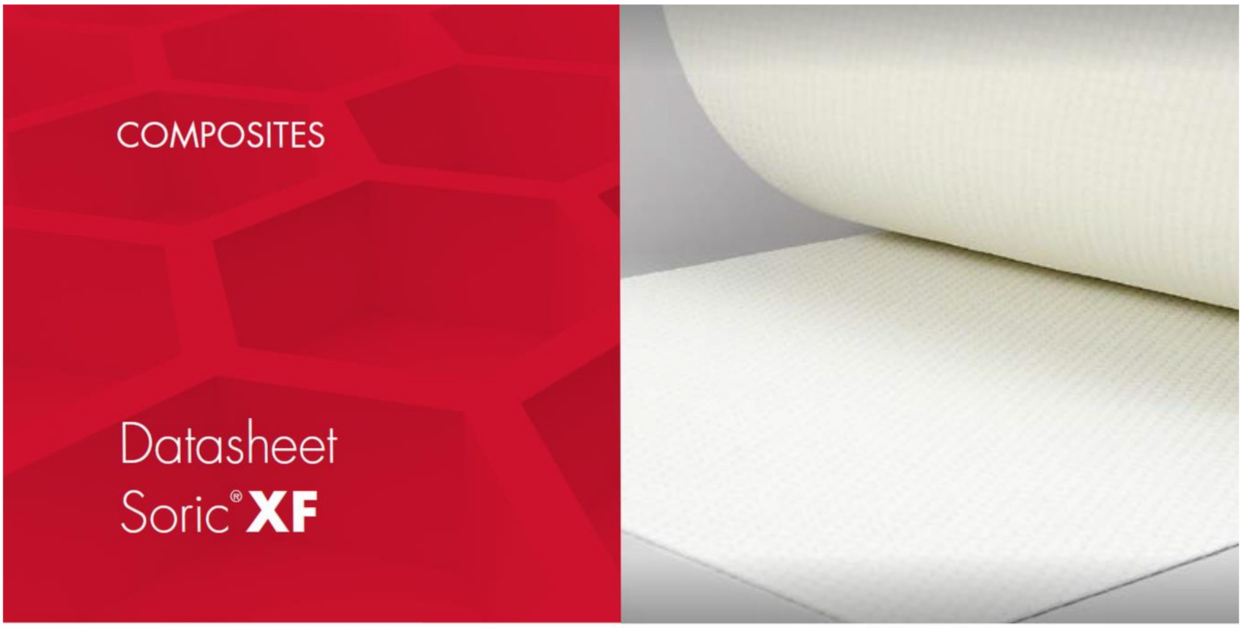

Lantor Soric®XF

- The cost effective solution for closed mould processes
- Is used as core material and infusion medium
- Is a pressure stable polyester nonwoven and compatible with all regular types of resins, including Polyester, Vinylester, Phenolic and Epoxy
- Is suitable for closed mould processes, including Infusion, RTM Light, RTM Heavy

Applications Lantor Soric®XF

- Marine: hulls, decks and structures of boats and yachts
- Transportation: parts and panels of cars, trailers, trucks and RV's
- Mass transit: interior and exterior of trains, light rail and buses
- Leisure: kayaks, surfboards, pools and tubs
- Industrial: cladding panels, fans, containers and tanks
- Wind Energy: nacelle and spinners

Dimensional data

Properties		XF 1.5	XF 2	XF 3	XF 4	XF 5	XF 6	XF 10
Thickness	mm	1,5	2,0	3,0	4,0	5,0	6,0	10,0
Roll length	m	70	80	50	40	30	25	15
Roll width	m	1,27	1,27	1,27	1,27	1,27	1,27	1,27
Thickness loss at 0,8 bar	%	<10	<10	<10	<10	<10	<10	<10
Max processing temp.	°C	170	170	170	170	170	170	170
Resin uptake	kg/m²	1,0	1,0	1,4	1,9	2,4	2,8	5,4
Dry weight	g/m²	100	135	180	250	320	345	625
Density impregnated	kg/m³	650	600	600	600	600	600	600

Typical mechanical properties of Lantor Soric®XF* impregnated with unsaturated polyester resin

Mechanical properties	unit	value	test method
Flexural strength	MPa	8	ASTM D790
Flexural modulus	MPa	800	ASTM D790
Tensile strength across layers	MPa	4	ASTM C297
Compression strength: 10% strain	MPa	8	ISO 844
Shear strength	MPa	3,5	ASTM C273-61
Shear modulus	MPa	35	ASTM C273-61
*Soric®XF 3			

The information contained in this document has been compiled in good faith by Lantor BV, but nevertheless no representation or warranty is given as to the accuracy or completeness of the (technical) information provided herein. Lantor BV can not be held liable of any damages arising from any (printing) errors or omissions in this information. Lantor BV reserves the right to make changes with respect to the information provided at any time without further notice.

Information

PO box 45 - 3900 AA
Verlaat 22 - 3901 RG
Veenendaal
The Netherlands
T +31(0) 318 537 111
composites@lantor.com

enabling performance
www.lantor.com

LANTOR

V2.0/02.2018

Technical Data Sheet

UNITED INITIATORS
driving your success

NOROX®KP-9

Methyl ethyl ketone peroxide
CAS#1338-23-4
Liquid mixture

Description

NOROX®KP-9 is a methyl ethyl ketone peroxide in phlegmatiser for the curing of unsaturated polyester resins at ambient temperature in combination with cobalt accelerators.

Technical Data

Appearance	Colourless and clear liquid
Active oxygen	9.0 - 9.2 %
Free hydrogen peroxide content	1.6 - 1.8 %
Water content	1.5 %
Flash point	> 80 °C (Method: Seta closed cup)
Density at 20 °C	1.12 - 1.15 g/cm³
Viscosity at 20 °C	9 - 15 mPa.s
Soluble in:	Oxygenated organic solvents
Slightly soluble in:	Water
Critical temperature (SADT)	65 °C
Recommended storage temperature	Max 30 °C.
Maintenance of activity at 30 °C as from date of delivery	6 months

Application

NOROX®KP-9 is a general purpose MEKP and is the workhorse of the United Initiators line. NOROX®KP-9 gives consistent room temperature performance with both resins and gelcoats. A reliable product of remarkable purity, NOROX®KP-9 assures quality in almost every system. Suitable applications are: Hand lay-up, spray-up, RTM, continuous laminating, centrifugal casting, filament winding, polyester concrete and vacuum infusion. A single MEKP initiator formulation cannot provide optimum results in all resin systems. Evaluation of each MEKP in each resin intended for use is absolutely essential before full-scale manufacturing is attempted.

Technical Data Sheet

UNITED INITIATORS
driving your success

Measurements

CURE CHARACTERISTICS

A reactivity test with an unsaturated polyester resin gave the following results:

Resin: Orthophthalic polyester Temperature: 25 °C
Initiator %: 1.5 Accelerator% 0,5%(1%cobalt)

Initiator	Gel time Min	Time to peak min	Peak exotherm temp °C
NOROX®KP-9	*25*	*61*	*88*
NOROX®KP-100	*18*	*48*	*106*
NOROX®SG-10	*13*	*44*	*101*

Reactivity of NOROX® MEKPs:

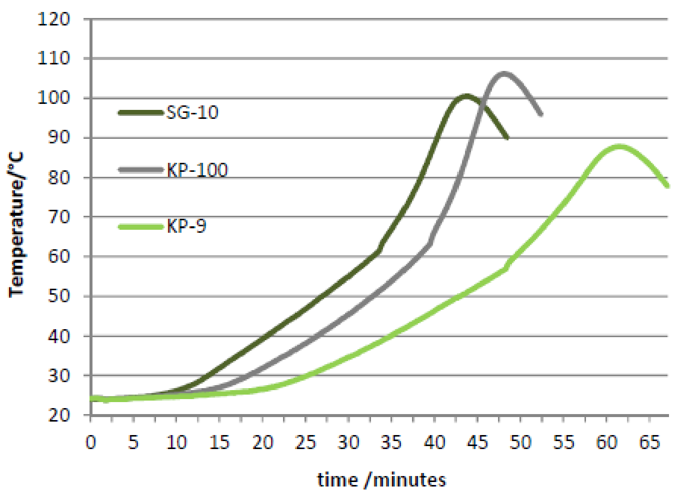

Standard Packaging

The standard package sizes of NOROX®KP-9 are 5 kg and 25 kg polyethylene bottles.

Technical Data Sheet

Disclaimer

This information and all further technical advice are reflecting our present knowledge and experience based on internal tests with local raw materials with the purpose to inform about our products and applications. The information should not be construed as guaranteeing specific properties of products described or their suitability for a particular application, nor as providing complete instructions for use. The information implies no guarantee for product and shelf life properties, nor any liability or other legal responsibility on our part, including with regard to existing third party intellectual property rights, especially patent rights. We reserve the right to make any changes according to technological progress or further developments.
Application and usage of our products based on our technical advice is out of our control and sole responsibility of the user. The user is not released from the obligation to conduct careful inspection and testing of incoming goods in order to verify the suitability for the intended application.

United Initiators
EU
T: +49 89 74422 237
F: +49 89 74422 6237
cs-initiators.eu@united-in.com

United Initiators
Nafta
T: +1 800 231 2702
F. +1 440 323 0898
cs-initiators.nafta@united-in.com

United Initiators
China
T: +86 20 6131 1370
F: +86 139 2503 8952
cs-initiators.cn@united-in.com

United Initiators
Australia
T: +61 2 9316 0046
F: +61 2 9316 0034
cs-initiators.au@united-in.com

www.united-initiators.com

Revision number: 1.0. Date: 03.03.14. Device M: TDS.

Bibliography

1. Raun, C., *DEVICE FOR USE IN A MOULD FOR THERMOFORMING, THE MOULDS OF THE TYPE PROVIDING A CURVED DOUBLE-CURVED, DYNAMICALLY RECONFIGURABLE SURFACE WITH AN OPEN STRUCTURE, WO2013104369.*, H. Consult, Editor. 2013.
2. Barnes, J.B.C.A.J., *Forming Fibre-Plastic Composites*. April 14,1987.
3. McGuinness, G.B.G.G.B., *Numerical analysis of stresses and deformations in composite materials sheet forming: central indentation of a circular sheet.* Composites Manufacturing, 1993. 4: p. 67-83.
4. Mallon, P.J. and C.M. O'Bradaigh, *Development of a pilot autoclave for polymeric diaphragm forming of continuous fibre-reinforced thermoplastics.* Composites, 1988. 19: p. 37-47.
5. Gutowski, T.G., et al., *Method and system for forming a composite product from a thermoformable material*. 1996, Google Patents.
6. Bhattacharyya, D., *Composite sheet forming*. Composite materials series, 0927-0108 ; 11; Composite materials series ; 0927-0108 11. 1997, Amsterdam :: Elsevier.
7. Parnas, R.S., *Liquid composite molding*. 2000, Munich :Cincinnati :: Hanser ;Hanser Gardner Publications.
8. L. Dupont, M.A.a.A.P. *An objective study of resin injection machines for resin transfer moulding of both low cost products and advanced composites*. in *ICCM-9*. 1993. Madrid.
9. Horrocks, A.R. and S. Anand, *Handbook of technical textiles*. 2000, CRC Press/Woodhead Pub.: Boca Raton, FL :.
10. Robroek, L.M.J., T. De Jong, and R. Marissen, *The development of rubber forming as a rapid thermoforming technique for continuous fibre reinforced thermoplastic composites: quality control by process control*. 1994, Delft University Press.
11. Bergsma, O.K., *Three Dimensional Simulation of Fabric Draping*. 1995, Delft University Press.
12. Committee, A.S.M.I.H., *ASM handbook. Volume 21, Composites*. 2001, ASM International: Materials Park, OH :.
13. Blanlot R., Billoet J.L., and G. H. *Study of Non-Polymerised Prepreg Fabrics in 'Off-Axes' Tests*. in *ICCM-9*. 1993. Madrid.
14. Potter, K.D., *The influence of accurate stretch data for reinforcements on the production of complex structural mouldings.* Composites, 1979. 10.
15. Van West, B.P., *A simulation of the draping and a model of the consolidation of commingled fabrics*. 1991.
16. Tam, A.S., *A deformation model for the forming of aligned fiber composites.* 1990.
17. Tam, A.S. and T.G. Gutowski, *Ply-Slip During the Forming of Thermoplastic Composite Parts.* Journal of Composite Materials, 1989. 23: p. 587-605.
18. Scherer, R., K. Friedrich, and N. Zahlan, *Modelling the interply slip process during thermoforming of thermoplastic composites using infinite element analysis.* 1990.
19. Talbott, M.F. and A.K. Miller, *A model for composite laminate bend-forming under arbitrary curvature distribution and extensive interlaminar sliding.* Polymer Composites, 1990. 11: p. 387-397.
20. III, C.L.T., *Forming of Advanced composites*. Advanced Composites Manufacturing, ed. T.G. Gutowski. 1997.
21. Advani, S.G., *Flow and rheology in polymer composites manufacturing*. Composite materials series, 0927-0108 ; 10; Composite materials series ; 0927-0108 10. 1994, Amsterdam :: Elsevier.
22. Hull, B.D., T.G. Rogers, and A.J.M. Spencer, *Theory of fibre buckling and wrinkling in shear flows of fibre-reinforced composites.* Composites Manufacturing, 1991. 2: p. 185-191.